The Pennsylvania State University

The Graduate School

Department of Mechanical Engineering

FILM COOLING CALCULATIONS WITH AN ITERATIVE CONJUGATE HEAT TRANSFER APPROACH USING EMPIRICAL HEAT TRANSFER COEFFICIENT CORRECTIONS

A Thesis in

Mechanical Engineering

by

Sushant Dhiman

Submitted in Partial Fulfillment
of the Requirements
for the Degree of

Master of Science

December 2010

The thesis of Sushant Dhiman was reviewed and approved* by the following:

Savas Yavuzkurt
Professor of Mechanical Engineering
Thesis Advisor

Anil K. Kulkarni
Professor of Mechanical Engineering

Karen Thole
Professor of Mechanical Engineering
Head of the Department of Mechanical Engineering Department

*Signatures are on file in the Graduate School

ABSTRACT

An iterative conjugate heat transfer technique was developed and automated to predict the temperatures on film cooled surfaces such as flat plates and turbine blades. Conventional approaches using a constant wall temperature to calculate heat transfer coefficient and applying it to solid as a boundary condition can result in errors of around 14% in internally cooled blades, as shown by previous research work. This indicates a need for conjugate heat transfer calculation techniques. However, full conjugate film cooling calculations also suffer from inability to correctly predict heat transfer coefficients in the near field of film cooling holes and require high computational cost making them impractical for component design in industrial applications. Iterative Conjugate Heat Transfer (ICHT) analysis is a compromise between these two techniques where the external flow convection and internal blade conduction are loosely coupled. The solution obtained from solving one domain is used as boundary condition for the other. This process is iterated until convergence. Flow and heat transfer over a film cooled blade is not solved directly, instead convective heat transfer coefficients resulting from external convection on a similar blade without film cooling and under the same flow conditions are corrected by use of experimental data to incorporate the effect of film cooling in the heat transfer coefficients. The effect of conjugate heat transfer is taken into account by using this iterative technique. Unlike full Conjugate Heat Transfer (CHT), the ICHT analysis doesn't require solving a large number of linear algebraic equations at once. It uses two separate meshes for external convection and blade conduction and thus problem can be solved in lesser time using less computational resources.

A demonstration of this technique using a commercial CFD solver FLUENT is presented for simulations of film cooling on flat plates and C3X turbine blade. Results are presented in form of film cooling heat transfer coefficients and surface temperature distribution which are

compared with results obtained from conventional approach where in which heat transfer data is usually obtained on test surface maintained at a constant temperature or heat flux condition.

For uncooled surfaces, the deviations were as high as 3.5% between conjugate and conventional technique results for the wall temperature. For film cooling simulations on a flat plate using the ICHT approach showed deviations up to 10% in surface temperature compared to constant wall temperature technique for a high temperature difference case and 3% for a low temperature difference case, since surface temperature is not constant over the surface when conjugate heat transfer is considered. In case of 2D full conjugate heat transfer simulation performed on a non film cooled C3X vane reasonable agreement to experimental data was observed for mid-span wall temperature distribution. Average deviations of around 6% on the pressure side and 7% on the suction side from experimental data were obtained.

Film cooling calculations performed on the C3X blade using the ICHT technique predicted wall temperature distribution in excellent agreement with the data. Temperature distribution obtained using ICHT were within 2 to 3 % of the experimental data i.e. well within the experimental uncertainty, while conventional technique predicted the same within 6 to 8% of the data. In all, for wall temperature distribution, an overall improvement of around 7% on the pressure side and 10% on the suction side over conventional technique was obtained using ICHT.

Results thus show that the ICHT technique is an effective tool for performing accurate film cooling calculations which reduces computational cost and complexity involved in meshing discrete film cooling holes. Moreover, it is physically more appropriate than conventional technique since it considers the effect of blade metal conduction.

TABLE OF CONTENTS

LIST OF FIGURES

LIST OF TABLES

NOMENCLATURE

Br_x = Local Brun number = $\frac{\lambda_f}{\lambda_s}\frac{b}{x}\ Pr^m Re^n$

Where $m = \frac{1}{3}, n = \frac{1}{2}$

b = thickness of the plate in mm

C_f = Skin friction coefficient

D = Diameter of injection hole

M = Blowing ratio or mass flux ratio

V_G = Mainstream gas inlet velocity

P = Static pressure

P_t = Stagnation pressure

Pr = Prandtl number

Re_x = Reynolds number based on length

Re_θ = Reynolds number based on momentum thickness

St = Stanton number

SNR = Stanton number ratio given by $SNR = 1 - h(\theta)/h_0$

Nu_D = Nusselt number based on diameter of tube

T_{AW} = Adiabatic wall temperature

T_b = Bulk temperature

T_C = Temperature of secondary gas or coolant

T_G = Temperature of mainstream gas

T_W = Temperature of fluid-solid interface surface

Tu % = Free stream turbulent intensity

x, y = Cartesian coordinates

h = Heat transfer coefficient (W/m^{2}K)

h_0 = Baseline heat transfer coefficient with no film cooling (W/m^{2}K)

h_f = Film heat transfer coefficient defined as follows

$$h_f = q_W/(T_{AW} - T_W)$$

$h(\theta)$ = Heat transfer coefficient defined as follows

$$h(\theta) = q_W/(T_G - T_W)$$

$q_W^{"}$ = Heat flux W/ m^2

Greek letters

α = Injection angle

η = Adiabatic film cooling effectiveness

$$\eta = (T_G - T_{AW})/(T_G - T_C)$$

θ = Dimensionless temperature

$$\theta = (T_G - T_C)/(T_G - T_W)$$

λ_f =thermal conductivity of fluid

λ_s= thermal conductivity of solid

Subscript

C = Secondary gas or coolant side

G = mainstream gas side

0 = No film cooling

Accent

$\bar{X}$ = laterally averaged quantity X like $\overline{\eta}$, $\overline{h(\theta)}$,$\overline{h_f}$

ACKNOWLEDGEMENTS

I would first like to thank my family for being forever supportive for all my endeavors. Next, I thank my graduate adviser Dr Savas Yavuzkurt for all his support and invaluable guidance not just on professional front but also on a personal level. It's been an absolute pleasure working with him. At this time I would also like to extend my gratitude to Dr Atul Kohli who was the project monitor for Pratt & Whitney for supporting my Masters Work. Without his encouragement and Pratt & Whitney's financial support I couldn't have worked on such a gripping technological challenge.

I am also grateful to the Mechanical Engineering Department which gave me an opportunity to study in such a sought after research institute like The Pennsylvania State University.

Finally, wish to say thanks to all my friends here at Penn State who made the two years of my masters such an enjoyable experience.

Chapter 1

INTRODUCTION & LITERATURE REVIEW

1.1 **Introduction**

An increase in the efficiency of gas turbines can be obtained by increasing the turbine inlet temperature. For engine power to double, the rotor inlet temperature should increase from 2500°F to 3500°F using compressor bleed air as pointed out by Je-Chin Han **[1]**.

The thermal stresses at these temperatures could lead to structural failure of blades. Moreover, these high temperatures could exceed the melting point of present blade materials, thus decreasing the component life significantly. An increase in the lifetime of gas turbine blades can be achieved by employing suitable cooling techniques.

Some of the most common techniques employed in cooling gas turbine blades are:-

1. Convection cooling
2. Impingement Cooling
3. Film Cooling
4. Transpiration Cooling

Convection Cooling: - Cooling air is passed through serpentine channels running interior of the hollow turbine blade. The walls of the hollow turbine blade separate the hot mainstream gas and cooler secondary gases. As it flows through these channels the coolant gases absorb heat by convection from the blade wall thus cooling it. These channels are ribbed and have turbulators and / or pin fins to increase the heat transfer rate.

Impingement Cooling: - The coolant gases flowing inside the channels in a hollow turbine blade impinge on the internal surface of the blade to absorb heat from the blade wall.

Film Cooling: - Cool air from the compressor is bled through holes on to the blade surface which forms a thin film of coolant to protect the blade surface from the mainstream hot gases. Secondary fluid or the cool air is usually injected into the external boundary layer right into the region where the thermal loads are the highest. The injected coolant not only protects the surface at the injection location but also the region downstream to the hole.

Transpiration Cooling: - Coolant gases exit the blade through small pores in its surface. Although it is a very effective way of drawing out heat from the blade metal but makes the structure weak and prone to clogging by dirt during the course of operation.

As evident from figure 1-1 discrete hole film cooling technique is an efficient way of cooling a turbine blade and still remains one of the most feasible and popular approach for gas turbine blade designers.

The present computational fluid dynamics study deals with a novel numerical technique of performing film cooling flow calculations which also take into account the effect of thermal resistance offered blade metal on the flow, thus making the technique as accurate and realistic as possible.

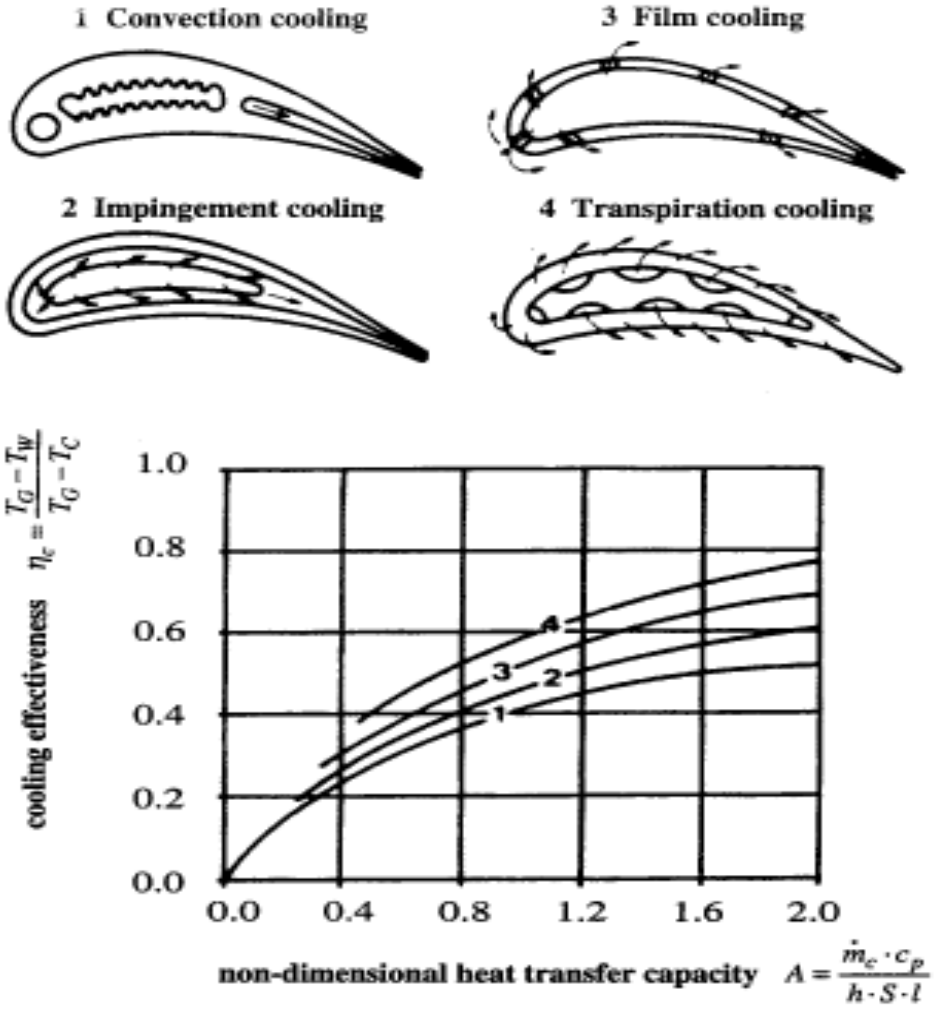

Figure 1-1 Various cooling configurations possible in a turbine blade, Sunden & Faghri [**2**].

1.2 Experimental Studies on Film Cooling

A review of some of the earliest studies on film cooling has been provided by Goldstein [**3**]. He provided a detailed summary of the effect of geometry and flow parameters on film cooling, through studies done prior to 1971. Much of the earlier work on film cooling was done on flat surfaces.

Ekkad et al **[4]** used transient liquid crystallography for gathering effectiveness and heat transfer data on a flat plate with compound injection angle of 0º, 45º & 90º at high free stream turbulence conditions of Tu=8.5% . They concluded that compound injection provides high film effectiveness as compared to simple angled holes. Apart from techniques like naphthalene sublimation and liquid crystallography mentioned above, two most commonly used methods for obtaining heat transfer data by researchers are constant temperature and constant heat flux technique. Both these techniques have been discussed later in greater detail.

Baldauf et al. **[5-8]** conducted a detailed study on flat plate film cooling, using constant wall temperature technique to obtain film cooling effectiveness and heat transfer coefficient data at engine like conditions, for various injection angles and blowing ratios and later reduced the data in form of experimental correlations. Yuen & Martinez **[9-12]** did an exhaustive study on film cooling characteristics of round hole and presented film cooling effectiveness and heat transfer coefficient data for various injection angles and orientations, they employed constant heat flux technique to obtain heat transfer data.

Gritsch et al **[13-14]** presented flat plate film cooling data at high Mach numbers (up to 0.6) for injection holes with expanded exits and blowing ratio of upto 2. They use constant temperature technique to obtain heat transfer coefficients. They found out that the holes with expanded exits provides better lateral spreading of the coolant jet as compared to the cylindrical holes thus improving overall film cooling performance. Sarginson et al. **[15]** used constant heat flux technique for determining heat transfer coefficients. They presented low speed flat plate heat transfer results using converging slot hole and compared the results with other film cooling geometries. They determined that hole of a console geometry has a thermal performance similar to that of a fan shaped hole but with lesser aerodynamic losses.

Most of the above mentioned researchers use constant heat flux or constant temperature to obtain heat transfer coefficient data while neglecting the effect of heat transfer to thermal resistance of the plate metal on the velocity field within the film or in other words the effect of metal conduction is not taken into account. In real life situations neither the heat flux nor the blade surface temperature remains constant. This implies that there is a need for running the experiments under conjugate conditions.

Relatively few conjugate heat transfer experiments on film cooling have been performed which take into account the effect of internal convection and metal conduction on the velocity field inside the film. One such study is by Hylton et al. **[16]** and they carried out measurements of external convective heat transfer coefficient on a C3X 2-D linear airfoil cascade. They employed part analytical and part experimental strategy. Experiments were first performed to determine internal and external boundary conditions at steady state. A finite element solver was then used for calculating the blade conduction to obtain normal gradients of temperature on the surface of the blade, using which the external convective heat transfer coefficients could be predicted.

1.3 Numerical Studies on Film Cooling

Computational studies on film cooling serves two fold purpose, it provides a better physical understanding of the complex flow structures (e.g. vortices created at the hole exit) , jet mixing and spreading involved in film cooling and more importantly in predicting the relevant film cooling performance variables like effectiveness and net heat flux reduction ratio .

Unfortunately, numerical calculations performed in the past to simulate such film cooling flows haven't always predicted the above mentioned film cooling performance variables correctly, mostly due to the closure problem associated with current turbulence models. Past work done by researchers on this field confirms this fact. Yavukurt and Habte **[17]** showed that in the near field of the jets [X/D<8] steady two equation turbulence models like *k-ε* and *k-ω* predict higher effectiveness indicating lower amount of mixing. **RNG** *k-ε* model under predicts the effectiveness data by as much as 80% while on the other hand *k-ω* model over predicts the data by around 16% in the near field region. This was despite the fact that the mesh was sufficiently resolved all the way up to the viscous sub layer where y+ < 1.

Similar numerical simulation of film cooling flows was performed by Azzi and Lakehal [**18**]. They tested out various versions of the *k-ε* turbulence models. Their results show that two-equation models like the universal *k*−ε model under predict the lateral spreading of the temperature field, leading to lower values of the laterally averaged adiabatic film cooling effectiveness. They also pointed out that film cooling calculations of the channel show that the thermal field is more difficult to predict. They conclude that even the non linear algebraic models under predict the lateral spreading of the jet as much as the isotropic model. Thus, due to inherent inadequacy of steady standard turbulence models accurate prediction of film cooling characteristics, especially in the near field of the jets, is very difficult.

Hoda and Acharya [**19**] compared several different turbulence models for film cooling flows and they concluded that, in general, the two equation turbulence models provide better results than algebraic models but are unable to predict the near field of the coolant jet accurately. On one hand where the lateral spreading and the mixing of the film cooling jet is under predicted by two equation model the vertical penetration of coolant jet is over predicted.

Acharya et al [**20**] suggested that lower lateral spreading can be attributed to the under estimation of eddy viscosity in the lateral direction since the two equation model assumes eddy viscosity to be an isotropic property. They also carried out a case study to evaluate the performance of several RANS models, LES and DNS modeling approaches as well. Their results showed that for two equation models the span-wise stresses were significantly lower than measured values indicating that they underestimate the jet growth in span-wise direction. Furthermore, even with the RSTM model, which accounts for the anisotropy, no significant improvement was achieved and instead it poorly predicted the kinetic energy. They concluded that the discrepancy usually comes from inability of this model to capture large scale unsteadiness in the near field.

Past studies by researchers have also highlighted the importance of including the effect of metal conduction into film cooling calculations. Silieti et al. **[21]** reported that the full conjugate heat transfer model shows a significant difference in temperature prediction when compared to adiabatic cases and confirmed that such an approach takes into account the mutual influence of heat transfer on fluid flow and vice versa. They compared the centerline effectiveness for both adiabatic and conjugate cases and observed a significant improvement in conjugate effectiveness of up to 3 times in the immediate region (x/D <6) of the coolant jet.

Bohn et al**. [22**] did a study on conjugate heat transfer in a film cooled turbine blade. They predicted 8% of difference in temperatures obtained from conjugate and decoupled conventional approach. Xiaochen et al. **[23]** concluded that the application of the conjugate method includes the influence of heat transfer on the velocity field within the boundary layer.

1.4 Conclusion from Literature Review and Motivation for Present Study.

Past work done by researchers, experimental as well as computational, in the field of film cooling reveal several key aspects of film cooling physics that forms the basis of the present study.

i. Heat transfer coefficient data is usually obtained by either maintaining constant heat flux or constant temperature on the film cooled surface where the data is collected. This implies that the effect of metal conduction is not taken into account while collecting the data as explained before.

In conventional technique, gas turbine blade designers use this heat transfer data as boundary condition to solve for metal conduction inside the blade and subsequently get the temperature field. However in practical situations, a turbine blade is subjected to external convection, blade conduction and internal convection. In such a case, neither the heat flux nor the temperature at the surface remains constant. It varies as the normal gradient of the temperature changes across the blade surface. Thus, using heat transfer coefficient data from the above mentioned technique usually leads to erroneous temperature field predictions inside the blade.

ii. This survey of literature on numerical studies of film cooling flow reveal that the current models of turbulence like the two equation standard k-ε are severely restricted in their ability to predict spreading and the mixing of the film cooling jet, leading to incorrect temperature field calculations. Even the more sophisticated RANS models like the RSTM, which accounts for the anisotropy of eddy viscosity, do not significantly improve the predictions and instead poorly predicts kinetic energy in the near field of coolant jet.

iii. As indicated by past computational studies on conjugate heat transfer any realistic flow calculations should solve external flow convection and blade metal conduction simultaneously. This type of fully coupled approach (i.e. conduction and convection are solved simultaneously) not only shows a significant improvement over a de-coupled solution but also the boundary condition at the fluid-solid interface need not be known by the blade designer.

However, the above mentioned problems associated inherently with steady turbulence models still persist, especially in the near field of coolant jet. Moreover, a fully coupled solution with internal convection and blade conduction means increased number of grid points i.e. solving large matrix of linear algebraic equations which require significant computational costs and increase the product design time.

1.5 Objectives of Present Research Work.

A careful investigation of the computational and experimental work on film cooling flows reveals several shortcomings in the approach taken by most present day researchers, some of which have been mentioned in the previous section.

The current research focuses on developing a new technique, *Iterative Conjugate Heat transfer or ICHT technique*, which can limit some of these known difficulties related to correct prediction of heat transfer related to film cooling flows.

The **main objectives** of this study can be summed up as follows:-

1. **Development of a computational technique i.e. ICHT.** In this technique film cooling flows is not modeled explicitly thereby overcoming the problems inherent to present turbulence models, especially in the near field region, as discussed in the literature review section. Instead, the effect of film cooling would be taken into account through the use of suitable film cooling correlations.

   In other words, only external mainstream flow calculations are performed with no secondary flow or coolant emanating from the jets thereby avoiding the complexities involved in turbulence modeling of mixing of these two flows.

2. **Development of a film cooling empirical correlation** based upon heat transfer data in published literature. These correlations would be used to correct external flow solution predicted by CFD to incorporate film effect.

3. **Inclusion of blade metal conduction** into film cooling flow analysis. As suggested by computational studies on conjugate heat transfer involving film cooling flows it is imperative to take into account the influence of thermal resistance of the blade metal and the effect of internal convection and blade conduction on the velocity field inside the coolant film on the surface.

4. **Automation of Iterative conjugate heat transfer technique.** In order to reduce the calculation time and manual effort, the whole process flow of ICHT was automated using a code written in a List programming language called SCHEME which is used as scripting language for ANSYS FLUENT.

Chapter 2

GOVERNING EQUATIONS AND TURBULENCE MODELS

The current study mainly makes use of one equation Spalart-Allmaras **(SA)** turbulence model, two equation standard *k-ε* (**SKE**) model developed by Launder and Spalding [**24**] in 1974 and two equation shear stress transport *k-ω* (**KW-SST**) model developed by Menter [**25**] in 1994. All the aforementioned models are Reynolds Averaged Navier Stokes (RANS) based models and each one of them yields a superior performance in different conditions. Therefore, it is important to know about the physics of the problem before choosing the right turbulence model. In order to obtain best results while performing CFD on turbulent flows one must take into account various complex phenomena involved in a fluid flow, some of which are listed below.

i. Flow separation

ii. Severe adverse pressure gradients

iii. Free sheer flows or wall bounded flows.

iv. Swirl, vortices in the flow

v. Transition in the flow

The complexity of flow physics is one of the most important things that should be taken into account while choosing a turbulence model. However, several other factors should also be considered as well.

i. Computational cost

ii. Robustness and convergence

iii. Near wall treatment

iv. Turnaround time and accuracy

For example a simple one equation model might be computationally inexpensive though it might not be able to capture the flow physics very well while on the other hand a 2 equation model or higher might yield superior answer but might have convergence difficulties and require a lot more computational resources.

But before dwelling deeper into turbulence and its modeling approach used for numerical predictions it is important to understand the fundamental laws and equations which govern fluid flow.

2.1 Governing Equations

The governing equations of flow for a Newtonian fluid are listed below in vector notation.

Conservation of Mass

$$\frac{\partial \rho}{\partial t} + \nabla.(\rho \boldsymbol{u}) = 0 \tag{2.1}$$

Conservation of Momentum

$$\frac{\partial (\rho \boldsymbol{u})}{\partial t} + \nabla.(\rho \boldsymbol{u}\boldsymbol{u}) = -\nabla p + \nabla.(\mu \nabla \boldsymbol{u}) + \rho \vec{g} \tag{2.2}$$

Conservation of Energy

$$\frac{\partial (\rho i)}{\partial t} + \nabla.(\rho i\, \boldsymbol{u}) = -p\, \nabla.\boldsymbol{u} + \nabla.(k \nabla T) + \phi \tag{2.3}$$

Here, $\boldsymbol{i}$ is the internal energy given by $i = h - \frac{p}{\rho} + \frac{v^2}{2}$. where h is the sensible enthalpy

$\boldsymbol{\phi}$ is known as the viscous dissipation, which is defined as the thermal energy created by viscous shear in the flow and is described by equation (2.4).

$$\boldsymbol{\phi} = \mu\left\{2\left[\left(\frac{\partial u}{\partial x}\right)^2 + \left(\frac{\partial v}{\partial y}\right)^2 + \left(\frac{\partial w}{\partial z}\right)^2\right] + \left(\left(\frac{\partial u}{\partial y}\right) + \left(\frac{\partial v}{\partial x}\right)\right)^2 + \left(\left(\frac{\partial u}{\partial z}\right) + \left(\frac{\partial w}{\partial x}\right)\right)^2 + \left(\left(\frac{\partial v}{\partial z}\right) + \left(\frac{\partial w}{\partial y}\right)\right)^2 + \lambda(\nabla.\boldsymbol{u})^2\right\} \quad (2.4)$$

$\boldsymbol{\phi}$ or viscous heating is generally negligible for incompressible flows and should be considered in CFD calculations when Brinkman number $\boldsymbol{Br_n} > 1$. In equation (2.4), $\boldsymbol{u}$ is the three dimensional velocity field given by $\boldsymbol{u} = \hat{\imath}u + \hat{\jmath}v + \hat{k}w$. P is the local pressure which remains constant across the boundary layer.

The above mentioned flow equations (2.1) & (2.2) are coupled since the unknowns u, v, w appear in each of them and must be solved simultaneously. Furthermore, the presence of non linear viscous term likes $\nabla.(\mu\nabla u)$ renders an analytical solution of these equations impossible, except for a few simplified cases. Therefore, CFD is the only way of obtaining solution of these equations when dealing with complex flow situation.

2.2 Turbulence Basics

What is turbulence?

Fluid flows which are unsteady, irregular and in which transported quantities (mass, momentum, scalar species) fluctuate in time and space are termed as a turbulent flows.

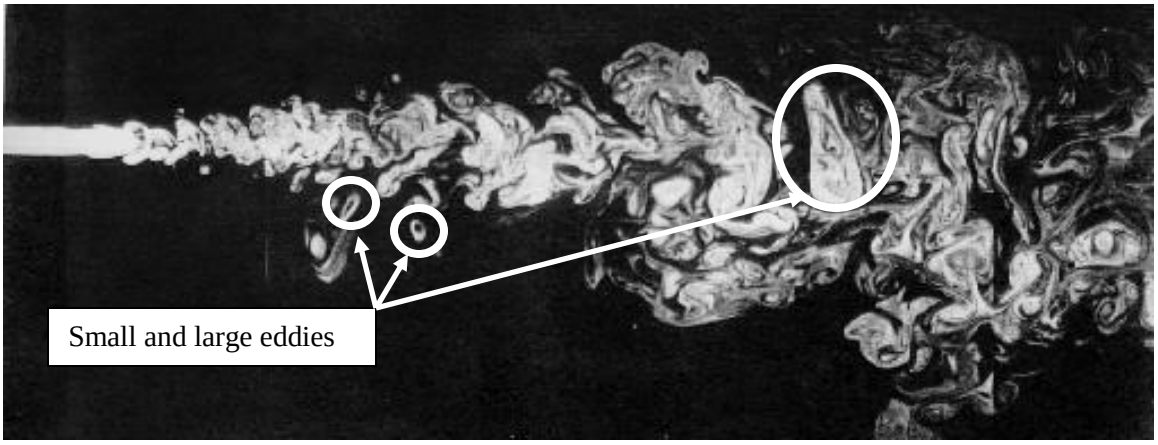

Figure 2-1 – Different scales of eddies in a turbulent flow.

Any turbulent flow contains a wide range of eddies which are nothing but energy carrying rotational flow structures as shown in figure 2-1. Thus, a turbulent flow has a wide range of length scales.

How is energy transferred during turbulence?

Energy is transferred from larger eddies to smaller eddies via the process of vortex stretching. Larger eddies extract the energy from the mean flow. Presence of mean velocity gradient in a turbulent flow stretches and distorts these eddies. Large eddies are dominated by inertial effects and are essentially inviscid and angular momentum is conserved during the process of vortex stretching. On the other hand, smaller eddies are stretched more by larger eddies than mean flow thus the kinetic energy is transferred down from larger to smaller rotational eddies in what is called energy cascade as shown in figure 2-2. Viscous effects are more dominant than inertial ones in smaller eddies. The larger eddies are highly anisotropic (directional properties) while the smallest eddies in a turbulent flow are isotropic (non directional properties).

2.3 Reynolds Averaged Navier-Stokes (RANS) Equations.

The computational requirement for direct numerical solution of time dependent Navier-Stokes equation of fully turbulent flows would be massive thus computational predictions are done using equations derived by time averaged properties of flow expressed in form of RANS equations.

Mean $\bar{\phi}$ of a flow property ϕ can be defined as

$$\bar{\phi} = \frac{1}{\Delta t}\int_0^{\Delta t} \phi(t)dt \tag{2.5}$$

Any instantaneous flow property ϕ can thus be expressed as

$$\phi = \bar{\phi} + \phi' \tag{2.6}$$

After taking the ensemble average of conservation of mass and momentum equations (2.1) & (2.3) we obtain equations for turbulent flows which are as follows, in vector notation .

Continuity equation,

$$\frac{\partial \rho}{\partial t} + \nabla.(\rho\bar{\boldsymbol{u}}) = 0 \tag{2.7}$$

RANS equations,

$$\frac{\partial(\rho\bar{u})}{\partial t} + \nabla.(\rho\bar{u}\bar{\boldsymbol{u}}) = -\frac{d\bar{p}}{dx} + \nabla.(\mu\nabla\bar{u}) + \left\{-\frac{\partial(\rho\overline{u'u'})}{\partial x} - \frac{\partial(\rho\overline{u'v'})}{\partial y} - \frac{\partial(\rho\overline{u'w'})}{\partial z}\right\} \tag{2.8}$$

$$\frac{\partial(\rho\bar{v})}{\partial t} + \nabla.(\rho\bar{v}\bar{\boldsymbol{u}}) = -\frac{d\bar{p}}{dy} + \nabla.(\mu\nabla\bar{v}) + \left\{-\frac{\partial(\rho\overline{u'v'})}{\partial x} - \frac{\partial(\rho\overline{v'v'})}{\partial y} - \frac{\partial(\rho\overline{v'w'})}{\partial z}\right\} \tag{2.9}$$

$$\frac{\partial(\rho\bar{w})}{\partial t} + \nabla.(\rho\bar{w}\bar{\boldsymbol{u}}) = -\frac{d\bar{p}}{dz} + \nabla.(\mu\nabla\bar{w}) + \left\{-\frac{\partial(\rho\overline{u'w'})}{\partial x} - \frac{\partial(\rho\overline{v'v'})}{\partial y} - \frac{\partial(\rho\overline{w'w'})}{\partial z}\right\} \tag{2.10}$$

2.4 Closure problem and Turbulence modeling

Six additional unknown terms appear in the RANS equations (2.8) to (2.10). These unknowns are called Reynolds stresses and can be expressed as ($\overline{u_i' u_j'}$) in tensor notation. Thus, in order to obtain a closure for the RANS equations these unknown Reynolds stresses have to be modeled.

One of the most popular ways of obtaining a closure for the RANS equations is through Boussinesq hypothesis which says that the Reynolds stresses can be linked to mean rate of deformation in the following fashion.

$$-\rho\overline{u_i' u_j'} = \mu_t \left(\frac{\partial \overline{u_i}}{\partial x_j} + \frac{\partial \overline{u_j}}{\partial x_i}\right) - \frac{2}{3}\left(\rho k + \mu_t \frac{\partial u_k}{\partial x_k}\right)\delta_{ij} \qquad (2.11)$$

Where, μ_t is known as eddy viscosity or the turbulent viscosity. This approach is used in one equation Spalart-Allmaras model, two equations *k*-ε and *k*-ω models.

Advantages of using Boussinesq hypothesis:-

i. The Boussinesq hypothesis is reasonable enough for simple turbulent shear flows-boundary layers, round jets, mixing layers, channel flows etc
ii. Low computational cost

Disadvantage of using Bousinesq hypothesis:-

i. It assumes that eddy viscosity μ_t is same in all direction i.e. isotropy, which is not completely true.

2.5 Turbulence Models

All the turbulence models employed in the present computational study are eddy viscosity models based on Boussinesq's hypothesis. Some perform better than the other in different situations.

Given below, is the description of various turbulence models employed in the current study, the notations and descriptions used for these turbulence models have been adopted from Fluent user manual [**26**] and Fluent training modules provided by ANSYS Inc.

2.5.1 Spalart-Allmaras (SA) Model

It is simple one equation turbulence model developed by Spallart and Allmaras [**27**] and is used extensively for turbo machinery applications. It solves the transport equation for a modified form of turbulent kinematic viscosity and it is not necessary to calculate a length scale related to the local shear layer thickness.

The transported variable in **SA** model is $\tilde{\boldsymbol{\nu}}$ and is appears in the transport equation (2.12).

The ($\tilde{\nu}$) transport equation

$$\frac{\partial(\rho\tilde{\nu})}{\partial t}+\frac{\partial(\rho\tilde{\nu}u_i)}{\partial x_i}=G_\nu+\frac{1}{\sigma_{\tilde{\nu}}}\left[\frac{\partial}{\partial x_i}\left\{\mu+\rho\tilde{\nu}\frac{\partial\tilde{\nu}}{\partial x_j}\right\}+C_{b2}\rho\left(\frac{\partial\tilde{\nu}}{\partial x_j}\right)^2\right]-Y_\nu+S_{\tilde{\nu}} \qquad (2.12)$$

where G_ν and Y_ν are the production and destruction term of turbulent viscosity in the near wall region. ν is the molecular kinematic viscosity and $S_{\tilde{\nu}}$ is the source term.

Turbulent viscosity ($\boldsymbol{\mu_t}$) is modeled as follows: -

$$\mu_t = \rho\check{\nu} f_{v1} \tag{2-13}$$

Where, f_{v1} is the viscous damping function, given by

$$f_{v1} = \frac{\chi^3}{\chi^3 + C_{v1}^3} \tag{2.14}$$

And $\chi = \tilde{\nu}/\nu$

Turbulent Production term ($\boldsymbol{G_\nu}$) is modeled as follows:-

$$G_\nu = C_{b1}\rho\tilde{S}\tilde{\nu} \tag{2.15}$$

Where,

$$\tilde{S} = S + \frac{\tilde{\nu}}{\kappa^2 d^2} f_{v2} \tag{2.16}$$

$$f_{v2} = 1 - \frac{\chi}{1+\chi f_{v1}} \tag{2.17}$$

S depends upon magnitude of vorticity and is defined in equation (2.18)

$$S = \sqrt{2\left(\Omega_{ij}\Omega_{ij}\right)} \tag{2.18}$$

Ω_{ij} is the mean rate of rotation tensor given in equation (2.19)

$$\Omega_{ij} = \frac{1}{2}\left(\frac{\partial \overline{u_i}}{\partial x_j} - \frac{\partial \overline{u_j}}{\partial x_i}\right) \tag{2.19}$$

Turbulent destruction term ($\boldsymbol{Y_\nu}$) is modeled as follows:-

$$Y_\nu = C_{w1}\rho f_w \left(\frac{\tilde{\nu}}{d}\right)^2 \tag{2.20}$$

$$f_w = g\left[\frac{1+C_{w3}^6}{g^6+C_{w3}^6}\right]^{1/6} \quad (2.21)$$

$$g = r + C_{w2}(r^6 - r) \quad (2.22)$$

$$r \equiv \frac{\tilde{\nu}}{S\kappa^2 d^2} \quad (2.23)$$

The constants in the SA model are

$C_{b1} = 0.1355, C_{b2} = 0.622\,,\ C_{v1} = 7.1,\ \sigma_{\tilde{\nu}} = 2/3$

$C_{w1} = \frac{C_{b1}}{\kappa^2} + \frac{1 + C_{b2}}{\sigma_{\tilde{\nu}}}\,, C_{w2} = 0.3, C_{w3} = 2.0\,, \kappa = 0.4187$

The **SA** model is a low Reynolds number formulation mainly intended for turbo machinery applications in flows with mild separation, such as supersonic/transonic flows over airfoils and boundary-layer flows subjected to adverse pressure gradients.

Advantages of SA model

1. Computationally inexpensive and economical for large meshes.
2. Good results for mildly complex external or internal flows and boundary layer flows under adverse pressure gradient (e.g. turbine blades, airfoils, wings, airplane fuselage, missiles, ship hulls).
3. Less sensitive to numerical error when non layered are used near the wall.

Disadvantages of SA model

1. Not suitable for complex engineering flows.
2. Unable to capture rapidly changing length scale e.g. wall bounded to free shear flows.
3. Isotropic eddy viscosity assumed due to Boussinesq hypothesis.
4. Performs poorly in massively separated flows.
5. Not validated thoroughly.

2.5.2 Standard *k-ε* (SKE) Model

This popular turbulence model developed by Launder and Spalding [**24**] is the de-facto standard against which all the CFD simulations are compared. It is a two equation semi-empirical high Reynolds number model based on modeled transport equation for turbulent kinetic energy ***k*** and dissipation rate ***ε.***

These two transport equations are solved giving two independent scales for calculating $\boldsymbol{\mu_t}$**.**

The turbulent kinetic energy (*k)* transport equation:-

$$\frac{\partial(\rho k)}{\partial t}+\frac{\partial(\rho k u_i)}{\partial x_i}=\frac{\partial}{\partial x_i}\left[\left(\mu+\frac{\mu_t}{\sigma_k}\right)\frac{\partial k}{\partial x_j}\right]+G_k+G_b-\rho\epsilon-Y_M+S_k \tag{2.24}$$

The turbulent dissipation rate (*ε)* transport equation:-

$$\frac{\partial(\rho\epsilon)}{\partial t}+\frac{\partial(\rho\epsilon u_i)}{\partial x_i}=\frac{\partial}{\partial x_i}\left[\left(\mu+\frac{\mu_t}{\sigma_k}\right)\frac{\partial\epsilon}{\partial x_j}\right]+\frac{C_{1\epsilon}\epsilon}{k}(G_k+C_{3\epsilon}G_b)-\frac{C_{2\epsilon}\rho\epsilon^2}{k}+S_\epsilon \tag{2.25}$$

where G_k is the turbulent kinetic energy production term due to mean velocity gradient, G_b is kinetic energy production term due to buoyancy and Y_M is the dilation dissipation term due to compressibility, to prevent over prediction of spreading rate in compressible flows.

Turbulent viscosity ($\boldsymbol{\mu_t}$) is modeled as follows:

$$\mu_t=\frac{\rho C_\mu k^2}{\epsilon} \tag{2.26}$$

The constants in the standard *k-ε* model are:

$$C_{1\epsilon}=1.44\,,C_{2\epsilon}=1.92,C_\mu=0.09,\sigma_k=1.0,\sigma_\epsilon=1.3$$

Advantages of standard *k*-*ε* model:-

i. Robust and computationally economic.

ii. Reasonably accurate for a wide range of flow and heat transfer simulations.

iii. Widely validated.

Disadvantages of standard *k*-*ε* model:-

i. Isotropic eddy viscosity assumed due to Boussinesq hypothesis.

ii. Overly diffusive for many situations.

iii. The dissipation rate ε equation contains a term which cannot be calculated at the wall, thus wall functions should be used.

iv. Performs poorly in flows with strong separations, large streamline curvature, swirl rotation and low Reynolds number flows.

v. Cannot predict jet spreading rate.

2.5.3 Renormalized *k*-*ε* (RNG) Model

This is a two equation model that was developed by Yakhot and Orszag [**28**].It was derived using a mathematical technique called Renormalization Group (**RNG**) Theory. It uses a scale-elimination technique applied to Navier-Stokes equations.

The transport equation for turbulent kinetic energy ***k*** is similar to that of standard *k*-*ε* model. The major difference is in the transport equation for turbulent dissipation rate ***ε*** which includes an additional strain term.

It has a differential viscosity model to account for low Reynolds number effects and an analytically derived algebraic formula for turbulent Prandtl number .It also has modifications to account for swirl.

The turbulent kinetic energy (*k*) transport equation:-

$$\frac{\partial(\rho k)}{\partial t}+\frac{\partial(\rho k u_i)}{\partial x_i}=\frac{\partial}{\partial x_i}\left[\sigma_k \mu_{eff}\frac{\partial k}{\partial x_j}\right]+G_k+G_b-\rho\epsilon-Y_M+S_k \quad (2.27)$$

The turbulent dissipation rate (*ε*) transport equation:-

$$\frac{\partial(\rho \epsilon)}{\partial t}+\frac{\partial(\rho \epsilon u_i)}{\partial x_i}=\frac{\partial}{\partial x_i}\left[\alpha_\epsilon \mu_{eff}\frac{\partial \epsilon}{\partial x_j}\right]+\frac{C_{1\epsilon}\epsilon}{k}(G_k+C_{3\epsilon}G_b)-\frac{C_{2\epsilon}\rho\epsilon^2}{k}+S_\epsilon-R_\epsilon \quad (2.28)$$

where G_k is the turbulent kinetic energy production term due to mean velocity gradient, G_b is kinetic energy production term due to buoyancy and Y_M dilation dissipation term due to compressibility to prevent over prediction of spreading rate in compressible flows

Turbulent viscosity ($\boldsymbol{\mu_t}$) is modeled as follows:-

$$d\left(\frac{\rho^2 k}{\sqrt{\epsilon\mu}}\right)=\frac{1.72\hat{\nu}}{\sqrt{\hat{\nu}^3-1+C_\nu}}d\hat{\nu} \quad (2.29)$$

Where,

$$\hat{\nu}=\mu_{eff}/\mu \quad (2.30)$$

$C_\nu = 100$

For high Reynolds number

$$\mu=\frac{\rho C_\mu k}{\epsilon} \quad (2.31)$$

The constants in the Renormalized *k*-*ε* model are:

$C_{1\epsilon} = 1.42$, $C_{2\epsilon} = 1.68$

Advantages of Renormalized *k*-*ε* model:-

i. Performs better than standard ***k*-*ε*** model for wider range of complex shear flows.

ii. Performs better than standard ***k*-*ε*** model for flows with high strain rates and swirl.

iii. Suitable for locally transitional flows.

iv. Suitable for flows with vortex shedding behind bluff bodies, stall in wide-angle diffusers, room ventilation.

Disadvantages of Renormalized *k*-*ε* model:-

i. Isotropic eddy viscosity assumed due to Boussinesq hypothesis.

ii. Difficult to obtain convergence.

2.5.4 Realizable *k*-*ε* (RKE) Model

This two equation ***k*-*ε*** model was proposed by Shih et al [**29**]. It is called realizable ***k*-*ε*** since it satisfies certain mathematical conditions imposed on Reynolds stresses, which are consistent with the physics of a turbulent flow. These mathematical constraints on Reynolds stresses are listed below:-

i. Normal stresses should be positive $(\overline{u_\alpha' u_\alpha'}) > 0$

ii. Schwarz' inequality should hold true for Shear stresses $(\overline{u_\alpha' u_\beta'})^2 \leq (\overline{u_\alpha^2 u_\beta^2})$

Both the two equation ***k*-*ε*** model listed before i.e. **SKE** and **RNG** are not realizable

While the transport equation for turbulent kinetic energy is the same as standard ***k*-*ε*** model, the following modifications were made to the standard ***k*-*ε*** model to obtain the realizable ***k*-*ε*** model:-

i. It include a new formulation for eddy viscosity which depends upon a variable C_μ.

ii. The transport equation for turbulent dissipation rate ***ε*** is based on mean –square vorticity fluctuations.

The turbulent kinetic energy *k* transport equation:-

$$\frac{\partial(\rho k)}{\partial t}+\frac{\partial(\rho k u_i)}{\partial x_i}=\frac{\partial}{\partial x_i}\left[\left(\mu+\frac{\mu_t}{\sigma_k}\right)\frac{\partial k}{\partial x_j}\right]+G_k+G_b-\rho\epsilon-Y_M+S_k \quad (2.32)$$

The turbulent dissipation rate ε transport equation:-

$$\frac{\partial(\rho\epsilon)}{\partial t}+\frac{\partial(\rho\epsilon u_i)}{\partial x_i}=\frac{\partial}{\partial x_i}\left[\left(\mu+\frac{\mu_t}{\sigma_k}\right)\frac{\partial \epsilon}{\partial x_j}\right]+\rho C_1 S_\epsilon-\frac{\rho C_2 \epsilon^2}{k+\sqrt{\nu\epsilon}}+\frac{C_{1\epsilon}\epsilon}{k}C_{3\epsilon}G_b+S_\epsilon \quad (2.33)$$

Where,

$$C_1=max\left[0.43,\frac{\eta}{\eta+5}\right] \quad (2.34)$$

$$\eta=\frac{Sk}{\epsilon} \quad (2.35)$$

$$S=\sqrt{(2S_{ij}S_{ij})}$$

where G_k is the turbulent kinetic energy production term due to mean velocity gradient, G_b is kinetic energy production term due to buoyancy and Y_M dilation dissipation term due to compressibility to prevent over prediction of spreading rate in compressible flows. σ_k and σ_ε are turbulent prandtl number for k & ε.

Turbulent viscosity ($\boldsymbol{\mu_t}$) is modeled as follows:-

$$\mu_t=\frac{\rho C_\mu k^2}{\epsilon} \quad (2.36)$$

Where C_μ is variable and is defined as

$$C_\mu=\frac{1}{A_0+\frac{A_S kU}{\epsilon}} \quad (2.37)$$

The constants in the Realizable *k*-ε model are:-

$C_{1\epsilon}=1.44\,, C_{2\epsilon}=1.9, \sigma_k=1.0, \sigma_\epsilon=1.2$

Advantages of Realizable *k*-*ε* Model:-

i. Predicts the spreading rate of both planar and round jets accurately.

ii. Superior performance in flows with separation and strong pressure gradients.

iii. Good for flows with large strain rate, recirculation and rotation.

Disadvantages of Realizable *k*-*ε* Model:-

i. Produces non-physical turbulent viscosities, in situations when the computational domain contains both rotating and stationary fluid zones e.g. sliding meshes.

ii. Suffers from Isotropic eddy viscosity assumed due to Boussinesq hypothesis.

2.5.5 k-ω Shear Stress Transport (KW–SST) Turbulence Model

The **KW–SST** was developed by Menter [**25**]. It behaves as a standard *k*-*ω* model in the near wall and as a standard *k*-*ε* model in the free stream. The reason for development of this model was that Wilcox' standard *k*-ω model is overly sensitive to the free stream value of ω, while standard *k*-*ε* model is not prone to such a problem. Most two equation models, including *k*-ε models, over-predict turbulent stresses in the wake (velocity-defect) region, which leads to poor performance of the models for boundary layers under adverse pressure gradient and separated flows. In this model, the turbulent viscosity is modified to account for the transport of the turbulent shear stress and a blending function is used to ensure that the model equations behave appropriately in both the near-wall and far-field zones.

The turbulent kinetic energy (*k*) transport equation:-

$$\frac{\partial(\rho k)}{\partial t}+\frac{\partial(\rho k u_i)}{\partial x_i}=\frac{\partial}{\partial x_j}\left[\Gamma_k \frac{\partial k}{\partial x_j}\right]+\bar{G}_k-Y_k+S_k \qquad (2.38)$$

The transport equation of specific dissipation rate (ω):

$$\frac{\partial(\rho\omega)}{\partial t}+\frac{\partial(\rho\omega u_i)}{\partial x_i}=\frac{\partial}{\partial x_i}\left[\Gamma_\omega\frac{\partial\omega}{\partial x_j}\right]+G_\omega-Y_\omega+S_\omega \quad (2.39)$$

where $\bar{G}_k$ represents the generation turbulence kinetic energy and G_ω is the source term for specific dissipation ω.

Effective diffusivity **(Γ)** is modeled as follows:-

$$\Gamma_k=\left(\mu+\frac{\mu_t}{\sigma_k}\right) \quad (2.40)$$

$$\Gamma_\omega=\left(\mu+\frac{\mu_t}{\sigma_\omega}\right) \quad (2.41)$$

Here, the turbulent viscosity **(μ_t)** is given as follows:-

$$\mu_t=\rho\frac{k}{\omega}\frac{1}{max\left[\frac{1}{\alpha},\frac{SF_2}{a_1\omega}\right]} \quad (2.42)$$

where, S is the strain rate magnitude.

Blending functions F_1 & F_2 are given by the following equations.

$$F_1=tan\,h(\phi_1^4) \quad (2.43)$$

$$\phi_1=min\left[\max\left(\frac{\sqrt{k}}{0.09\omega y},\frac{500\mu}{\rho y^2\omega}\right),4\rho k/(\sigma_{\omega,2}D_\omega^+y^2\right] \quad (2.44)$$

$$D_\omega^+=max\left[\frac{2\rho1}{\sigma_{\omega,2}}\frac{1}{\omega}\frac{\partial k}{\partial x_j}\frac{\partial\omega}{\partial x_j},10^{-10}\right] \quad (2.45)$$

$$F_2 = tan\,h(\phi_2^4) \tag{2.46}$$

$$\phi_2 = max\left[2\,\frac{\sqrt{k}}{0.09\omega y}, \frac{500\mu}{\rho y^2 \omega}\right] \tag{2.47}$$

Here, D_ω^+ is the positive part of the cross diffusion term given by equation (2.48)

$$D_\omega = \frac{2(1-F_1)\rho\sigma_{\omega,2}}{\omega}\,\frac{\partial k}{\partial x_j}\frac{\partial \omega}{\partial x_j} \tag{2.48}$$

This term is used to blend the standard *k-ω* and standard *k-ε* functionalities together.

Advantages of *k-ω* shear stress transport model:-

i. Reliable and accurate for a wider range of flows with adverse pressure gradients, transonic shock waves.

ii. Performs better than ***k-ε*** models for boundary layer flows.

Disadvantages of *k-ω* shear stress transport model:-

i. Dependency on wall distance makes this less suitable for free shear flows.

ii. Separation is typically predicted to be excessive and early.

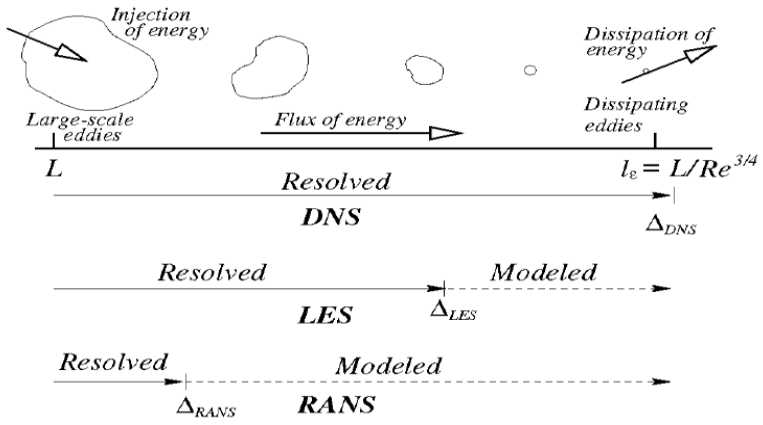

Figure 2-2 Energy cascade and length scales captured by different turbulence models.

Chapter 3

FLUENT CODE VALIDATION: BENCHMARK TESTS

Any CFD simulation cannot be called successful and its results reliable, until appropriate validation has been performed to check whether the numerical simulation agrees with the physical reality of the problem. In most cases, the validation is performed by comparison to experimental results. Therefore, before attempting to do complex CFD simulations on film cooling flows benchmark tests on a flat plate tests were performed to compare accuracy of the CFD research tool against known correlations and experimental results.

The current research work uses ANSYS FLUENT which is a general purpose commercially available code based on finite volume method.

Part of verification process in a CFD study is done through sensitivity analysis, performed on the meshing scheme. This is done in order to be assured that the solution is grid independent. The current study employs grids of 3 different sizes to check grid independence.

3.1 Computational Domain and Boundary Conditions

Figure 3-1 shows the final computational grid and boundary conditions employed for preliminary study of flow on a flat plate. Three different mesh sizes were used to perform grid sensitivity

Mesh no.	*Grid points - X direction*	*Grid points - Y direction*	*First cell height(m)*	*Growth Ratio*	*Number or rows*
1	200	120	1E-03	1.1	80
2	220	150	1E-04	1.1	100
3	250	300	1E-05	1.06	200

Table 3-1 Grid sizes used for sensitivity analysis

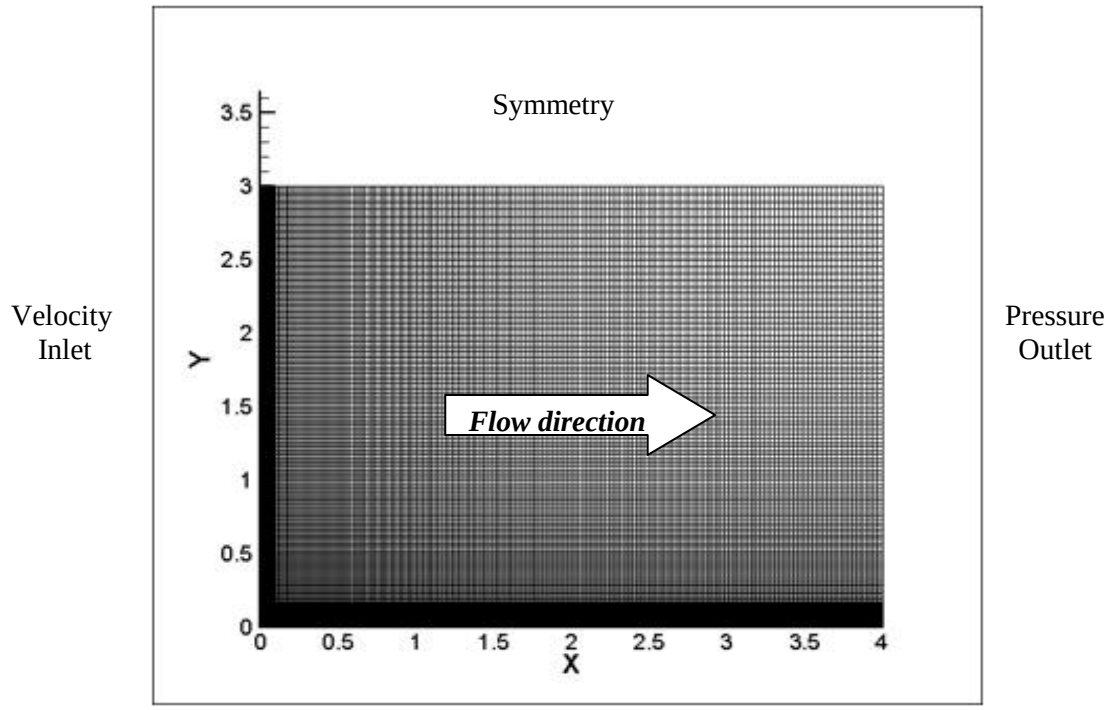

Figure 3-1 Computational grid and zones for benchmark tests on flat plate flow study (shown in table 3-1) before choosing the appropriate grid for benchmark tests on flat plate.

The boundary conditions employed for inlet of the flat plate were a mainstream velocity of 20 m/s and constant temperature of 303 K. A low free stream turbulence intensity of 0.01% was also provided at the inlet. The flat plate was kept under isothermal condition of 295K.

3.2 Grid Sensitivity Analysis

Wall $\mathbf{y}^+$ value for all the grids was kept below 5, thereby ensuring that the first cell lies in the laminar sublayer. Any computational grid should be suitably refined such that the first cell doesn't fall in the buffer region or $5 < \mathbf{y}^+ < 30$. If the mesh is relatively coarse in the near wall then log wall function options can be explored.

It is evident from figure 3-2, which shows the non dimensional turbulent velocity profiles and Stanton number distribution over the flat plate for various grid sizes, that Grid 1 used in conjunction with enhanced wall treatment options is sufficient enough to carry out computation over flat plate. Further increase in grid size is an unnecessary computational expense.

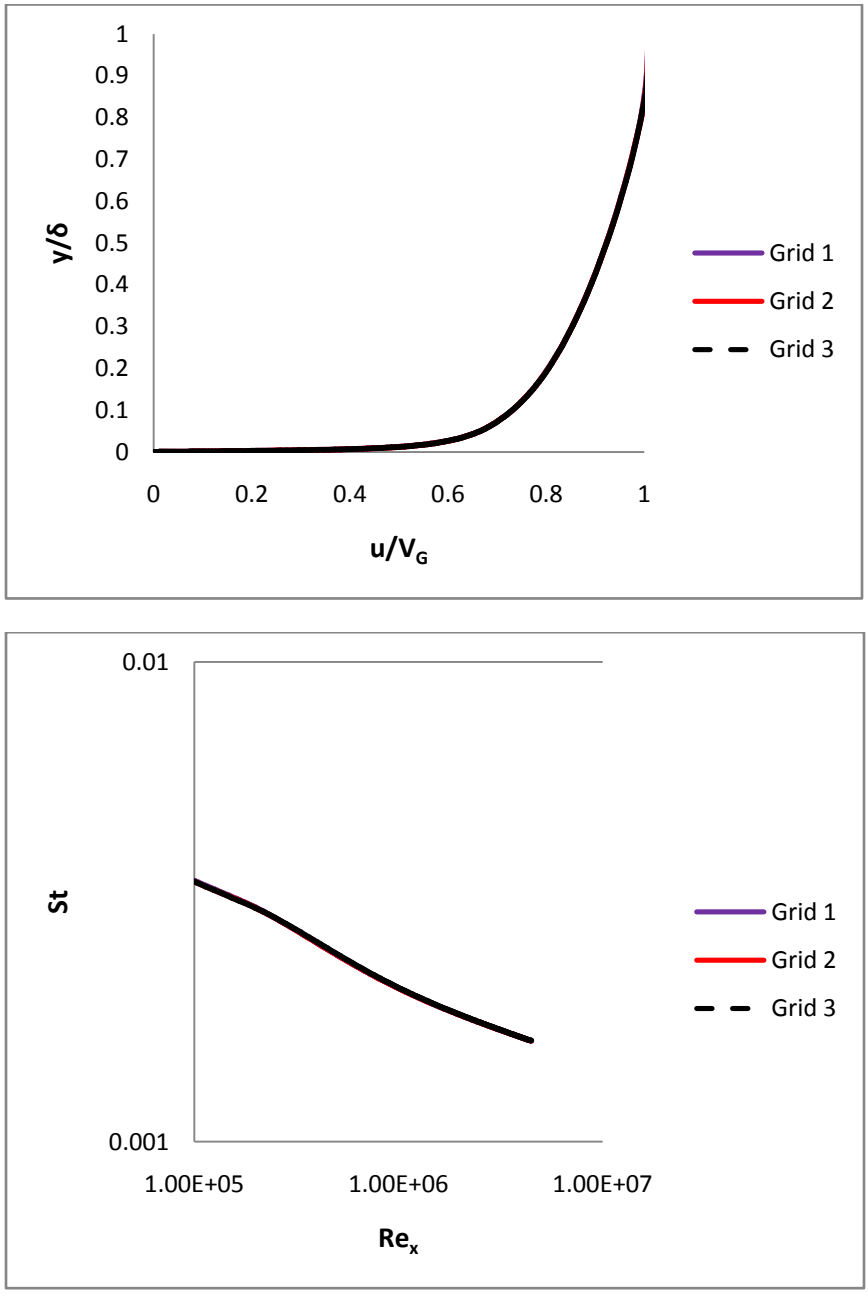

Figure 3-2 Grid sensitivity analysis using meshes of different sizes.

3.3 Results for Benchmark Tests on Flat Plate

3.3.1 Flow Validation

Figure 3-3 shows turbulent velocity profiles, plotted at x=0.25m, for each of the turbulence models employed in the present study which are compared against known experimental correlation provided by Kays and Crawford [**30**] given by equation (3.1).

$$\frac{u}{V_G} = \left(\frac{y}{\delta}\right)^{1/7} \tag{3.1}$$

where V_G is the free stream velocity of 20m/s and δ is the hydrodynamic boundary layer thickness. A low free stream turbulence intensity of 0.01% was also provided at the inlet boundary.

All turbulence models were in close agreement with the $1/7^{th}$ velocity correlation suggested by Kay and Crawford [**30**] that is to say that they were well within experimental uncertainty. Even the relatively simple one equation model like **SA** was able to perform boundary layer calculations with great accuracy. The worst prediction however was made by **KW-SST** model which was around 6% off from the experimental correlation indicating some error in prediction of hydrodynamic boundary layer growth.

Figure 3-4 shows non dimensionalized turbulent kinetic energy (TKE) profiles, plotted at x=0.25m, for each of the turbulence models employed in the present study which are compared against known experimental data for low free stream turbulence by Chien [**31**].
Here again the *k-ε* family of turbulence model predict a TKE levels near the wall with great accuracy of around 7% maximum deviation from low free stream intensity data of Chien [**31**], However, **KW-SST** model predicted high local deviation of around 20 % from the same.

Figure 3-5 shows skin friction coefficient vs momentum thickness based Reynolds number along the length of the flat plate, for each of the turbulence models employed in the present study. Results are compared against known experimental correlation provided by Kays and Crawford [**30**] given by

$$C_f = 0.025 * Re_\theta^{-0.25} \tag{3.2}$$

In addition to the above correlation, experimental data from Weighardt and Tillman [**32**] is also employed to verify the skin friction coefficient. Both one equation and two equation models predicted results well within 2% of the known correlation and experimental data suggesting accurate prediction of normal velocity gradient at wall in the boundary layer and shear stresses.

3.3.2 Heat Transfer Validation

Stanton number vs length based Reynolds number is an excellent method to validate heat transfer for fully turbulent region. For turbulent flow on flat plate with unheated starting length the correlation is given by correlation provided by Kays and Crawford [**30**]

$$St * Pr^{0.4} = 0.03 * Re_x^{-0.2} \tag{3.3}$$

Figure 3-6 reveal that CFD predictions of Stanton number along the length of the flat plate by various turbulence models reveal close agreement with the above correlation i.e. within 2% of the correlation data indicating all models are apt for heat transfer modeling including turbulent flows in situations with favorable pressure gradients.

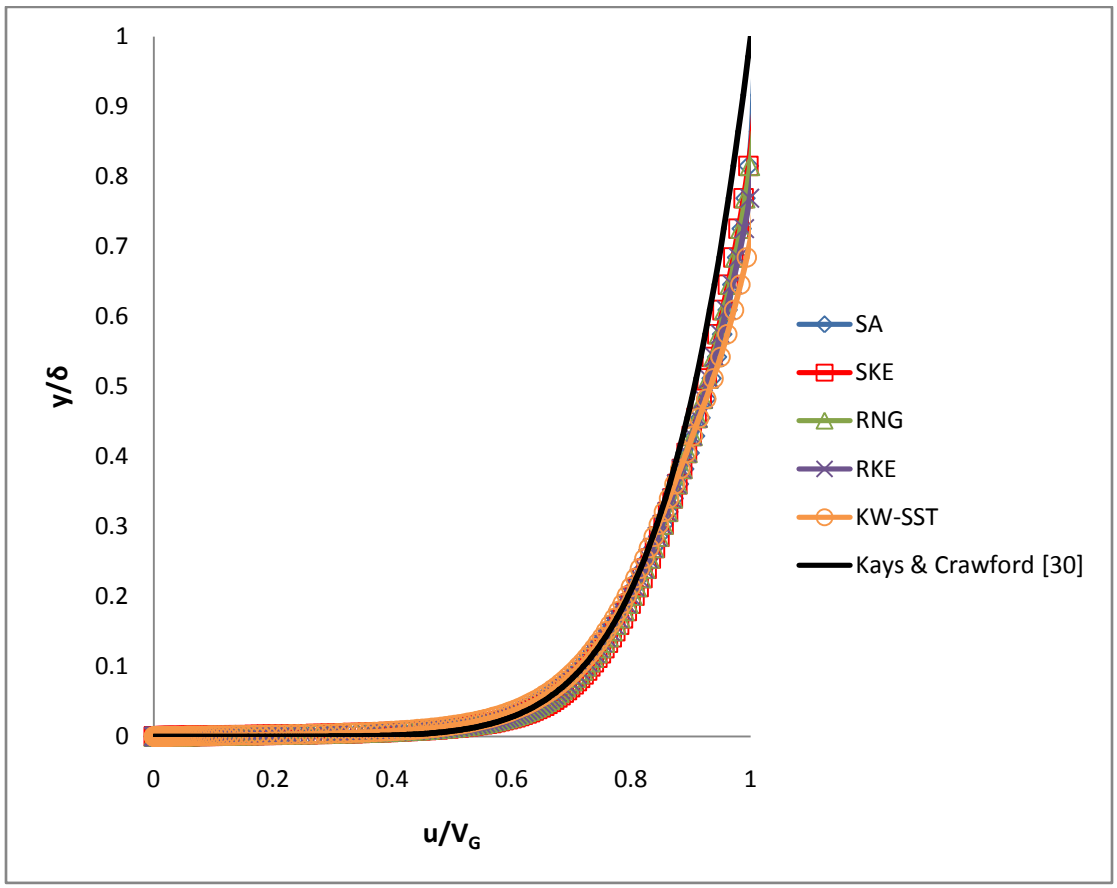

Figure 3-3 Turbulent velocity profile at x=2m. Comparison of various turbulence

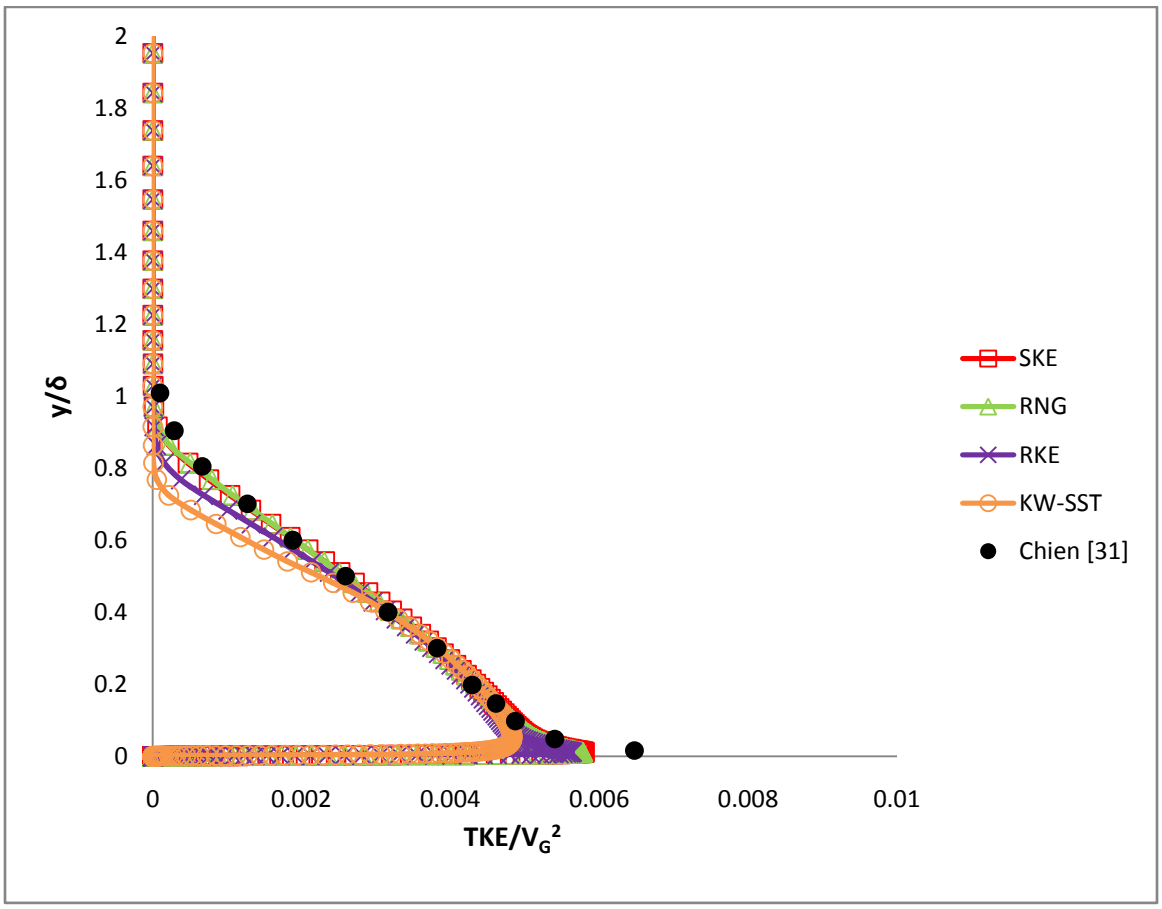

Figure 3-4 Turbulent kinetic energy profile at x=2m. Comparison of various turbulence models.

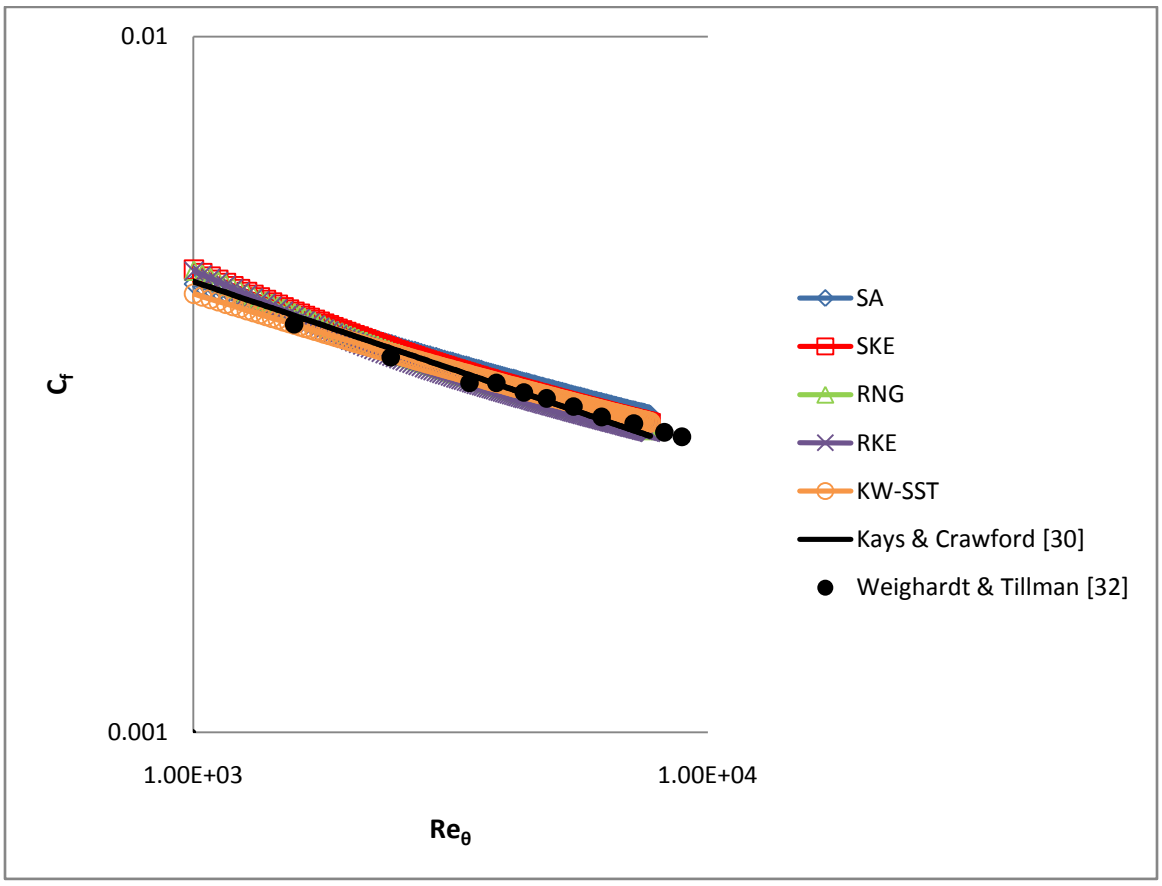

Figure 3-5 Variation of skin friction coefficient along the length of the plate. Comparison of various turbulence models.

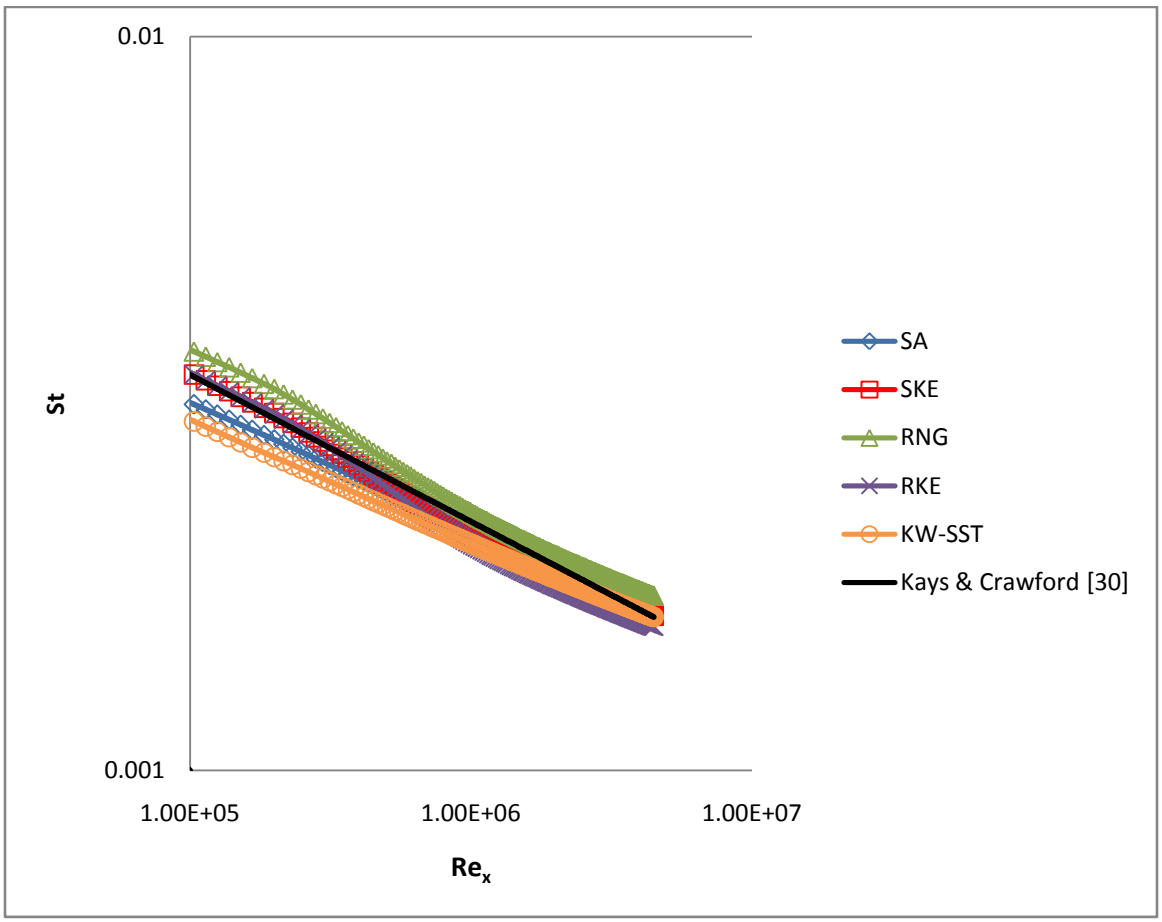

Figure 3-6 Variation of Stanton number with local Reynolds number along the length of the plate. Comparison of various turbulence models

Chapter 4

FILM COOLING THEORY & RELATIONS

"Film cooling is the introduction of a secondary fluid (coolant or injected fluid) at one or more discrete locations along the surface exposed to a high temperature environment to protect that surface not only in the immediate region but also in the downstream region"- Goldstein [**3**]. Film cooling provides the necessary thermal protection by reducing the net heat load to the blade surface. Since local temperatures on these blade surfaces are very important from design point of view, we therefore investigate the fundamentals and important relations for a film cooled surface.

4.1 Film Cooling Relations

As shown in figure 4-1 for a film cooled surface the heat flux $q_W^{"}$ from hot main stream gas to wall surface can be written as follows:-

$$q_W^{"} = h(\theta)(T_G - T_W) \tag{4.1}$$

Where, θ is the dimensionless temperature and can be defined as follows:-

$$\theta = (T_G - T_C)/(T_G - T_W) \tag{4.2}$$

The same heat flux entering the surface for film cooling flow can also be written as follows:-

$$q_W^{"} = h_f(T_f - T_W) \tag{4.3}$$

For adiabatic condition at wall surface, $T_f = T_{AW}$. Therefore, equation (4.3) can be rewritten as follows:-

$$q_W^{"} = h_f(T_{AW} - T_W) \tag{4.4}$$

The method used to arrive at external heat transfer coefficients $h(\theta)$, at any arbitrary temperature, is similar to that of Eckert [**33**].

The equation (4.5) for $h(\theta)$ is obtained by superimposition of temperature fields at two different temperatures one in which the coolant temperature is equal to mainstream temperature or $T_C = T_G$, i.e. $\theta = 0$ and another in which coolant temperature is equal to the wall temperature $T_C = T_W$, i.e. $\theta = 1$.

$$h(\theta) = h(0) + \theta(h(1) - h(0)) \tag{4.5}$$

The first point $\theta = 0$ of the line represented by equation (4.5) designates an isothermal situation in which film cooling temperature has no effect on external heat transfer coefficient $h(\theta)$ i.e.

$$h(\theta = 0) = h_f \tag{4.6}$$

The second point $\theta = 1$ of the line represented by equation (4.5) designates adiabatic situation or no heat flux to the wall i.e. $q_W^{"} = 0$. Rewriting equation (4.5) using equation (4.6) we get equation (4.7).

$$\frac{h(\theta)}{h_f} = (1 + K\theta) \tag{4.7}$$

Where, $K = \big(h(1) - h_f\big)/h_f$

Now, equation (4.1) can be rewritten as follows:-

$$q_W^{"} = h_f(1 + K\theta)\,(T_G - T_W) \tag{4.8}$$

Using the definition of θ , we get equation (4.9).

$$q''_W = h_f[T_W - T_G - K(T_C - T_G)] \tag{4.9}$$

Comparing equation (4.9) with equation (4.4) we get equation (4.10).

$$T_{AW} = T_G - K(T_C - T_G) \tag{4.10}$$

Now, comparing equation (4.10) with the definition of adiabatic film effectiveness η

$$\eta = (T_{AW} - T_G)/(T_C - T_G) \tag{4.11}$$

We can now determine K which is given by equation (4.12).

$$K = -\eta \tag{4.12}$$

Substituting the value of K in equation (4.7) we get external heat transfer coefficient $h(\theta)$ for film cooled surface at any arbitrary temperature.

$$\boldsymbol{h(\theta) = h_f\,(1 - \eta\theta)} \tag{4.13}$$

4.2 Commonly Performed Experiments to Determine Heat Transfer Coefficients for Film Cooled Surfaces

Two most commonly employed experimental techniques based on Eckert **[33]** calculation methods for film cooling are mentioned here. Heat transfer coefficient h can be obtained by using either **constant heat flux or constant temperature** as boundary condition on the surface where data is collected.

4.2.1 Experiments Performed using Constant Wall Heat Flux

a. The coolant is injected at T_C with heat flux q''_W as zero on the wall surface. "Adiabatic wall temperature" for this situation is obtained which denoted as T_{AW}. Film effectiveness can thus be calculated using the equation (4.12).

b. A finite amount of heat flux, q_w, is applied onto the wall surface with coolant temperature T_C equal to mainstream temperature T_G **i.e.** $\theta = 0$ **.**In this situation, the line represented by equation (4.5) for $h(\theta)$ gives $h(\theta) = h_f$.

4.2.2 Experiments Performed using Constant Wall Temperature

Heat transfer coefficients are obtained by keeping the wall temperature constant and two sets of experiments are performed for use in linear superposition approach.

a. Coolant is injected at a temperature equal to mainstream temperature,$T_C = T_G$ or $\theta = 0$.
b. Coolant is injected at a temperature equal to wall temperature, $T_C = T_W$ or $\theta = 1$
c. Heat transfer coefficient are obtained at the above temperatures i.e.at $\theta = 0$ and $\theta = 1$ and local heat transfer coefficients for any temperature can be calculated by using equation (4.5).

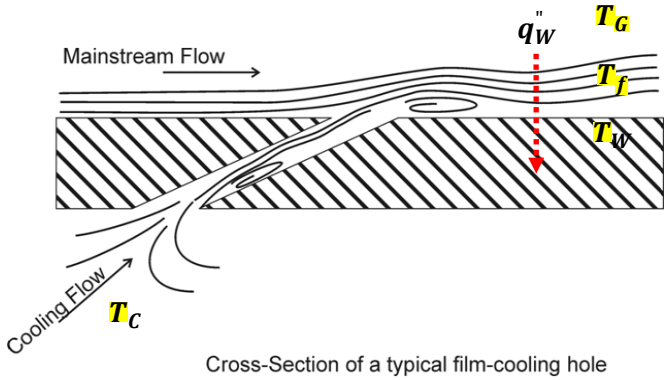

Figure 4-1 A typical film cooling configuration

Chapter 5

BLADE TEMPERATURE CALCULATION TECHNIQUES

The aero-thermal design of a film cooled blade is often an extremely difficult task for designers. It is almost impossible to accurately predict the heat transfer on the external and interior surfaces of the turbine blade. Techniques commonly employed during the design process often fail to accurately predict blade metal temperatures. For modern blade configuration even a small deviation (≈ 50˚F) in predicting the wall temperatures correctly can lead to "hot-spots" (shown in figure 5-1) caused by thermal stresses, which might ultimately lead to failure.

Therefore a new technique which is capable of predicting accurate temperature distribution in a film cooled blade is needed. The following are two most commonly employed techniques for determining heat transfer and wall temperature distribution on the blade.

5.1 Conventional Technique in Blade Design

The conventional technique is a design process which adopts a relatively simpler strategy. In order to predict temperature field of the turbine blade, the designer should know heat transfer coefficients on the internal and external surfaces of the blade which is usually obtained from numerical predictions, empirical correlations and designer's experience.

It is a three step approach in solving the temperature field inside the blade:-

i. First, external convection calculation is performed to determine film heat transfer coefficients $\boldsymbol{h_f}$ using either constant wall temperature or constant heat flux boundary condition discussed in previous section. That means that the effect of metal conduction on the flow field is isolated in this step.

ii. In the next step, these heat transfer coefficients are modified using empirical correlations to get heat transfer coefficient $\boldsymbol{h(\theta)}$ which include the effect of film cooling. These heat transfer coefficient are then used as boundary condition for conduction calculation in the blade metal.

iii. Heat conduction calculation in the blade metal gives the temperature field inside and on the surface of the blade.

Based upon these temperatures a suitable cooling configuration can then be designed so as to minimize the thermal stresses on the blade. A schematic of the conventional technique in blade design is shown in figure 5-2. Calculating the blade temperature using such experimental data, for film heat transfer coefficient $\boldsymbol{h_f}$ and film effectiveness $\boldsymbol{\eta}$ results in inaccuracies, since in real applications neither the wall heat flux nor the surface temperature distribution remain constant. The blade temperature distribution is highly dependent on local heat transfer coefficient and fluid flow interaction at internal and external surfaces, Bohn et al. **[22].** Thus, it is important to take into account also the effects of internal convection and blade metal conduction. When conjugate heat transfer is considered wall temperature and heat flux distribution becomes variable. The temperature gradient at the surface changes thus the convective heat transfer coefficients change leading to different surface and blade temperature distributions.

5.2 Full Conjugate Heat Transfer (CHT) Technique

Full CHT analysis, in which the both the external flow and metal conduction are coupled together, provides more realistic results. Also it is easier to specify boundary conditions in case of CHT analysis as conditions at interface need not be known. It is evident from the work of researchers Kane & Yavuzkurt **[34]** who performed numerical simulation on a non film cooled blade reported 30% deviation from data of Hylton et al. **[35]** in using conventional constant wall

temperature approach, whereas full conjugate results were much closer to the data with an overall deviation about a few percent. However, a full conjugate simulation involves solving large set of linear algebraic equations, which is both computationally expensive and time consuming. In case of full coverage film cooling this problem becomes even worse as it requires massive computational resources. Moreover, the steady turbulence models employed in CHT simulation suffers from their inherent inadequacies discussed earlier. Thus a completely reliable prediction of heat transfer coefficients, in the near field of the jets, cannot be obtained using a full CHT simulation. A schematic of the CHT technique in blade design is shown in figure 5-3.

5.3 Iterative Conjugate Heat Transfer Technique (ICHT)

The ICHT technique is a practical compromise between full conjugate simulations and conventional techniques, to determine surface temperature distribution, with which one can limit the inaccuracies of full CHT by providing experimental input to correctly predict the temperature field.

In this methodology, convection and conduction domains are loosely coupled, such that external convective heat transfer coefficient provides the boundary condition for conduction in blade metal. The subsequent surface temperature distribution arising from conduction domain solution is used as updated boundary condition for external convection calculation. This process is iterated until continuity of temperature is obtained at the fluid-solid Interface i.e. $T_{fluid} = T_{solid}$ at interface cells in fluid and solid domain respectively. While temperature continuity is reached at the interface, heat flux matching is always enforced at each step of the iteration as shown in equation (5.1) where T_{solid} is the temperature of the solid zone cell and T_G is the temperature of mainstream gas.

$$-\lambda_s \left(\frac{dT}{dy}\right)_{solid} = h(\theta)(T_{solid} - T_G) = q" \quad (5.1)$$

Flow over a film cooled blade is not solved directly and instead convective heat transfer coefficients calculated on a similar blade without film, under the same flow conditions, are corrected by use of experimental data to incorporate the effect of film cooling on the heat transfer coefficients. The effect of conjugate heat transfer is taken into account by using this iterative technique. Figure 5-4 shows the schematic of the ICHT process. As mentioned earlier, the calculations are iterated until convergence is obtained as indicated by the continuity of temperature and heat flux at the fluid-metal interface. Initial temperature guess is so provided such that it is physically feasible one. For example, if one has little idea about the temperature at the interface would start his simulation by assuming a temperature between T_G and T_C**.** Moreover, no matter what physically realistic initial guess is provided, always the same solution is obtained upon convergence.

It is important to note that the main distinction between the iterative conjugate heat transfer technique (ICHT) and the conventional technique in blade design is that in ICHT updated blade surface temperature boundary condition resulting from blade metal conduction is included in the external convection calculation for next iteration level to calculate heat transfer coefficients while in conventional technique constant wall temperature is used for calculation of local heat transfer coefficient at any arbitrary temperature $h(\theta)$ *which is then directly used for calculation of blade temperature field.*

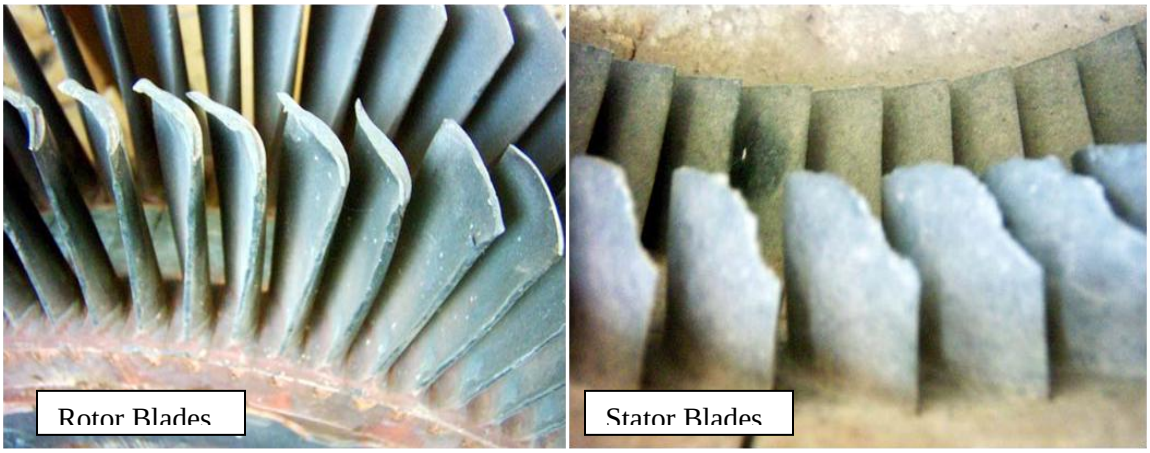

Figure 5-1 Failure & Deformations in Stator & Rotor Blades of a turbine Naeem et al [**36**].

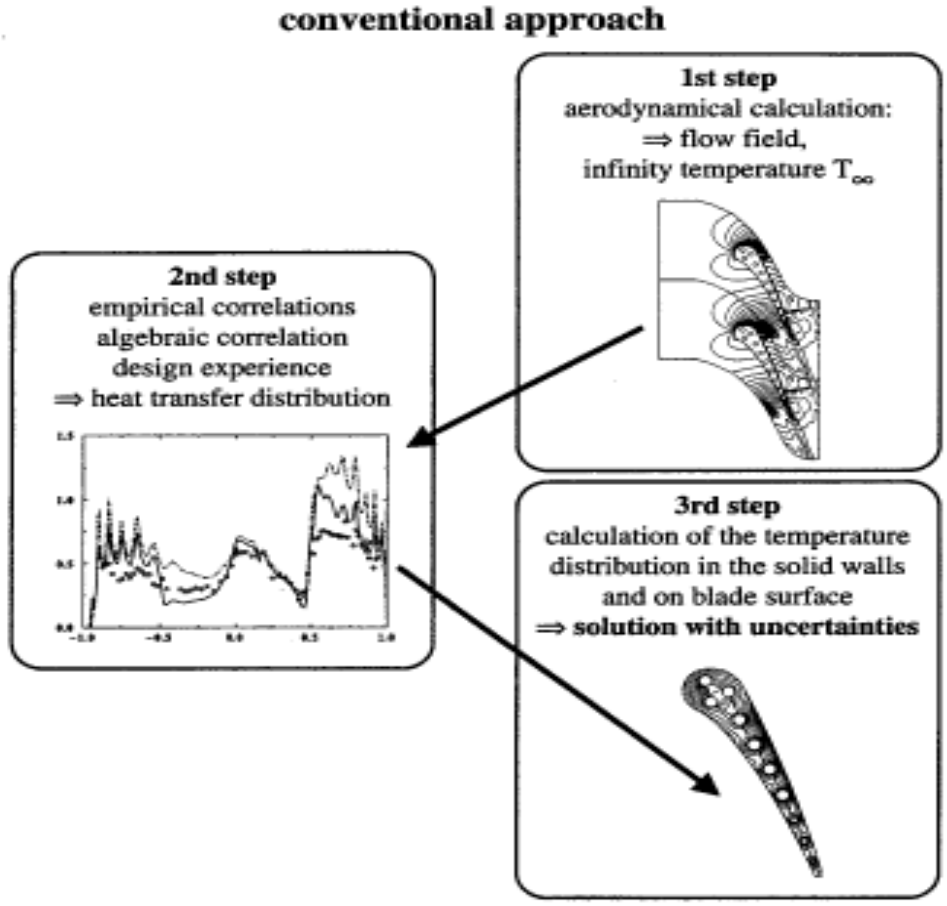

Figure 5-2 Conventional Technique in Blade Design process for cooled blades from Sunder and Faghri [**2**].

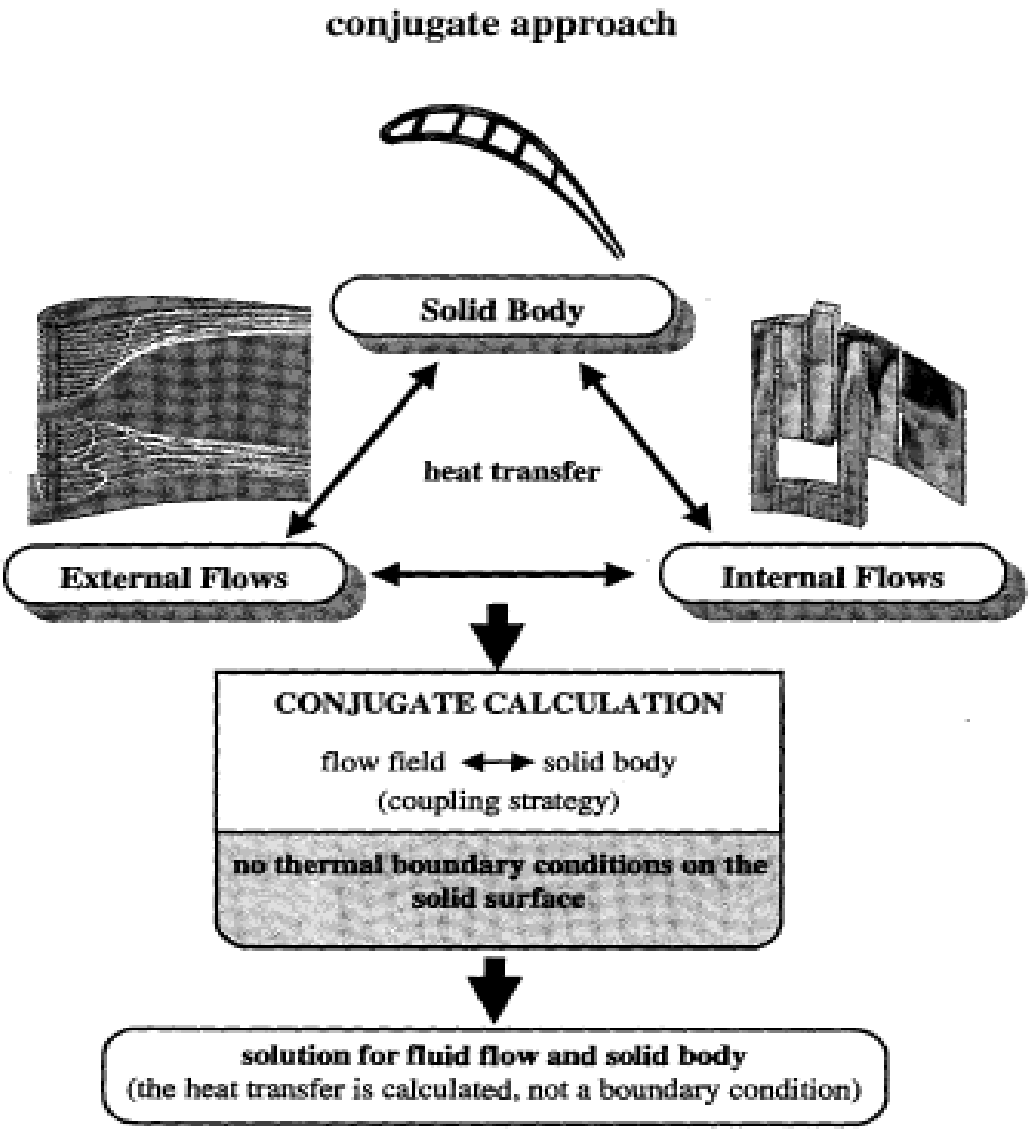

Figure 5-3 Full Conjugate or Coupled technique in Blade Design process for cooled blades from Sunder and Faghri [**2**].

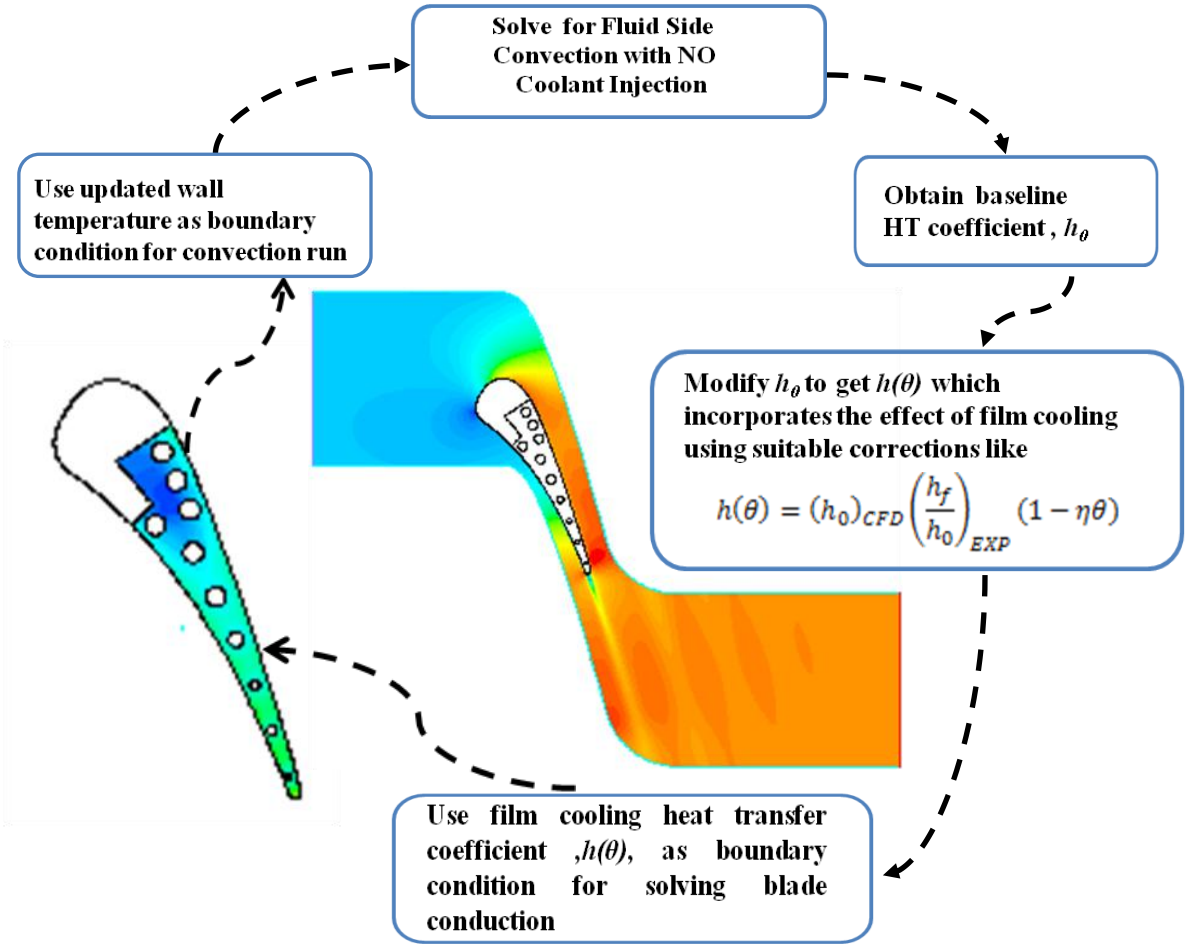

Figure 5-4 Schematic of the Iterative Conjugate Heat Transfer technique (ICHT).

5.4 Implementation of Iterative Conjugate Heat transfer technique (ICHT)

The ICHT process was automated using a scheme code in conjunction with a MATLAB script. Scheme is a list programming type of language which is the scripting language employed by ANSYS FLUENT12. The ICHT code was run on the commercial CFD solver ANSYS FLUENT 12. Two separate meshes are used to carry out the technique. One mesh is used as a computational domain for external forced convection calculations and another as computational domain for blade metal conduction.

Figure 5-5 shows the complete flowchart of the ICHT technique:

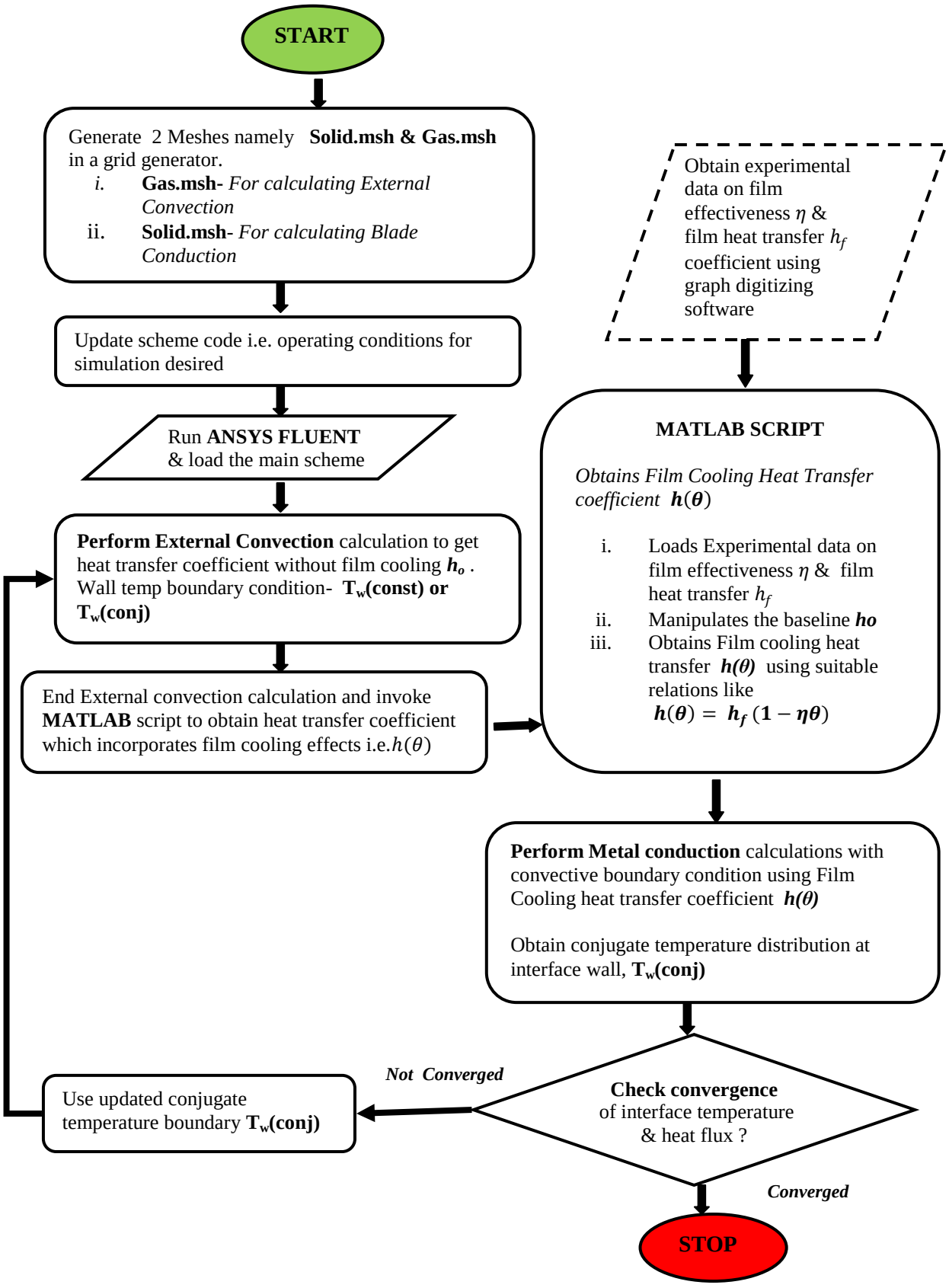

Figure 5-5 Process flowchart for Iterative Conjugate Heat transfer technique

Chapter 6

ICHT CODE VALIDATION

Code validation is defined by (AIAA G-077-1998) as "The process of determining the degree to which a model is an accurate representation of the real world from the perspective of the intended uses of the model". It means it is imperative to check whether the numerical simulation is consistent with physical reality and this check can be highlighted by comparison of numerical predictions to experimental results

In order to validate The ICHT approach numerical solution obtained by ICHT scheme code was compared to analytical solution obtained by Luikov **[37].** Laminar flow over a flat plate under conjugate conditions was considered. Montomoli **[38]** also performed a similar validation technique for his CFD code.

6.1 Numerical Domain and Boundary Conditions

Here, a plate of 100mm thickness and 500mm length was used. A thermal conductivity of the plate material λ_s is 4W/mK. A constant temperature $T_b = 600K$ was imposed on the bottom side of the plate and the sides were maintained at adiabatic conditions. Mach number of $Ma = 0.13$ and a total temperature of $T_0 = 1400K$ was kept at the inlet.

It is necessary to check when conjugate heat transfer should be considered in coupled cases. Luikov **[37]** proposed conjugacy criteria according to which if the $Br > 0.1$ the flow should be solved as a conjugate one. For the validation case $Br = 1.91$, thus thermal resistant offered by the plate is quite high and should be considered.

6.2 Results from Code Validation

The ICHT code was used to simulate the laminar flow under the above conditions. Static temperature at the wall was non dimensionalized using total inlet temperature and was compared against analytical solution of Luikov [**37**]. The result for this simulation is in good agreement with the analytical solution, within 1%, as shown in figure 6-1, depicting thermal boundary layer at x=80mm.

However, small difference between the ICHT and analytical solution of Luikov [**37**] can be attributed to the approximations and constant air property assumption in the arriving at the analytical solution while the simulations were carried out at variable air property in order to be more physically realistic.

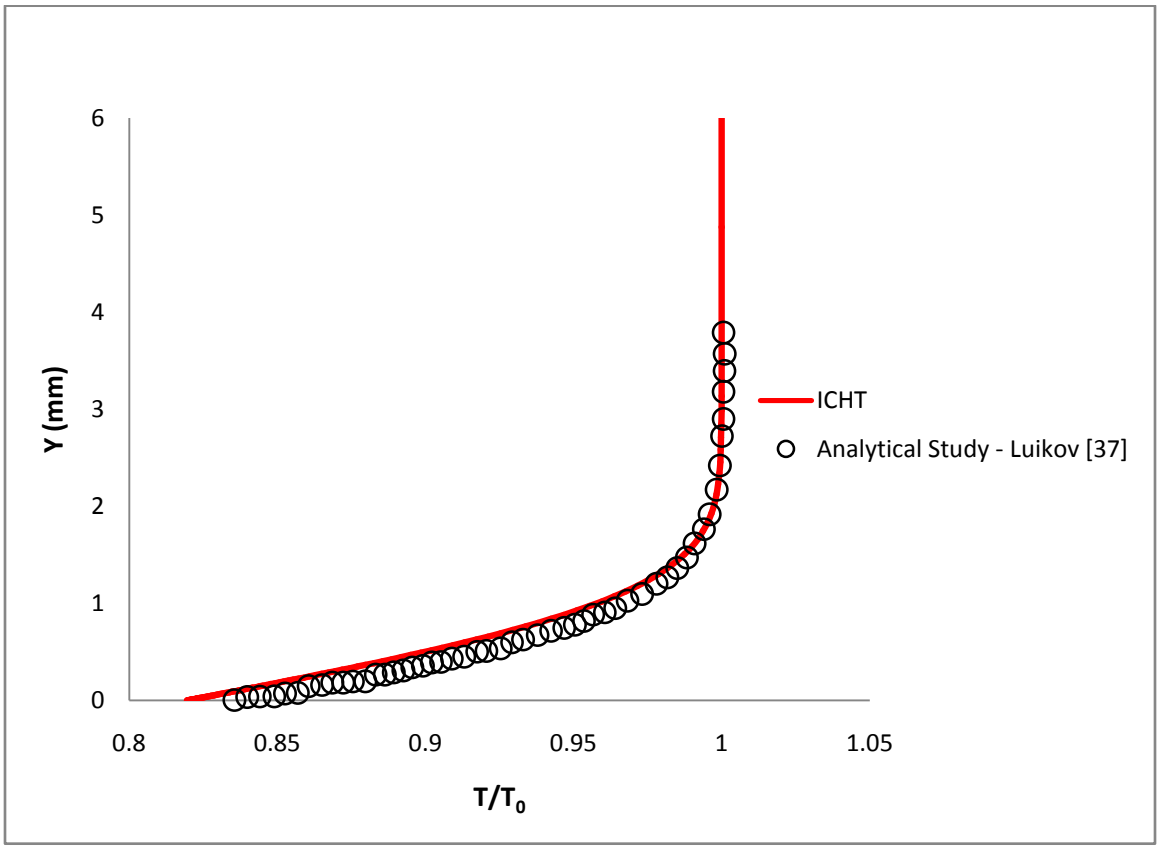

Figure 6-1 Dimensionless temperature distribution normal to the wall in a flat plate boundary layer under conjugate heat transfer

Chapter 7

TEST SIMULATIONS PERFORMED USING ICHT

The effect of conjugate heat transfer was first analyzed on a flat surface, employing **no** film cooling correction to heat transfer coefficients. The experiments simulated were so chosen such that they represent the two techniques employed in obtaining their respective heat transfer data as illustrated in chapter 5 i.e. constant wall temperature and constant heat flux techniques. Film cooling simulations were then performed for two different cases, at high and low temperature difference between the mainstream and secondary flow. The idea being that variable air property effects are directly proportional to the temperature difference between the mainstream and the secondary flow. Moreover, effects arising from conjugate heat transfer are expected to enhance at elevated temperature differences.

For all grids on which flat plate film cooling calculations were performed the wall $\mathbf{y}^+$ value was kept lower than 4, i.e. the 1st cell height was sufficiently resolved up to the viscous sub layer. Enhanced wall treatment option was used over standard wall functions since the mesh was sufficiently refined in near wall / boundary layer region. CFD simulations were performed to closely match flow and thermal boundary conditions of the actual film cooling experiment so that heat transfer coefficients could directly be used to compare against the data available from the literature. All flows were solved as conjugate ones based on fact that the calculated Brun number was greater than 0.1 as suggested by Luikov [**37**]. All the results presented are laterally averaged quantities.

7.1 Flat Plate Simulation with No Film Cooling

7.1.1 Numerical Setup and Boundary Conditions

A flat plate of finite thickness with forced convection of hot gas over it was chosen. Flat plate geometry was modeled keeping the dimensions and boundary conditions as close as possible to experimental conditions of a Mark-II blade in Hylton et al **[16].** The objective of such a simulation is to analyze the effect of conjugate heat transfer alone without modeling any film cooling effect. The Brun number for this situation was calculated to be 0.13 indicating the need of conjugate heat transfer analysis. Figure 7-1 shows the schematic of the simple flat plate geometry simulated with $1/7^{th}$ power turbulent velocity profile and a free-stream velocity of 106 m/s imposed at the hot gas inlet. Variable property effect was taken into account since the temperature changes inside the boundary layer, this effect is even more predominant in elevated temperature differences. Given below are the boundary conditions for flat plate simulation without film cooling using ICHT

BOUNDARY CONDITIONS	
Inlet conditions	
Mainstream gas velocity, $\mathbf{V_G}$	106m/s
Mainstream temperature, $\mathbf{T_G}$	788K
Free stream turbulence, **Tu %**	6.5 %
Conditions at plate bottom (representing internal convection)	
Average heat transfer coefficient	1943.67 W/m^2K
Mean Temperature	336.36 K
Material Properties	
Material of Plate	ASTM 310, Stainless Steel
Conductivity of ASTM 310 **(k)**	16.0 W/mK

Table 7-1 Boundary Conditions for ICHT simulation of flat plate with no film cooling

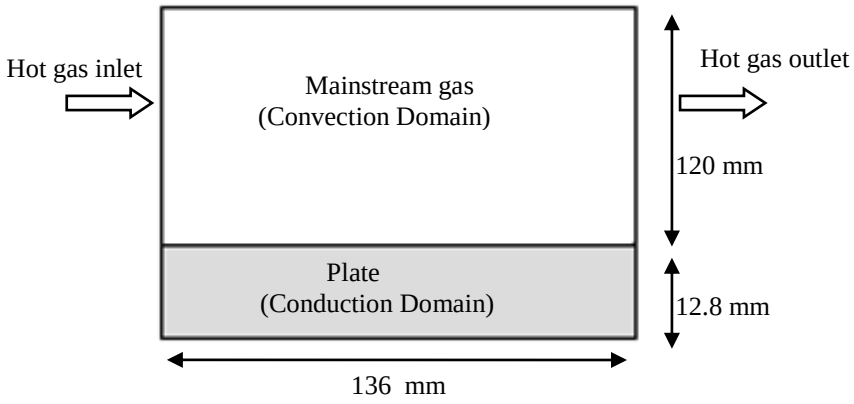

Figure 7-1 Flat Plate geometry with no film cooling chosen for ICHT simulation.

Computational grid used to simulate iterative conjugate heat transfer (**ICHT**) is similar to the one on which benchmark tests were performed. The technique requires convection and conduction to be solved on separate grids namely Gas.msh & Solid.msh as shown in figure 7-2

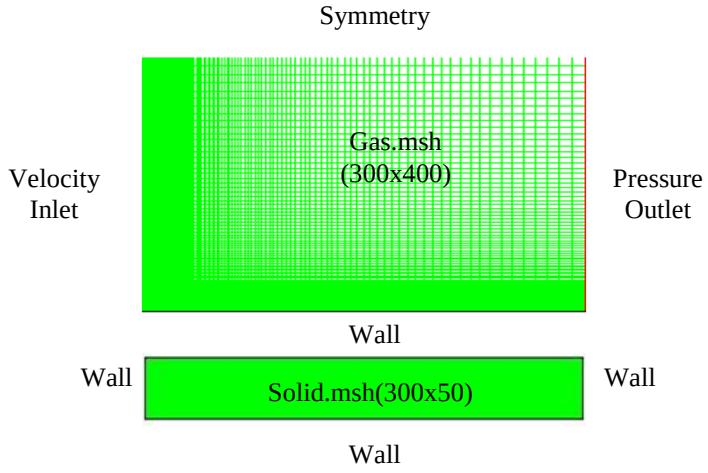

Figure 7-2 Grid used for CFD simulation of flat plate with no film cooling.

Here heat transfer coefficients obtained at each iteration level, of the ICHT technique, were used directly without modification for film cooling effect as boundary condition for conduction run

7.1.2 Results

This simulation was performed to independently analyze the effect of conjugate heat transfer and variable air properties in situations where high temperature difference exists between the mainstream and the surface. The results were obtained using variable air properties since at high temperature differences such a simulation is more realistic as temperature inside thermal boundary layer changes significantly.

As shown in figure 7-4, Iteration 1 depicts the results obtained from conventional constant wall temperature technique in which conduction in the plate (Corning Macor, ceramic) is ignored. Iteration 5 is the final iteration and represents the ICHT result of the same. As observed from figures 7-3 and figure 7-4 , it is clear that significant differences exists between the conventional constant wall temperature technique and ICHT results irrespective of using constant or variable properties since thermal resistance offered by the plate is not considered at all in the conventional technique.

As seen in these figures, for variable property simulation, deviations as high as 3.5% in wall temperatures and around 20% in convective heat transfer coefficient are observed between ICHT and conventional technique. In other words the difference induced is caused by the introduction of metal conduction into the system.

Therefore, the effect of conjugate heat transfer on external heat transfer coefficients is significant and must be taken into account for flows involving high temperature difference between mainstream and coolant flow. Temperature differences in actual gas turbine blades would be higher leading to larger deviations.

It can be inferred that Full Conjugate and ICHT (final iteration) solutions for both heat transfer coefficient and wall temperature distributions match closely indicating that simulation was performed correctly by successfully taking into account the conduction in the plate metal.

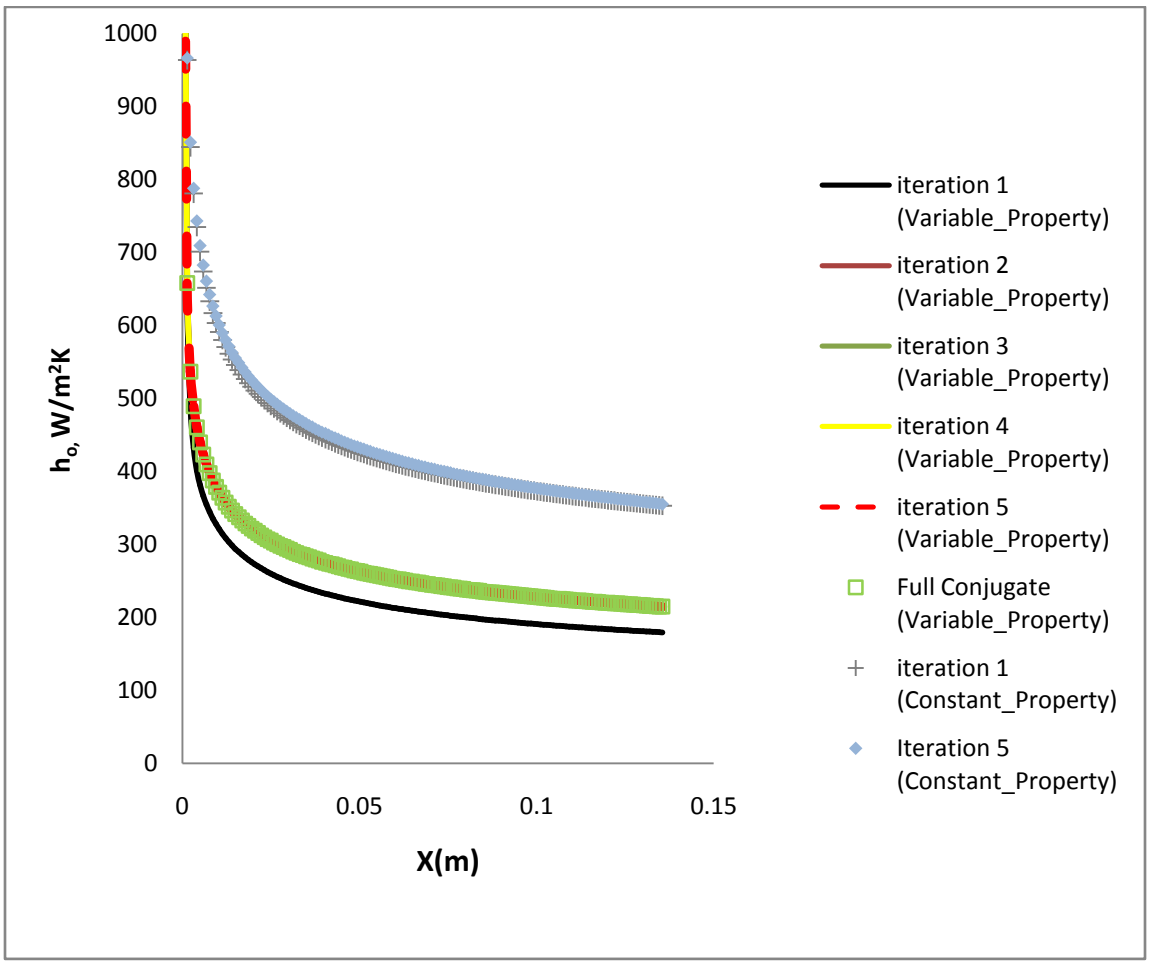

Figure 7-3 Heat transfer coefficient variation using conventional and ICHT approaches on a flat plate with no film cooling

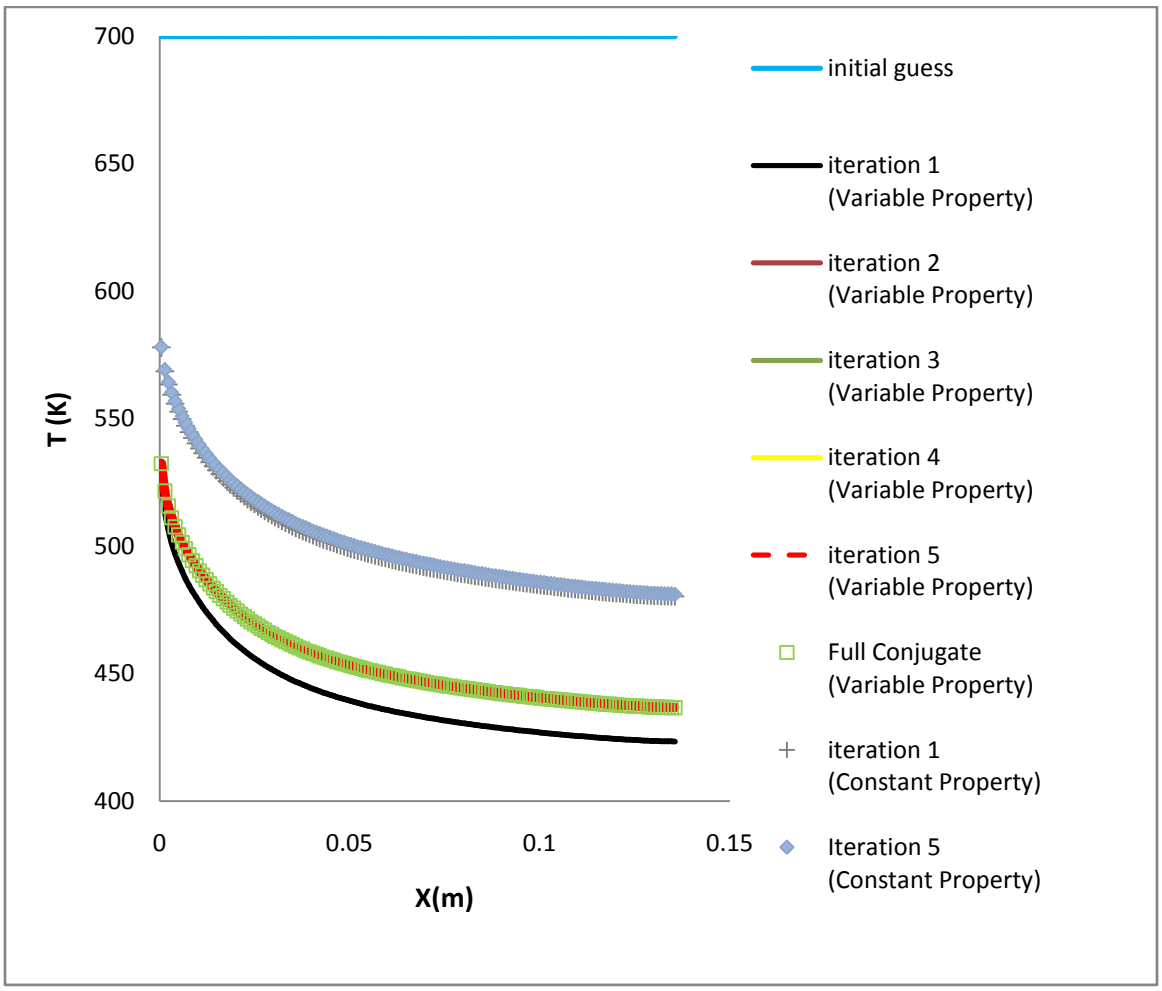

Figure 7-4 Wall temperature variation using conventional and ICHT approaches on a flat plate with no film cooling

7.2 Flat Plate Film Cooling Simulation at Low Temperature Difference using ICHT

7.2.1 Setup and Boundary Conditions

Flat plate film cooling was simulated using a 2-D computational domain, with experimental data from Yuen et al [**9-12**] which has an extensive data set on various film cooling configurations and blowing ratios. Figure 7-5 shows the experimental setup for the same. The injection plate shown in figure 7-5 has 2 rows of holes out of which one is covered during the experiment. The single row of holes used in this numerical simulation corresponds to the origin of X-Y axis in figure 4. A constant heat flux of 410 W/m^2 was used on the bottom surface of metal slab as used in Yuen et al [**12**].The simulation was performed with an unheated turbulent boundary layer tripped 265mm prior to the origin i.e. knife edge shown in the experiment by Yuen et al [**12**]. The ICHT technique was carried out in the region representative of downstream of the coolant hole.

A slab of 50 mm thickness was used to investigate the effect of metal conduction. The Brun number for this situation was calculated to be around 1.2 again indicating the need to solve the problem as a conjugate one.

Numerical simulation employed a mesh of size 360x225 for solving the external convection and a mesh of size 200x50 for solving conduction as shown in figure 7-6.Boundary conditions employed for simulation of the same are presented in table 7-2. The wall y^+ was kept 5 in order to resolve the mesh completely down to the viscous sublayer since standard k-ε model was used. Since the mesh was sufficiently refined wall treatment option was preferred to standard wall functions.

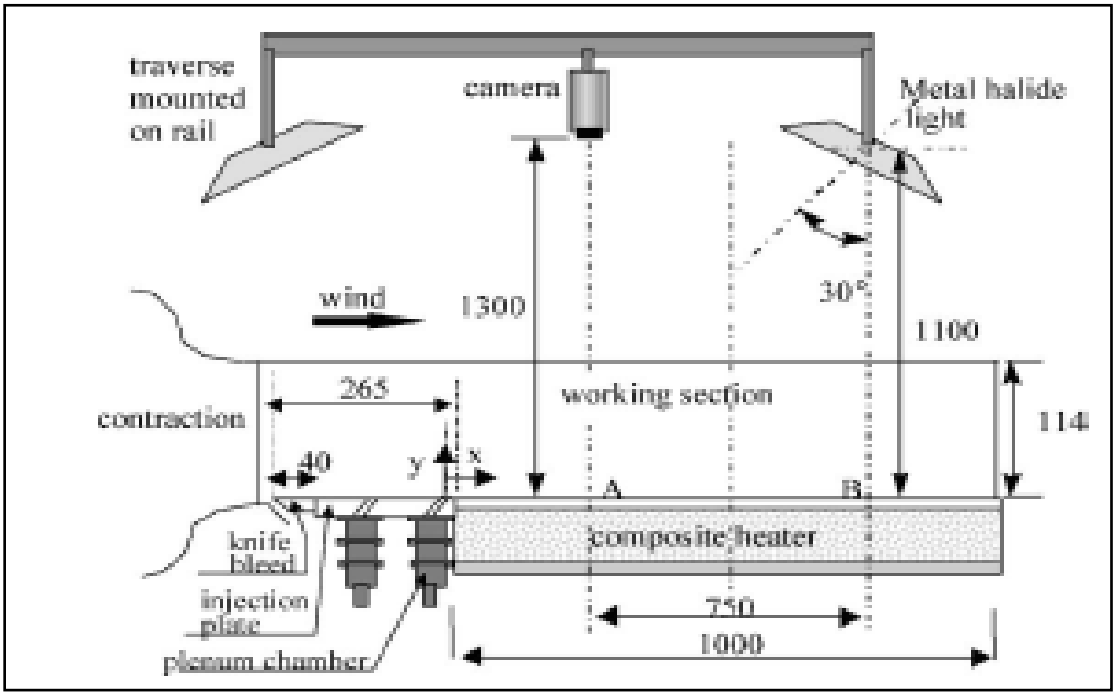

Figure 7-5 Flat plate with film cooling. Experimental setup of Yuen et al **[12]**

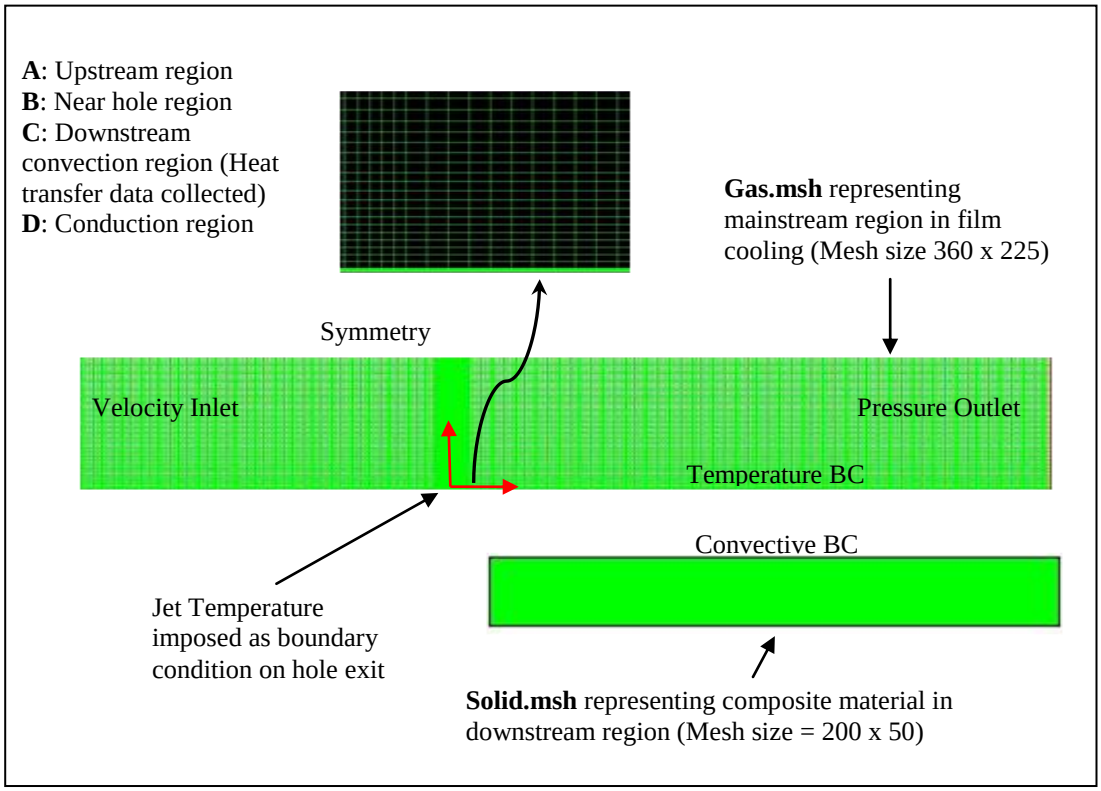

Figure 7-6 Numerical grid to simulate flat plate film cooling experiment of Yuen et al **[12]**, using ICHT.

BOUNDARY CONDITIONS	
Injection angle $\alpha=30^{o}$ Diameter of hole, **D=10mm**	
Inlet Conditions	
Mainstream gas velocity, $\mathbf{V_G}$	**13m/s**
Mainstream temperature, $\mathbf{T_G}$	**300K**
Free stream turbulence, **Tu %**	**2.7 %**
Plate bottom (representing internal convection)	
Constant heat flux	410 W/m^2
Coolant Temperature **Tc**	**280K**
Blowing Ratio **M**	0.5
Material Properties	
Material of Plate	Composite Material
Conductivity Composite (**k**)	1.5 W/mK

Table 7-2 Boundary conditions used for ICHT simulation as used in Yuen et al [**12**].

7.2.2 Results

This computation was performed to simulate the flat plate film cooling experiment performed by Yuen et al [**12**] for which the data was collected using constant heat flux technique. At low temperature differences effects arising out of variable air properties could be ignored given the temperature difference between mainstream and coolant flow ≈ 20K.

The entire simulation takes about 6 iterations to reach the desired level of convergence. Iteration 1 in figure 7-8 shows the wall temperature distribution that would be obtained using conventional (constant heat flux) technique. As mentioned before, the conventional technique

uses the experimentally determined heat transfer coefficient, shown in figure 7-7, to predict wall temperatures. This technique does not take into account the conduction of the plate.

As seen in figure 7-8, the computation starts with an initial guess of 285K on the film cooled surface. Results shown in figure 7-8 reveal a maximum difference of 3% observed between wall temperatures obtained from ICHT and conventional techniques. Since at low temperatures, variable air property effects are almost negligible, the differences can solely be attributed to thermal resistance of the metal plate due to conduction.

As seen in figure 7-9, the heat transfer coefficients obtained from conventional technique (iteration 1) and ICHT technique (iteration 6) differs by an order of 2. This striking difference can be explained by examining wall temperatures distribution which suggests high value of negative dimensionless wall temperatures θ yielding large values of local heat transfer coefficients $h(\theta)$.

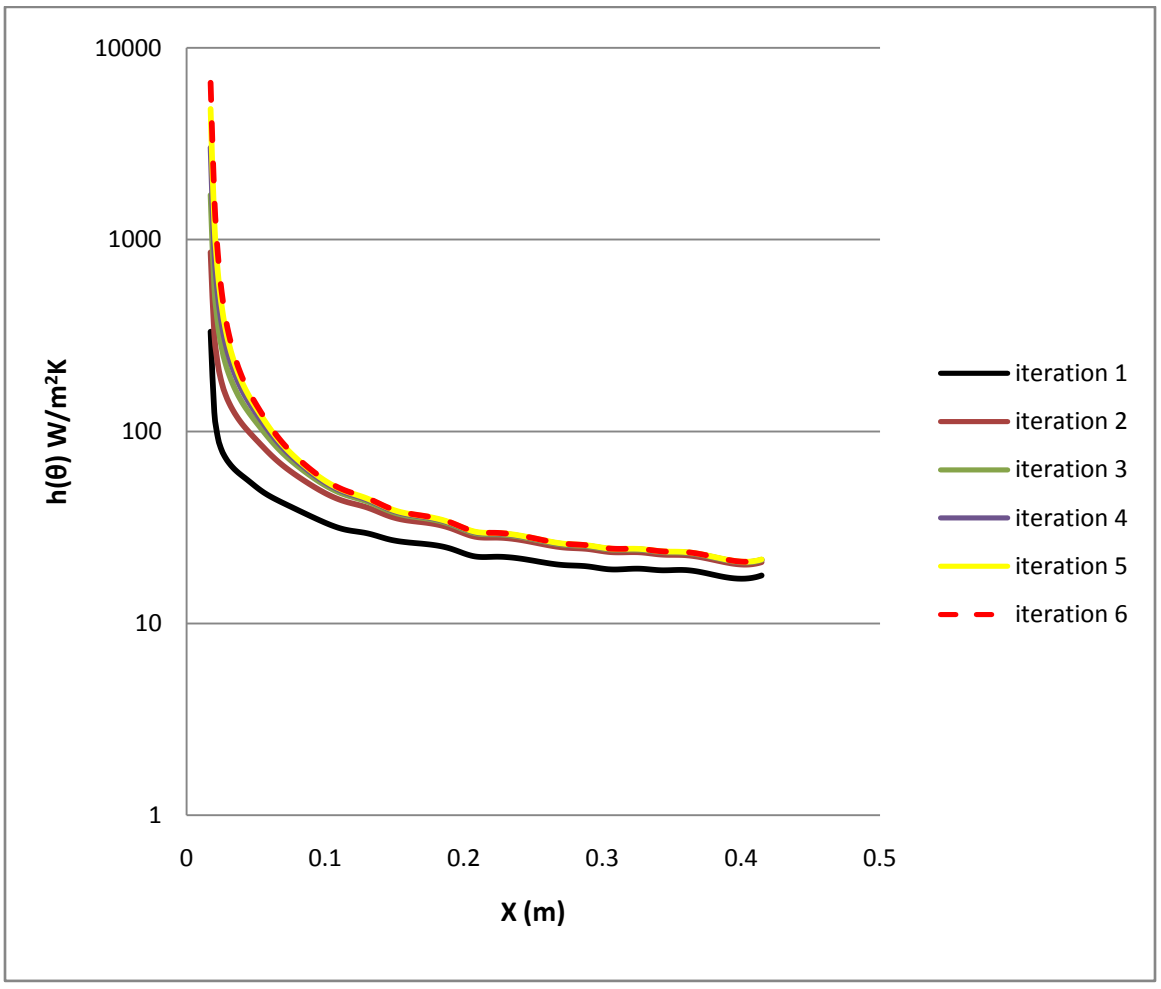

Figure 7-7 Variation of film cooling heat transfer coefficient during ICHT process

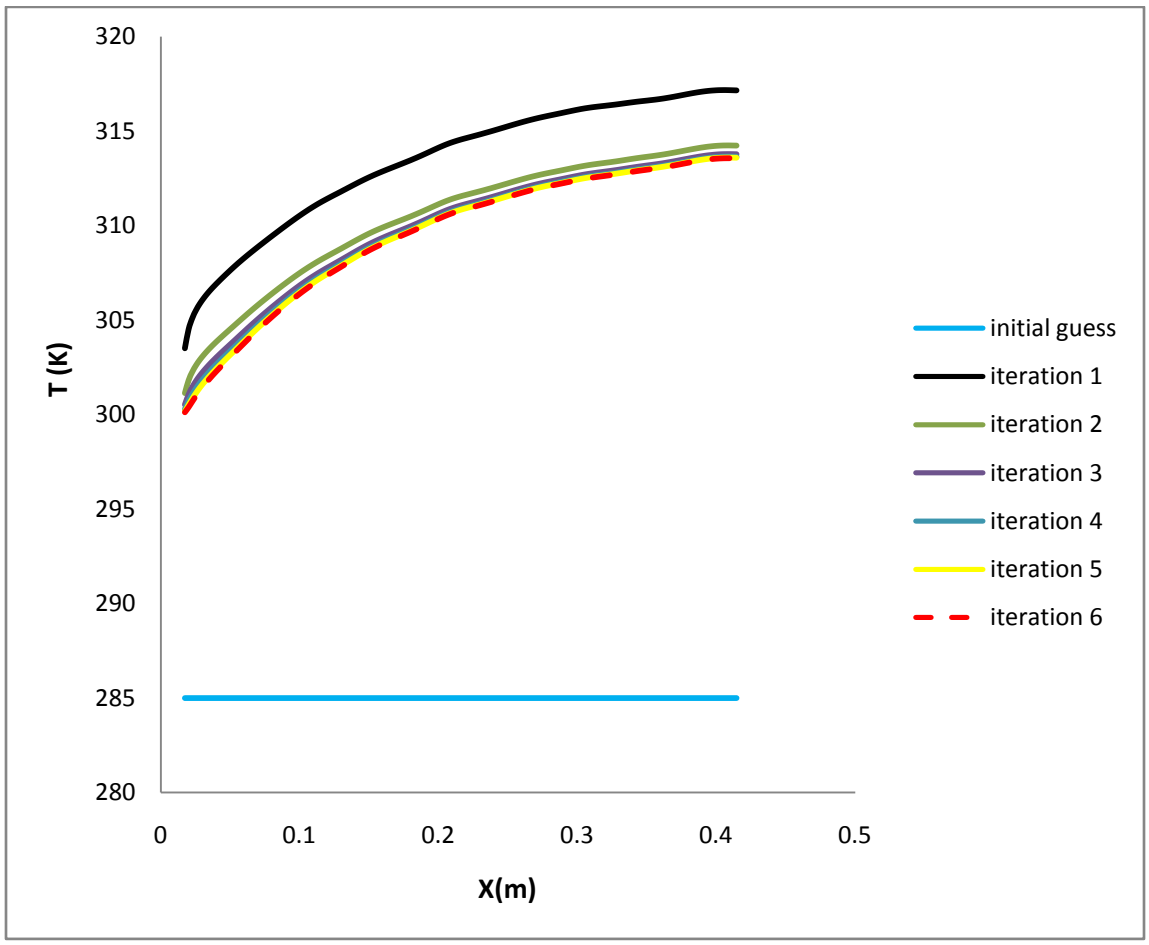

Figure 7-8 Variation of surface temperature during ICHT process

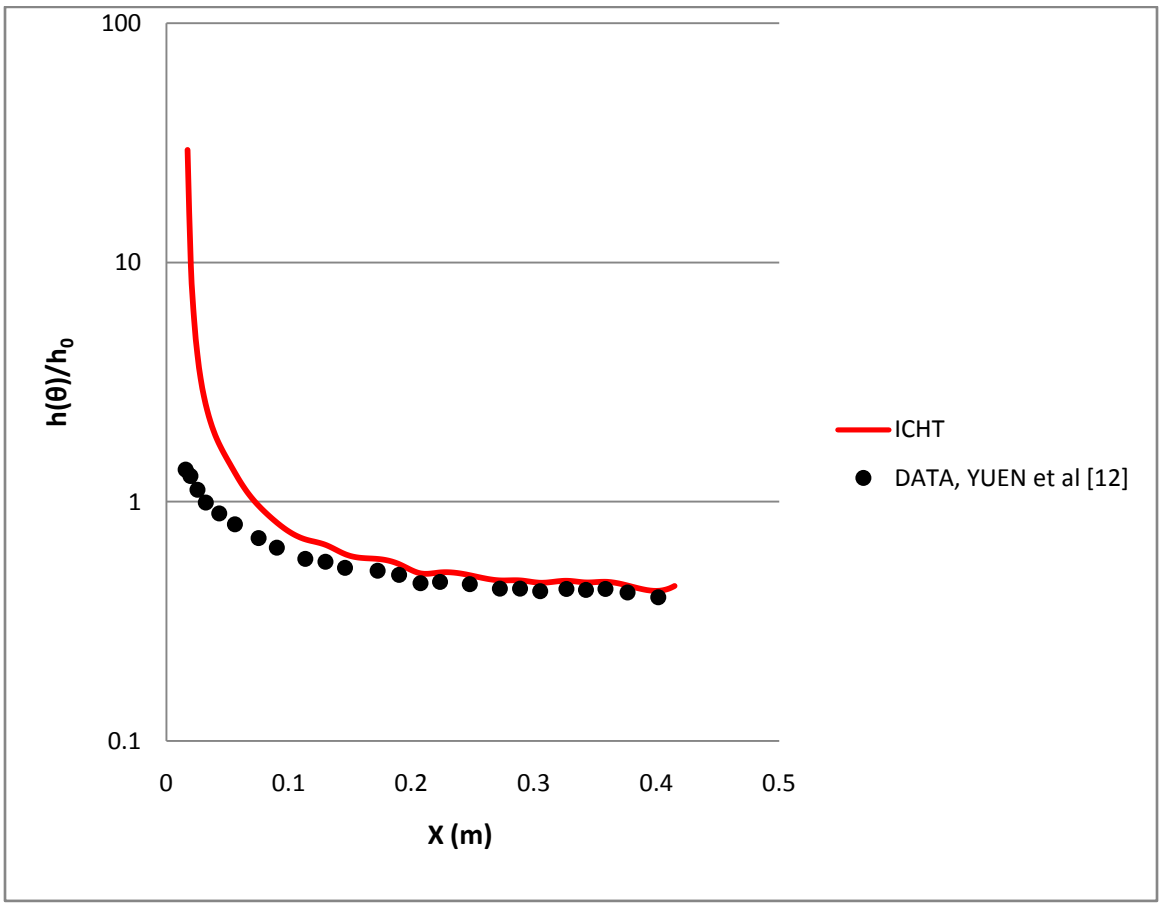

Figure 7-9 Normalized heat transfer coefficient $h(\theta)/h_0$ for flat plate with film cooling

7.3 Flat Plate Film Cooling Simulation at High Temperature Difference using ICHT

7.3.1 Setup and Boundary Conditions

Flat plate film cooling was simulated on a 2-D computational domain. Baldauf et al. **[5-8]** experiment was used due to availability of data set $\frac{\overline{h_f}}{h_0}$ vs $\boldsymbol{x/D}$ and $\overline{\boldsymbol{\eta}}$ vs $\boldsymbol{x/D}$ which is needed in ICHT technique. This experiment was carried out by employing constant temperature technique, in which a constant temperature of 300K is employed at the plate bottom. The Brun number for the given flow was calculated to be around 0.35. Figure 7-10 shows the schematic of the simple flat plate geometry simulated with appropriate 1/7th power turbulent velocity profile applied at the mainstream inlet.

Numerical simulation employed two separate grids one representing the recovery region in the convection side and another metal conduction below the same. Grid of size 150 x 250 was employed for external convection and 150x50 for metal conduction, as shown in figure 7-11.

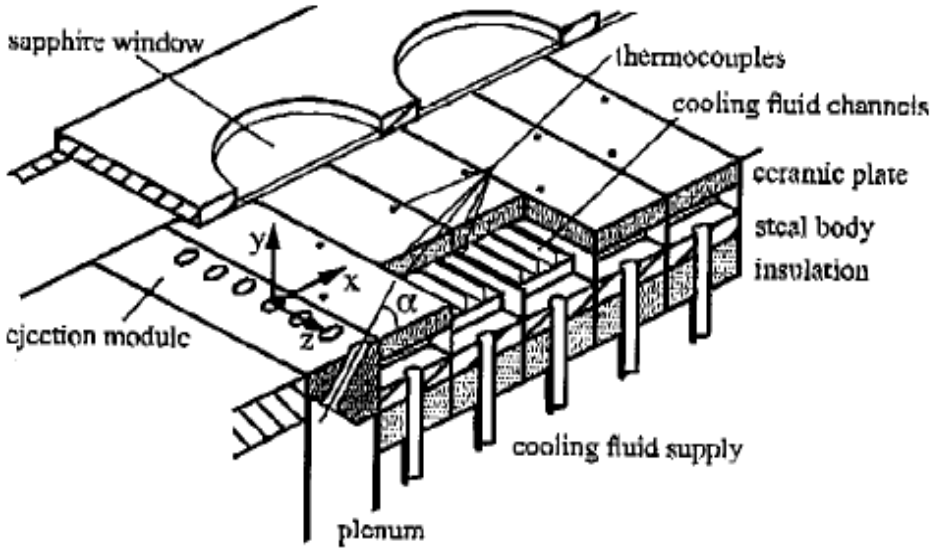

Figure 7-10 Flat plate with film cooling. Experimental setup of Baldauf et al **[8].**

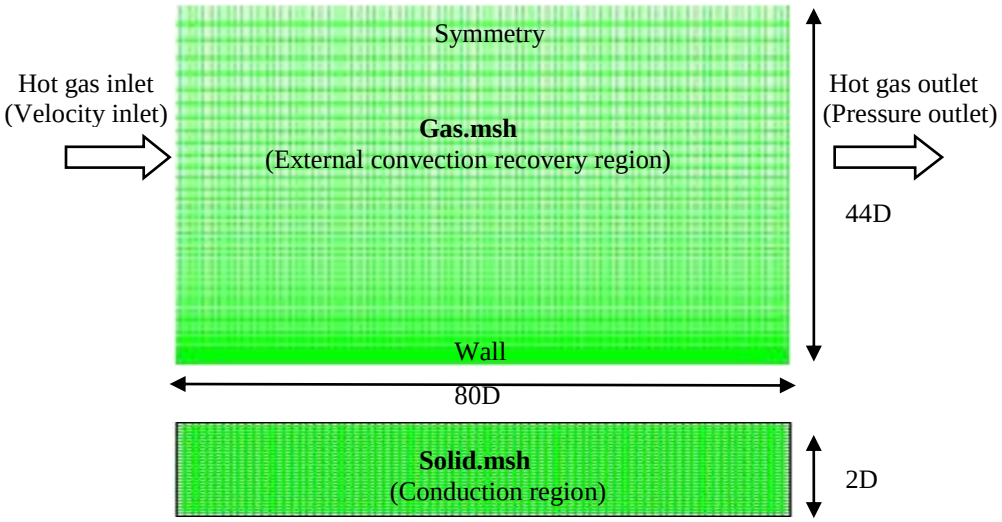

Figure 7-11 Numerical grid to simulate flat plate film cooling experiment of Baldauf et al [**7**] using ICHT.

BOUNDARY CONDITIONS	
Injection angle α=30 Diameter of hole, **D** = 5mm	
Inlet Conditions	
Mainstream gas velocity, $\mathbf{V_G}$	60m/s
Mainstream temperature, $\mathbf{T_G}$	550K
Free stream turbulence, **Tu %**	1.5 %
Plate bottom (representing internal convection)	
Constant Temperature	300K
Coolant Temperature $\mathbf{T_C}$	300K
Blowing Ratio **M**	1
Material Properties	
Material of Plate	Corning Macor (Ceramic)
Conductivity Corning Macor **k**	2.0 W/mK

Table 7-3 Boundary Conditions used for ICHT simulation as used in Baldauf et al [**7**].

7.3.2 Results

This simulation was performed to investigate the workings of the ICHT code using film cooling corrections for heat transfer coefficient and test its convergence. Baldauf et al. **[7]** experiment was chosen due to its simple geometry and availability of heat transfer data, collected by employing constant wall temperature technique, as discussed earlier.

Results in figures 7-12 and figures 7-13 show that it takes around 6 iterations to reach the final solution for ICHT technique. Iteration 1 shows the heat transfer coefficient $h(\theta)$ that would have been obtained using conventional technique. Whereas iteration 5 shows the distribution of heat transfer coefficient obtained using ICHT technique. A maximum deviation of around 60% from conventional technique in terms of heat transfer coefficients is observed in figures 7-12. As seen in figures 7-13 , around 10% difference in terms of wall temperature is observed between conventional and ICHT technique. These differences can be explained by changing of fluid temperature gradients at the wall in the direction of flow, due to conduction in the metal. This in turn alters the convective heat transfer coefficients, leading to a changed surface or blade temperature distribution. This is the conjugate heat transfer effect.

Figures 7-14 shows normalized heat transfer coefficients. The heat transfer coefficients $h(\theta)$ values were well below the heat transfer coefficients for no injection (h_0) indicating reduced heat flux to the plate, at the same temperature difference between mainstream gas and the surface, indicating the effects of film cooling. The apparent wavy nature of the $h(\theta)/h_0$ plot is attributed to the experimental input from Baldauf et al. **[7].**The same figure also shows the spanwise-averaged film cooling effectiveness obtained from experiments.

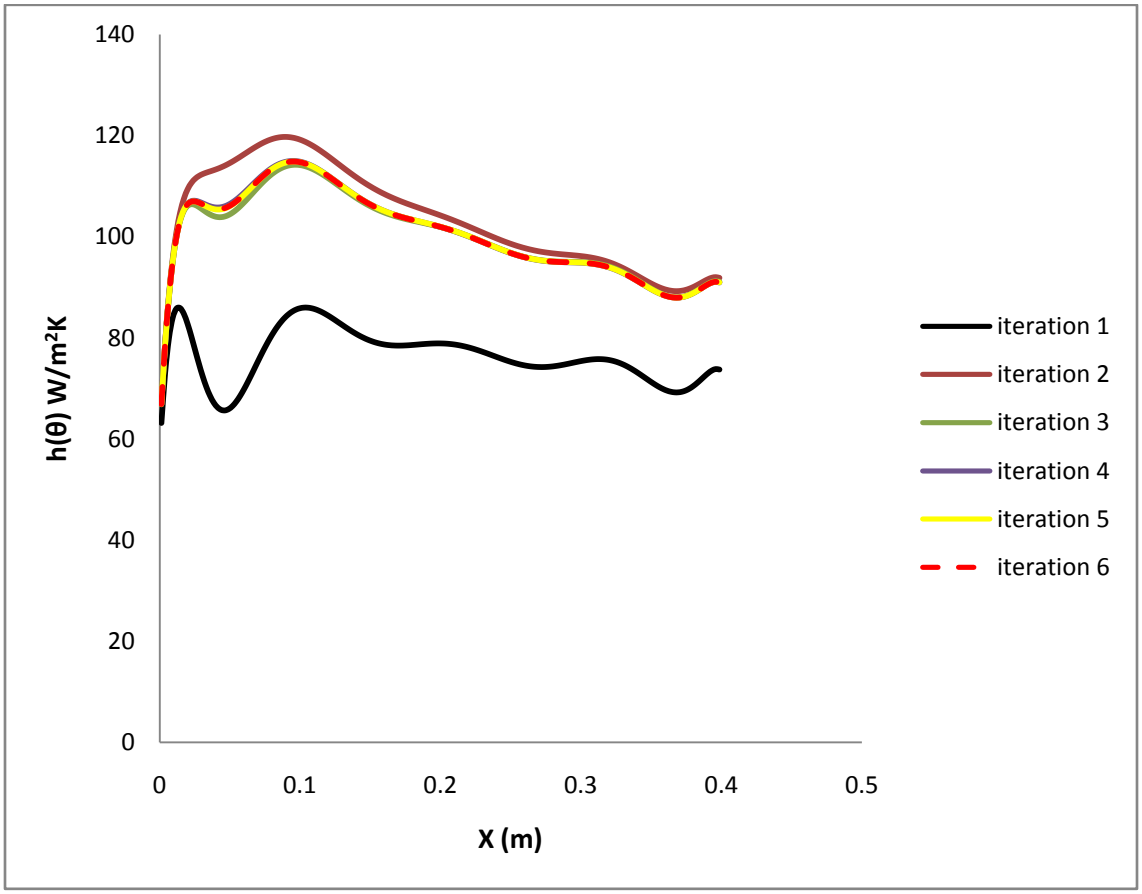

Figure 7-12 Variation of film cooling heat transfer coefficient during ICHT process.

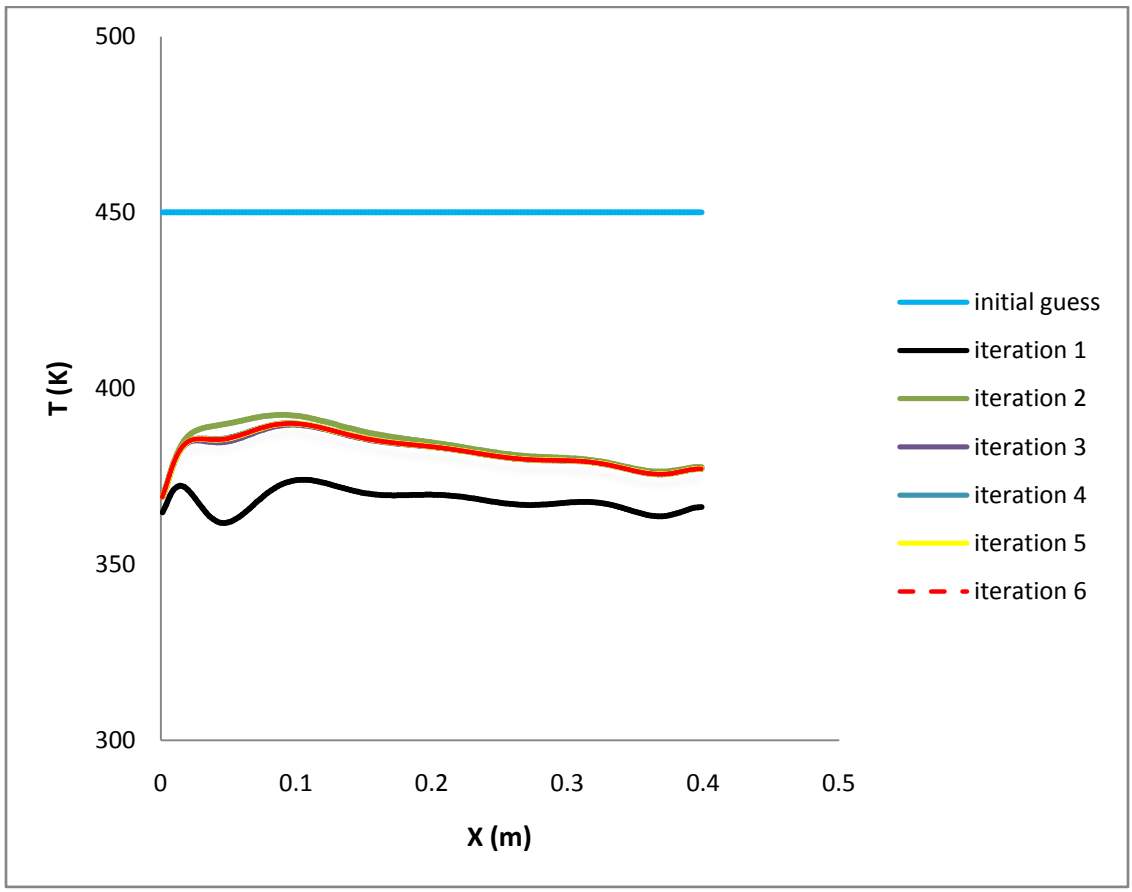

Figure 7-13 Variation of surface temperature during ICHT process.

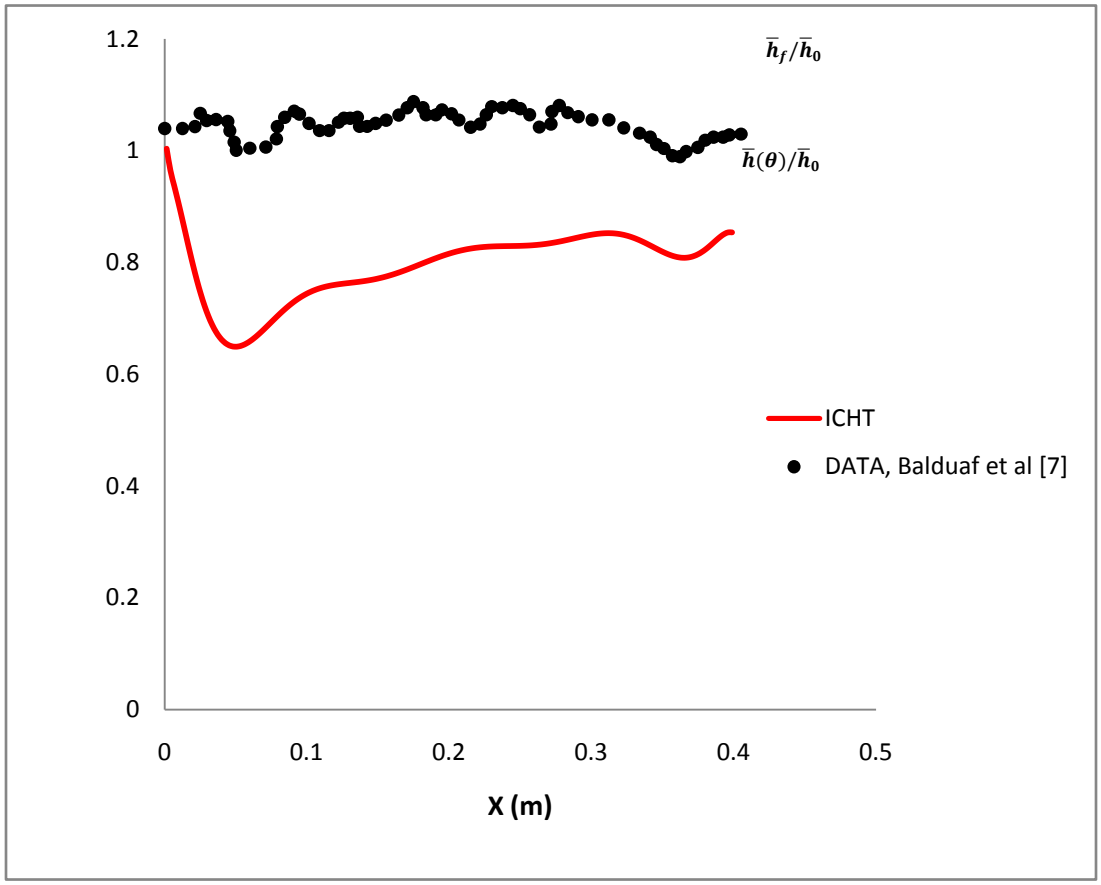

Figure 7-14 Normalized heat transfer coefficient $\boldsymbol{h(\theta)/h_0}$ for flat plate with film cooling.

7.4 Film Cooling Simulation Performed on a 2D Turbine Blade Cascade using ICHT

ICHT code was tested to model film cooling on a linear cascade of C3X turbine vane as used by Hylton et al [**16**]. Experimental data required to model film cooling using Iterative Conjugate Heat Transfer (ICHT) technique was obtained from Hylton et al [**16**].

The experimental investigation was performed in Allison aero-thermal cascade facility which conducted research on turbine components at high temperatures. Extensive heat transfer data under conjugate conditions is available and summarized through the NASA report prepared by authors.

The experimental results are important for validating the ICHT technique for 2D blade cascade since thermal data like heat transfer coefficient and wall temperature distribution was obtained under conjugate conditions by the investigators.

7.4.1 Experimental Setup

The setup consisted of a 2D linear cascade of C3X blade. Test facility included a burner a convergent section a free stream section and optical access, a test section with instrumentation, a quench zone with back pressure regulation and an exhaust system as shown in figure 7-15.

The test section consisted the of 2 inlet total pressure rakes with 5 pressure probes , 2 inlet total temperature rakes with 5 thermocouples and eighteen endwall static pressure taps . The converging transition duct had 7 endwall static pressure taps. 37 endwall static pressure taps are located in the endwall of the cascade at the exit plane as shown in figure 7-16.

The test vane was internally cooled by an array of 10 radial holes. The vane was film cooled by using leading edge, suction surface and pressure surface holes. The leading edge employed a showerhead array of five equally spaced holes while the downstream had 2 rows of holes each on pressure and suction side respectively, as shown in figure 7-17. Detailed geometric

orientation of the film cooling holes is given in table7-4. The film cooling section was thermally isolated from the blade metal using a Z-shaped thermal barrier as shown in the figure 7-17.

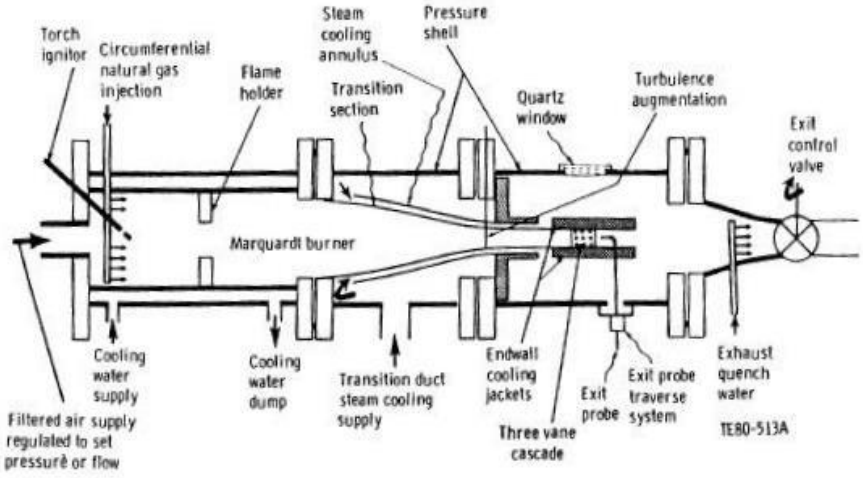

Figure 7-15 Aero-thermo dynamic test cascade facility used by Hylton et al [**16**].

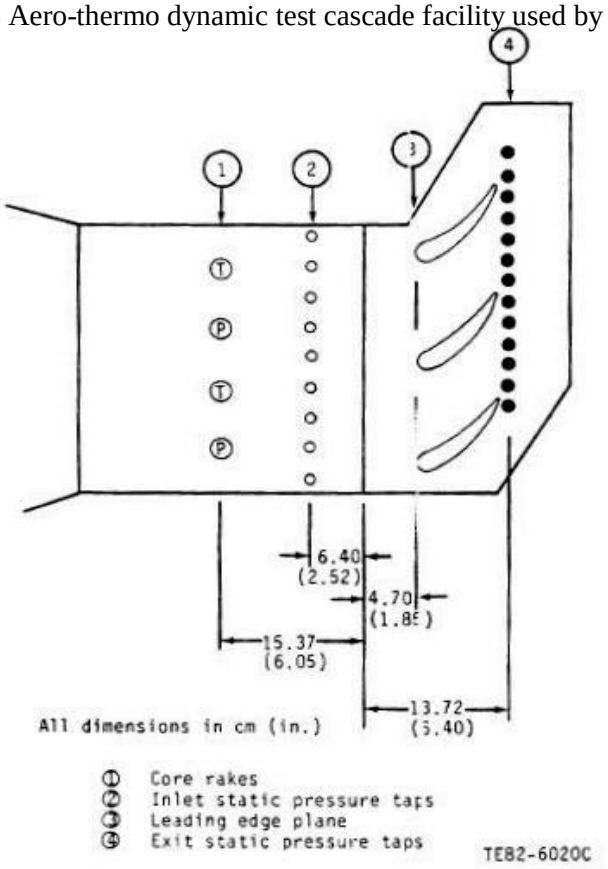

Figure 7-16 Blade cascade setup and instrumentation, Hylton et al [**16**].

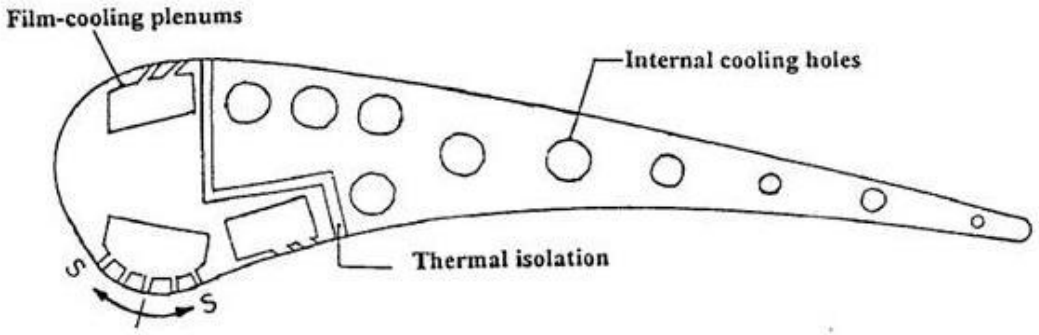

Figure 7-17 C3X vane with film cooling and internal cooling holes, Hylton et al [**16**].

Leading Edge parameters	***Values***
Rows of holes	5
Hole diameter (D)	0.099
Pitch to diameter ratio (P/D)	4
Spacing to diameter (S/D)	7.5
Slant angle (α)	45
Skew angle (β)	90
Downstream parameters	***Values***
Rows of holes	2
Hole diameter (D)	0.099
Pitch to diameter ratio (P/D)	4
Spacing to diameter (S/D)	3.0
Slant angle (α)	90
Skew angle (β)	20,35

Table 7-4 Geometric orientation of film cooling holes of the C3X vane, Hylton et al [**16**].

7.4.2 Computational Setup

Prior to performing 2D film cooling calculation on the C3X blade , 3D simulation full conjugate heat transfer was performed to find out the approximate internal boundary conditions at the midspan of the blade. Boundary conditions for the internal radial cooling holes were not directly available from the Hylton et al [**16**], 1988 NASA report. These were obtained from a CFD study done by Laskowski et al [**39]** on the same C3X blade. A full conjugate 2D heat transfer CFD analysis was done using the obtained boundary conditions to validate the flow and heat transfer results over the C3X blade. Film cooling calculations using ICHT technique was carried out on a similar grid using the same internal boundary condition for cooling holes employed in 2D full conjugate heat transfer simulation.

Ideal gas assumption and variable air properties were used for the hot mainstream gas over the blade. This is important since temperature changes inside the boundary layer as so does the air properties. The C3X blade was made of ASTM 310 stainless steel with material properties as follows

Material	$\boldsymbol{\rho}$ **(kg/m^3)**	$\boldsymbol{C_P}$ **(KJ/kg-K)**	$\boldsymbol{k}$**(W/m-K)**
ASTM 310 Steel	7854	434	6.811+0.020176*T

Table 7-5 Material properties of the C3X vane taken from Ledezma et al [**40**].

Various numerical grids employed to carry out these CFD calculations on a C3X blade are as follows:-

i. *3D grid for full conjugate heat transfer simulation of C3X vane with no film cooling*

Figure 7-18 shows the grid used for full conjugate heat transfer calculations on the C3X vane which consists of 205820 hexahedral cells and 227640 wedge shaped cells (prismatic cells). Such a hybrid mesh has advantages in terms of reduced false numerical diffusion and relative

ease of construction for complex blade geometries. Grid generator GAMBIT was used for construction of this mesh. The details for the grid are mentioned in table 7-6.

Grid Type	***Number of Cells***	***1st Cell height near blade surface (m)***	***1st Cell height near cooling hole (m)***	***Wall Y^+***	***Periodic Interface***
Hybrid	433460	1e-05	1e-03	< 30	Conformal

Table 7-6. Specification of grid used for 3D Full Conjugate Heat Transfer simulation.

ii. 2D grid for full conjugate simulation of a non film cooled C3X Vane

For 2D full conjugate analysis of a non film cooled C3X vane 2 hybrid grids were evaluated. Hybrid Grid 1, shown in figure 7-19, contains quad cells in a structured arrangement for solving external convection and an unstructured region with triangular cells for solving blade metal conduction. The structured free stream region is created and smoothed using an elliptic solver for grid generator POINTWISE.

Hybrid Grid 2, shown in figure 7-20, uses an unstructured meshing scheme for solving both free stream flow and blade metal conduction. In addition to that a fine structured boundary layer is used for convection region close to the C3X blade surface. Further details of the two grids are available in Table 7-7.

Grid Type	***Number of Cells***	***1st Cell height near blade surface (m)***	***1st Cell height near cooling hole (m)***	***Wall Y^+***	***Periodic Interface***
Hybrid Grid 1	120856	1e-05	1e-02	< 0.1	Non Conformal
Hybrid Grid 2	109626	1e-05	1e-02	< 0.04	Conformal

Table 7-7. Specification of grid used for 2D Full Conjugate Heat transfer simulation.

iii. 2D grid for ICHT simulation of film cooled C3X Vane

Two grids were used to perform model film cooling using the iterative conjugate technique. Tests were performed using both structured and unstructured grid for external convection simulation since unstructured grids are known to be more susceptible to false numerical diffusion and is less effective in capturing intricate flow features.

External convection and blade conduction were solved on different meshes as described in the ICHT methodology.

For external convection a hybrid grid as shown in figure 7-21 was considered which contains a structured boundary attached to the C3X turbine blade and an unstructured triangular cells for free stream region. The grid was created in a preprocessor called GAMBIT which is specifically designed for the CFD solver ANSYS FLUENT. Relevant grid specifications are enlisted in Table 7-8.

Grid Type	***Number of Cells***	***1st Cell height (m)***	***Wall Y^+***	***Periodic Interface***
Structured	90288	1e-05	< 0.1	Non Conformal
Hybrid	96032	1e-05	< 0.04	Conformal

Table 7-8. Specification of grid used for external convection in ICHT

For blade conduction again a hybrid grid was considered as shown in figure 7-22. A fine structured grid was applied to region near the cooling holes was accurately capturing the temperature gradients. The mesh was generated in GAMBIT and the specifications are given in Table 7-9.

Grid Type	***Number of Cells***	***1st Cell height (m) (Near Cooling holes)***
Hybrid	13594	1e-02

Table 7-9. Specification of grid used for blade in ICHT.

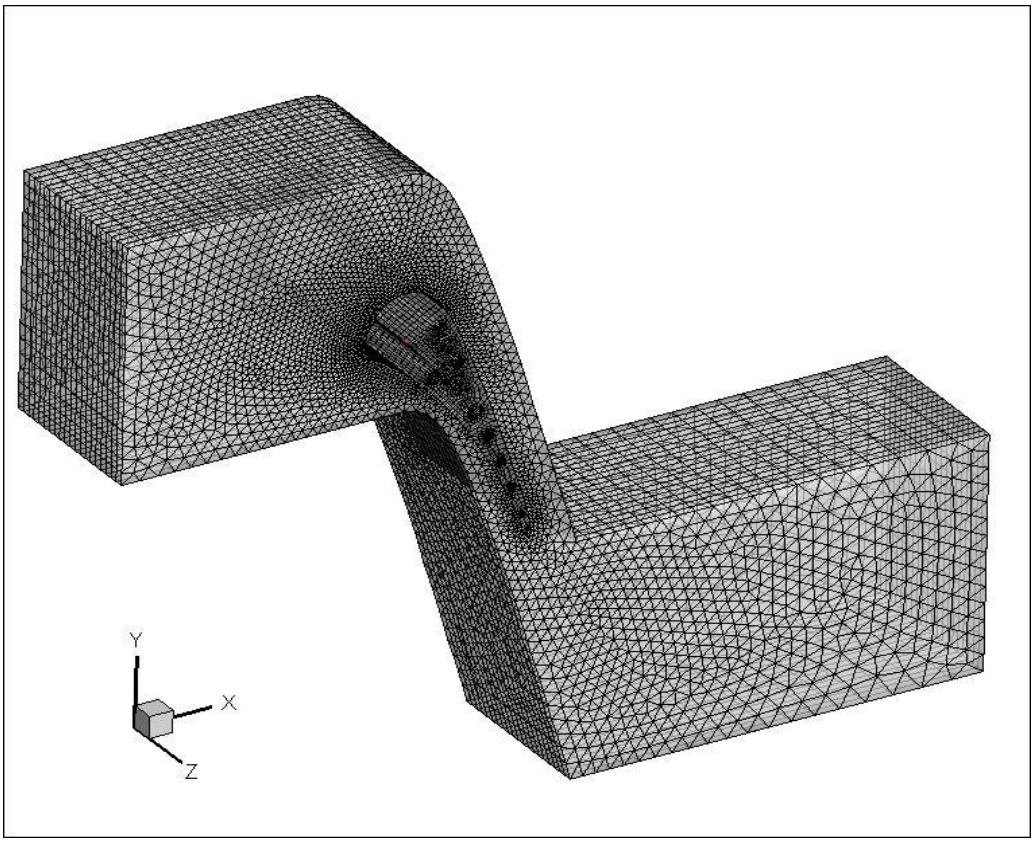

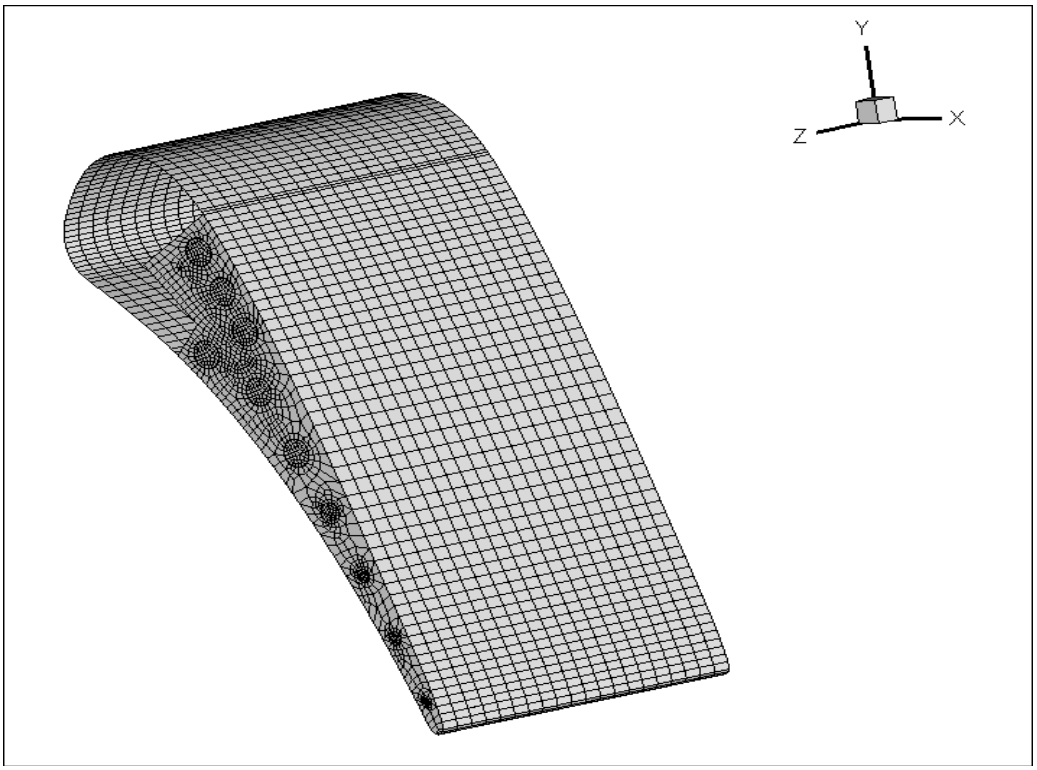

Figure 7-18 **3D** Grid used for full conjugate simulation of C3X vane with no film cooling.

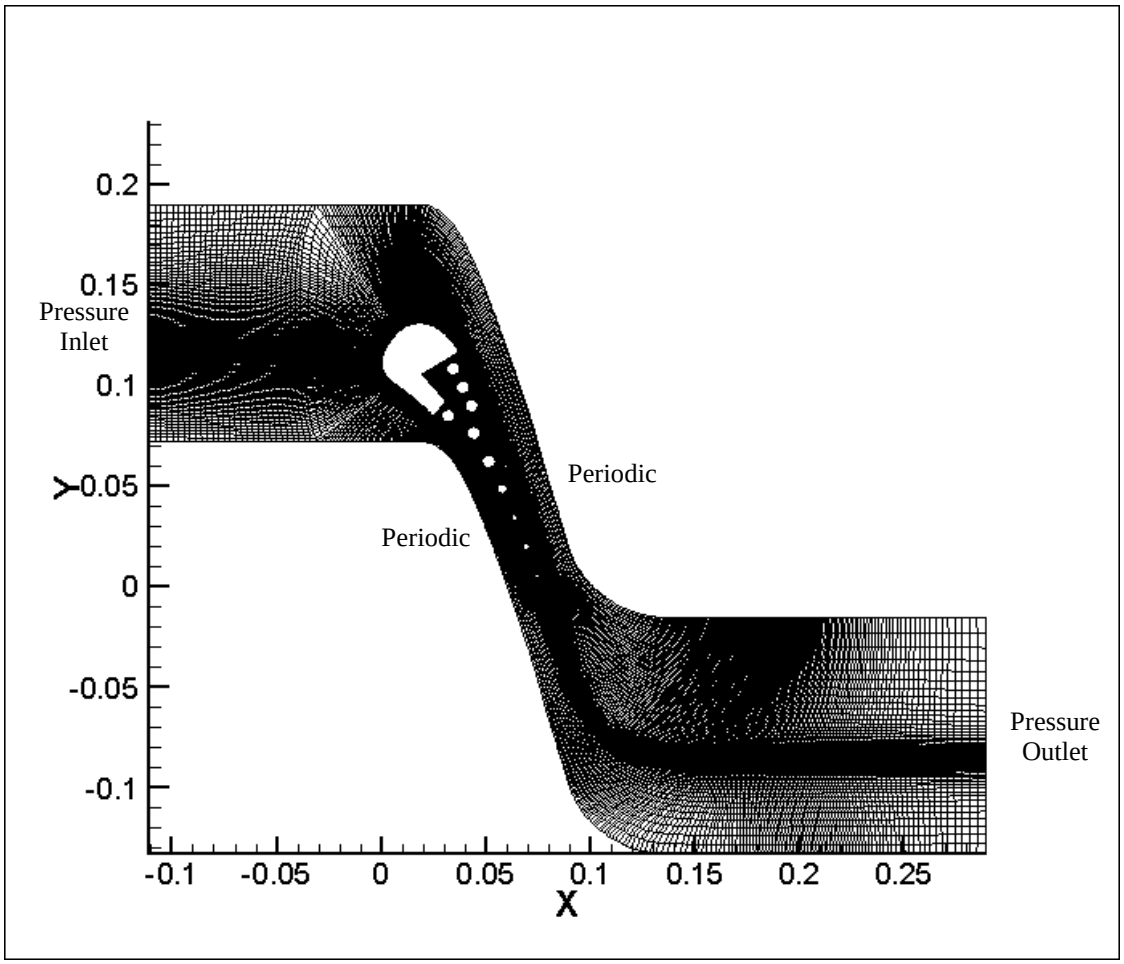

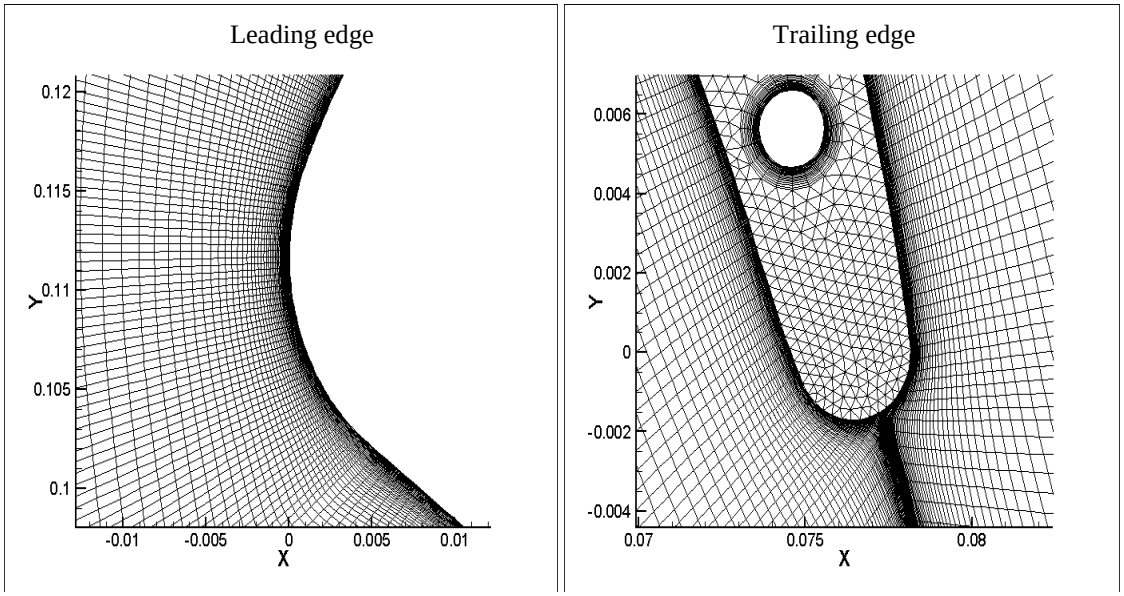

Figure 7- 19 Hybrid Grid 1, used for 2D full conjugate heat transfer simulation on a non film cooled C3X vane.

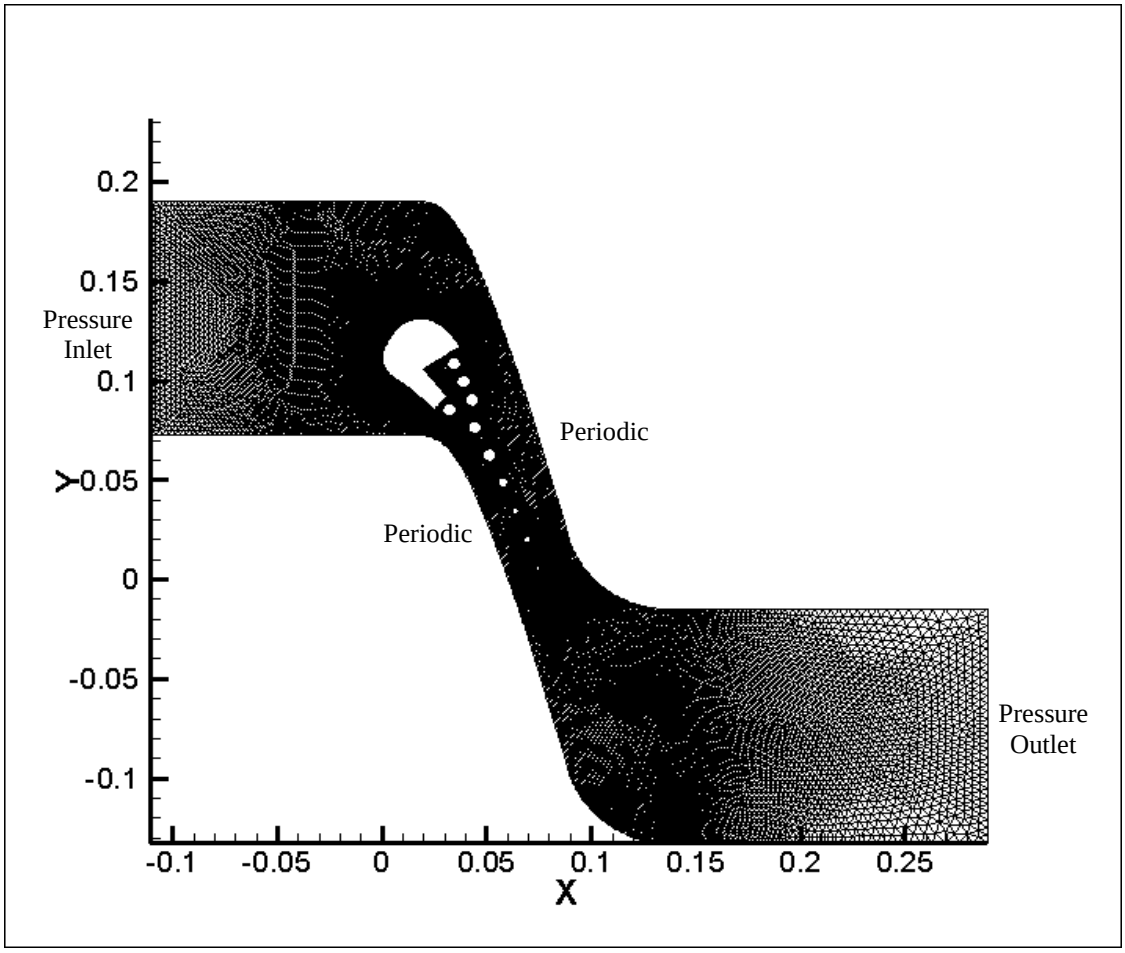

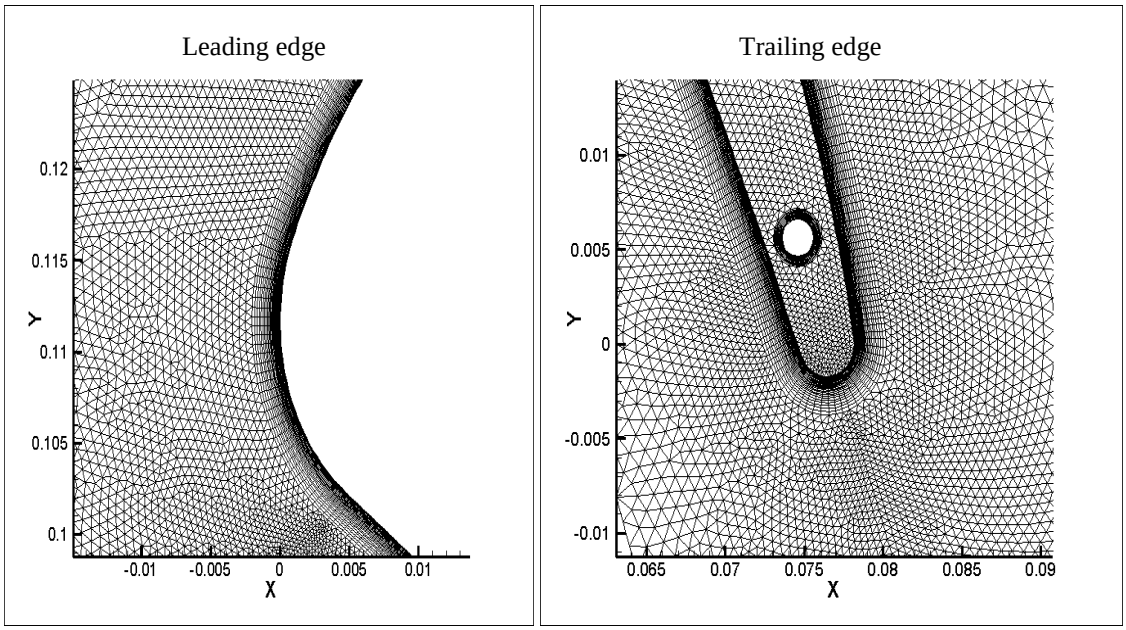

Figure 7-20 Hybrid Grid 2, used for 2D full conjugate heat transfer simulation on a non film cooled C3X vane.

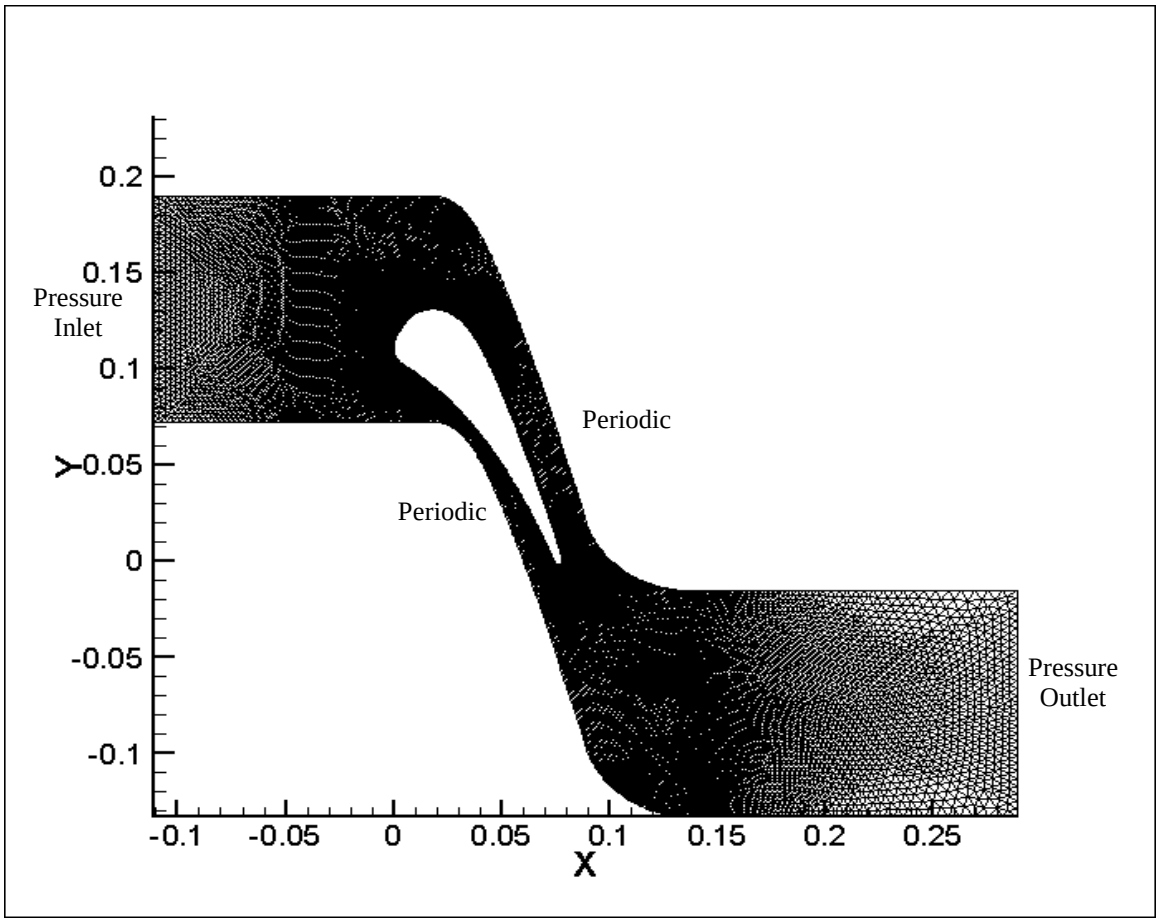

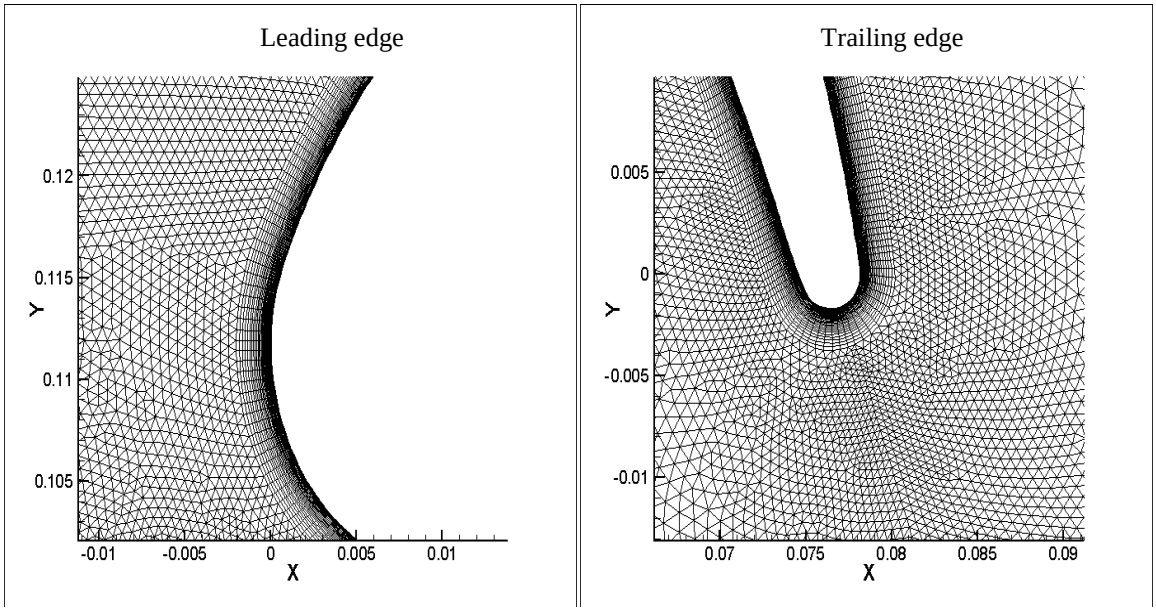

Figure 7- 21Hybrid Grid used for external convection simulation for film cooling calculation on a C3X blade using ICHT.

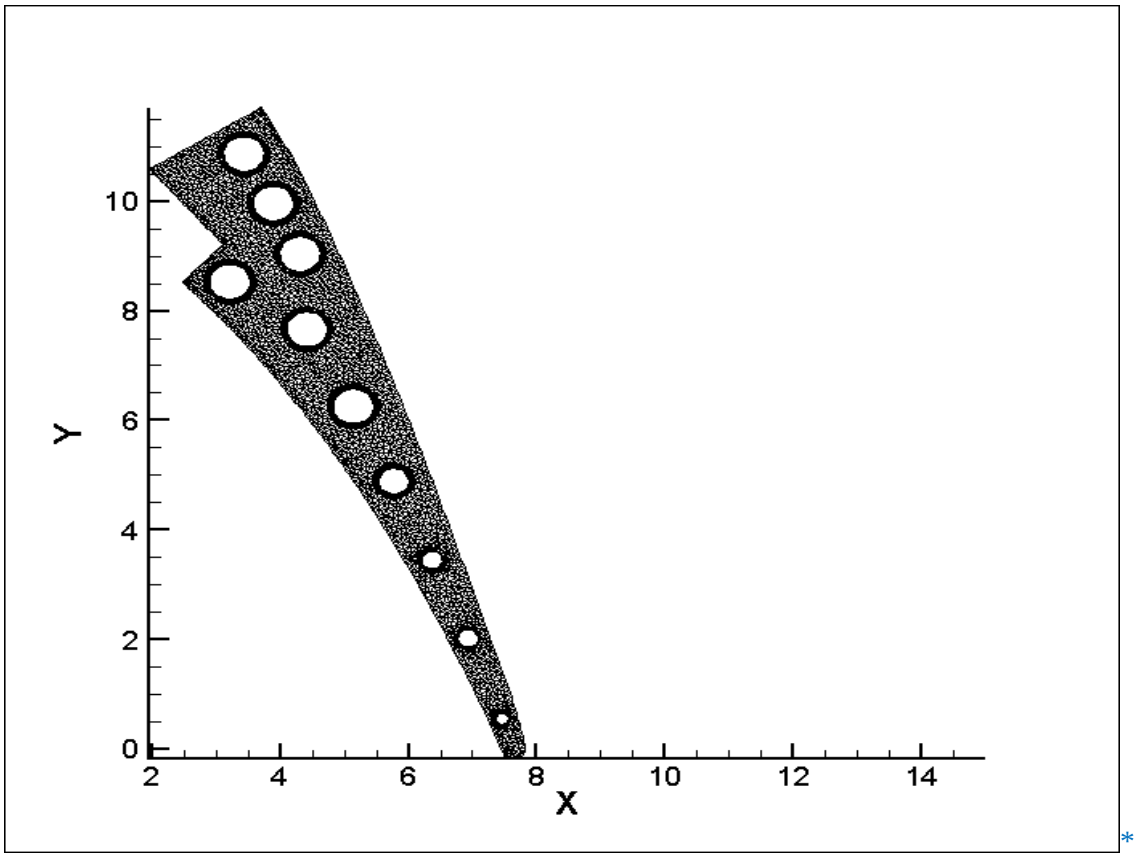

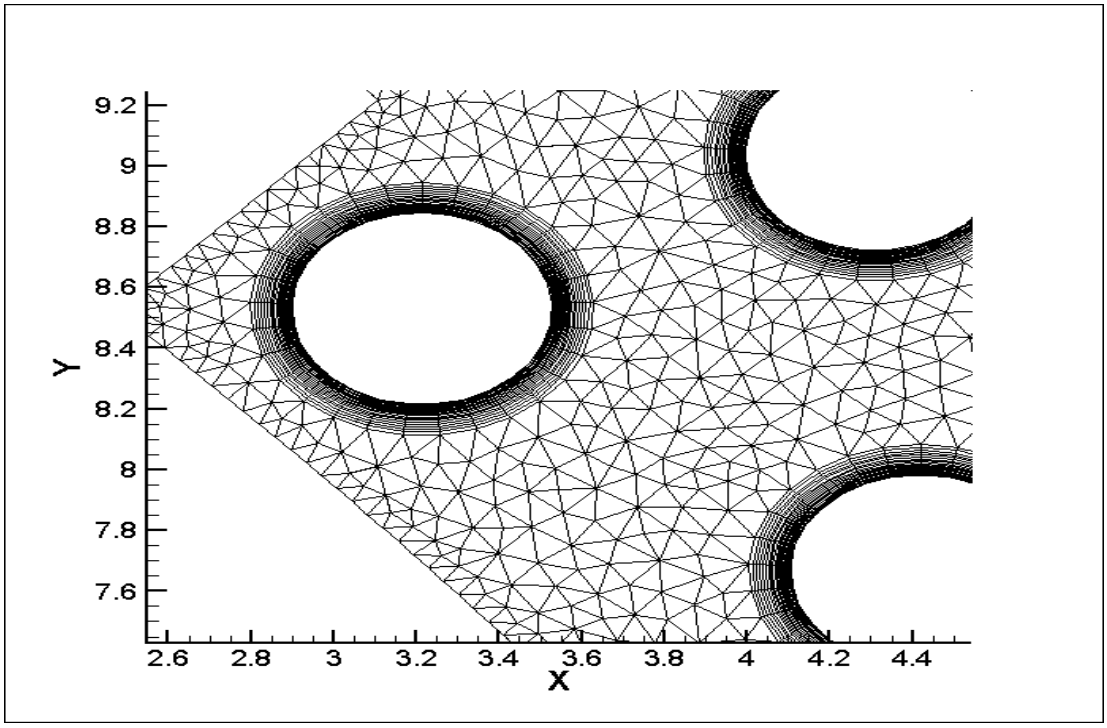

Figure 7-22 **2D** Grid used for blade conduction for film cooling simulation using Iterative conjugate heat transfer technique.

7.4.3 Boundary Conditions

i. 3D full conjugate heat transfer simulation of C3X vane with no film cooling

Test case 44000 of Hylton et al [**16**] was used to perform full conjugate 3D analysis of the C3X vane with no film cooling. The one equation Spallart – Allmaras (**SA**) turbulence model was used in the present setup since it performs well for boundary layer subjected to adverse pressure gradients, which is usually the case in turbo machinery application.

The internal boundary conditions for the radial cooling holes were not documented in the 1988 NASA report by Hylton et al [**16**] and were obtained from Laskowski et al [**38**] who used an "inverse" procedure to find out the missing flow conditions.

Mass flow and temperature conditions at inlet of ten radial cooling channels resulting from inverse solution to be used for 1988 C3X case are provided in Laskowski et al [**38**] and are shown in table 7-10.

Hole Number	$\dot{m}$ **(kg/s)**	T**(K)**
1	0.00784	425.25
2	0.00793	367.06
3	0.00794	350.79
4	0.00826	402.94
5	0.00748	325.1
6	0.00691	326.76
7	0.00752	360.59
8	0.0077	422.46
9	0.00473	379.99
10	0.00357	421.32

Table 7-10. Mass flow and temperature conditions at inlet of the radial cooling holes of the C3X blade.

External flow conditions for Test case 44000 are mentioned in table 7-11.

ii. 2D full conjugate heat transfer simulation of C3X vane with no film cooling

Approximate internal boundary conditions of the C3X blade were obtained from Nusselt number correlation for tubes and bulk temperature obtained at the midspan of the C3X blade after running a 3D full conjugate heat transfer simulation. Bulk temperature T_b for any cross section area in the tube, laminar or turbulent flow, can be calculated using the equation (7.1).

$$T_b = \frac{1}{UA}\int uT \; dA \tag{7.1}$$

Average heat transfer coefficients were calculated by using Nusselt's number correlation for internal flow in a tube. For a close approximation all the air properties were evaluated at the bulk temperature at the midspan. The correlation used for the current study is given in Hylton et al [**16**] and is as follows:-

$$Nu_D = Cr\ (0.22\ Pr^{0.5}\ Re_D^{0.8}) \tag{7.2}$$

Here, Cr is the correction factor which is a function of Prandtl number (Pr), the tube diameter (D) ,Reynolds number (Re_D), and the streamwise coordinate at the cooling hole diameter (x/D), to correct the Nu expression for a fully developed thermal, boundary layer to account for thermal entrance region effects. Average heat transfer coefficient $\bar{h}$ for the internal convection in the cooling tube could then be calculated using the definition of Nusselt's number based on the diameter of that hole.

$$Nu_D = \frac{\bar{h}D}{k} \tag{7.3}$$

Boundary conditions so obtained are given in the following table 7-11.

Hole	*Diameter (m)*	*Cr*	*k (W/m-K)*	*ρ (kg/m^3)*	*v (m^2/s)*	*$\dot{m}$ (kg/s)*	*Re_D*	*Nu_D*	*$\bar{h}$ (W/m^2K)*	*T_b (K)*
1	0.0063	1.118	0.03574	0.81875	0.0000297	0.00784	65159.52	143.9797	816.79	431.74
2	0.0063	1.118	0.031872	0.93943	0.0000236	0.00793	72135.19	156.1841	790.14	376.45
3	0.0063	1.118	0.030765	0.97944	0.0000220	0.00794	74231.84	159.8053	780.38	361.13
4	0.0063	1.118	0.034151	0.86515	0.0000271	0.00826	71201.46	154.5646	837.86	408.66
5	0.0063	1.118	0.02908	1.0461	0.0000197	0.00748	73095.61	157.8454	728.59	338.18
6	0.0063	1.118	0.029377	1.03381	0.0000201	0.00691	67206.43	147.5868	688.19	342.20
7	0.0047	1.09	0.031893	0.93872	0.0000236	0.00752	91645.75	184.4138	1251.38	376.74
8	0.0031	1.056	0.036116	0.80853	0.0000303	0.0077	129092.3	234.9965	2737.78	437.18
9	0.0031	1.056	0.036668	0.79372	0.0000312	0.00473	78449.04	157.7652	1866.10	445.32
10	0.00198	1.025	0.037108	0.782231	0.0000320	0.00357	91655.13	173.4309	3250.33	451.83

Table 7-11. Internal boundary conditions for radial cooling tubes of the C3X blade.

External flow conditions around the C3X blade used for full conjugate heat transfer simulation with no film cooling are given in table 7-12.

Test Case	*Total Temperature T_t (K)*	*Total Pressure P_t(Pa)*	*Inlet Mach number Ma_1*	*Outlet Mach number Ma_2*
44000	709	280350	0.19	0.89

Table 7-12. Boundary condition for full conjugate heat transfer simulation with no film cooling.

iii. 2D film cooling simulation on C3X blade using ICHT

Boundary condition employed for the internal convection cooling holes is in form of average heat transfer coefficients and bulk temperature as mentioned before. These are listed in table 7-11. Test case 44344 was carried out to simulate film cooling and analyze the results along the midspan of the C3X blade. The operating conditions for Test case 43444 are mentioned in table 7-13.

Test Case	***Total Temperature T_t (K)***	***Total Pressure P_t(Pa)***	***Inlet Mach number Ma_1***	***Outlet Mach number Ma_2***
44344	701	285130	0.17	0.89

Table 7-13. Boundary condition for film cooling simulation on C3X blade.

7.4.4 Film Cooling Experimental Correlation / Data used

Film cooling heat transfer data in the form of Stanton Number Ratio (**SNR**) was employed for correcting the baseline heat transfer coefficient obtained from the external convection solution at each iteration level. Such a strategy was adopted instead of using correlation for film effectiveness η and augmentation ratio $\frac{h_f}{h_0}$, as these quantities are not widely available in open literature and are usually propriety information of gas turbine designers.

Stanton Number Ratio (**SNR**) is given in the equation (7.4).

$$SNR = 1 - \frac{St(\theta)}{St_0} \tag{7.4}$$

Where, $St(\theta)$ is the Stanton number at any arbitrary temperature for a film cooled surface and St_0 is the Stanton number for surface with no film cooling.

If the ratio of film cooled Stanton number to baseline non-film cooled Stanton number is determined using data obtained at equivalent exit Mach number and exit Reynolds number conditions, SNR would be approximately equal to the actual heat transfer coefficient reduction. This is possible, because $\rho C_p V_G$ will be same for both film cooled and non film cooled case. Thus, SNR can now be defined by

$$SNR = 1 - \frac{h(\theta)}{h_0} \tag{7.5}$$

7.4.5 Other Important Parameters

Since flow is in the compressible range i.e. Mach number > 0.3 all the transported variables momentum, density, turbulence viscosity and energy were discretized using a QUICK scheme (Quadratic Upstream Interpolation for Convective Kinetics) which is second order accurate in space. This type of scheme gives more accurate results and can resolve and shock waves present in the flow. Pressure and velocity were coupled using the SIMPLE algorithm (Semi Implicit Pressure Linked Equation).

7.4.6 Results and Discussion

i. 3D full conjugate heat transfer simulation of C3X vane with no film cooling

Full conjugate 3D heat transfer simulation was carried out for Test case 44000 of Hylton et al [**16**] on a C3X vane with only internal cooling. Results of both flow and heat transfer showed good agreement with the experiment data of Hylton et al [**16**]. As seen in figure 7-23, the pressure distribution along the midspan of the blade shows a maximum local deviation of around 6% and an average deviation of around 3% on the pressure side. On the other hand suction side results reveal a maximum local deviation of 18% and an average deviation of 4% from the

experimental data. Results have therefore shown that the flow around the blade was calculated correctly using the **SA** turbulence model.

Heat transfer results were compared in the form of temperature and heat transfer coefficient normalized over mainstream gas temperature and an arbitrary heat transfer coefficient value of 1135 W/m^2K respectively. Figure 7-24b shows temperature predicted by the **SA** model over the midspan of C3X blade revealing a maximum deviation of 7% and 5% on the pressure and suction side respectively from experimental data for non film cooled blade. On the other hand deviations recorder for heat transfer coefficients were well outside the maximum experimental uncertainty of 22.5% .The observed deviations for pressure and suction side were around 45% and 26% respectively from the data as shown in figure 7-25. However, the since the temperature results compared reasonably well with the experimental data therefore this case was used to find out the approximate internal boundary conditions for radial cooling tube.

ii. 2D full conjugate heat transfer simulation of C3X vane with no film cooling

This simulation was performed to validate flow and heat transfer over the C3X blade and to ensure that the internal boundary conditions, obtained through the technique illustrated in section 7.4.3, are correctly implemented. A grid sensitivity study was carried out on hybrid grid 1 & hybrid grid 2 as shown in figure7-26a and flow results were compared against the available data. No significant gain was found through the use of a smoothed structured hybrid grid 1. Hybrid grid 2 was chosen for all the further simulations since it was easier to prepare and converged faster to a solution. Both the one equation **SA** model and two equations **KW-SST** model were compared against the data to see if there are any noticeable benefits of using a more complicated model like **KW-SST**, which is considered advantageous for situations with complex boundary layer flows under adverse pressure gradient and separation.

Flow results shown in figure 7-26b results in form of pressure distribution obtained using hybrid grid 2 through **KW-SST** & **SA** turbulence model follow a similar trend. Both models show an average deviation of 3% & 10% on the pressure and suction side respectively. A maximum local deviation of 23% is also observed on suction side. Small peaks in pressure distribution observed towards the trailing edge can be attributed to the flow separation and counter rotating vortex near in the wake region as seen in figure 7-27. Pressure and velocity contours of the entire flow field can also be visualized in figure 7-27 & figure 7-28 respectively. The entire flow regime is close to transonic i.e. Mach number ≈ 0.8.

Temperature contours shown figure 7-29 reveal the most effective cooling takes place close to the air barrier region which progressively worsens as we approach the trailing edge. Temperature distribution predicted by these turbulence models shows a maximum local deviation of 7% & 6% on the suction and pressure side respectively, as observed from figure 7-30. An overall deviation of around 2 to 4 % is observed for both the sides which fall close to the uncertainty of 2% in experimental measurements. The predicted heat transfer coefficients, shown in figure 7-31, does not fall within experimental uncertainties for any of the two models even though the **KW-SST** model performed slightly better than the one equation **SA** model. Both these models over predicted normalized heat transfer coefficients by as much as 132% on the pressure side and under predicted the same by as much as 67% on the suction side. These deviations can be attributed to the fact, that heat transfer is modeled analogous to the flow, for all the above mentioned **RANS** models and such discrepancies are an outcome of the closure approach used in turbulent flow heat transfer modeling. Moreover, discrepancies in flow and heat transfer results, near the trailing edge of the blade might be a result of inaccurate prediction of flow, by both the models in this region. This happens in flows with suddenly changing strain rates for which linear relationship between Reynolds stress and strain rate does not hold true.

iii. 2D Film cooling simulation on C3X blade using ICHT

This simulation was performed on two separate hybrid grids, whose description is available in table 7-11 & table 7-12. ICHT simulation of test run 44344 of Hylton et al [**16**], which uses a film cooled C3X vane, is performed. As discussed earlier all the calculations were performed keeping in mind the compressibility effects of air at such high speeds. Figure 7- 37 confirms that compressibility effects are taken in to account as the density does change from 0.833 to 1.85. A weak shock is also observed near the trailing edge of the suction side which is confirmed in figure 7-36 indicating a maximum mach number of 1.02.

The ICHT process is started with an initial guess of 600K on both pressure and suction side. It takes about 2 full iterations to get the desired convergence on temperature as seen in figure 7-32. An improvement of around 7% on the pressure side and 10% on suction side, over conventional technique (iteration 1), is observed for wall temperature distribution obtained using ICHT. Figure 7-32 also show that wall temperature distribution obtained using ICHT technique is within 3% of the experimental value on pressure side and 2% of the experimental value on the suction side. On the other hand wall temperature distribution obtained using conventional technique (iteration 1) predicts temperature within 6% on pressure side & within 8% on suction side. Temperature contours of the 2D blade midspan, as shown in figure 7-34 & figure 7-35, suggest that there is an approximate difference of around 20 – 30 K between film cooled and non film cooled blade. However, heat transfer coefficients, shown in figure 7-35, obtained through the ICHT technique were off from experimental data by 85% on the pressure side and 62% on the suction side both near the trailing edge. A maximum improvement of around 21% over the conventional technique is also observed but only on the suction side.

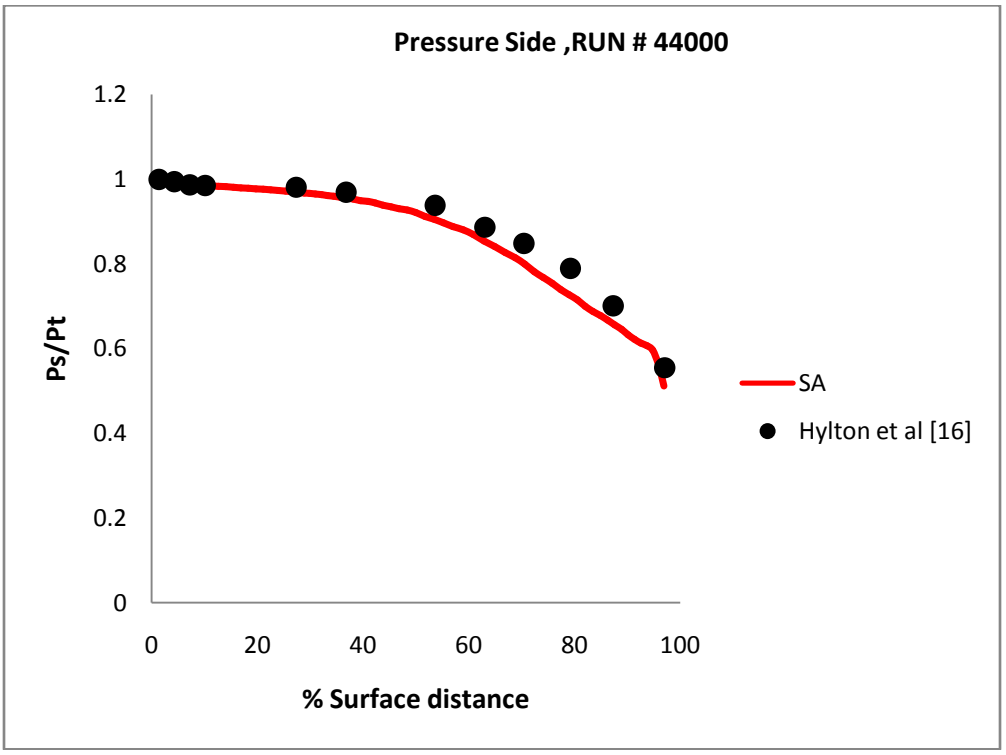

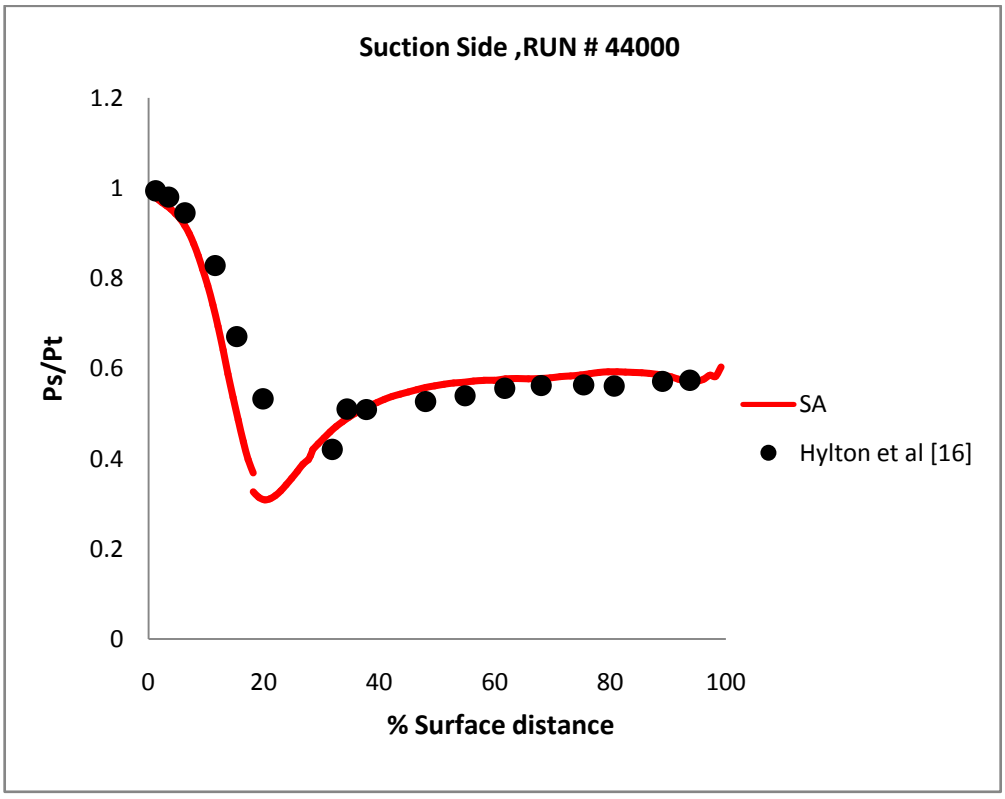

Figure 7-23 Pressure distributions obtained from 3D full conjugate simulation of C3X vane with no film cooling, **Run #44000**

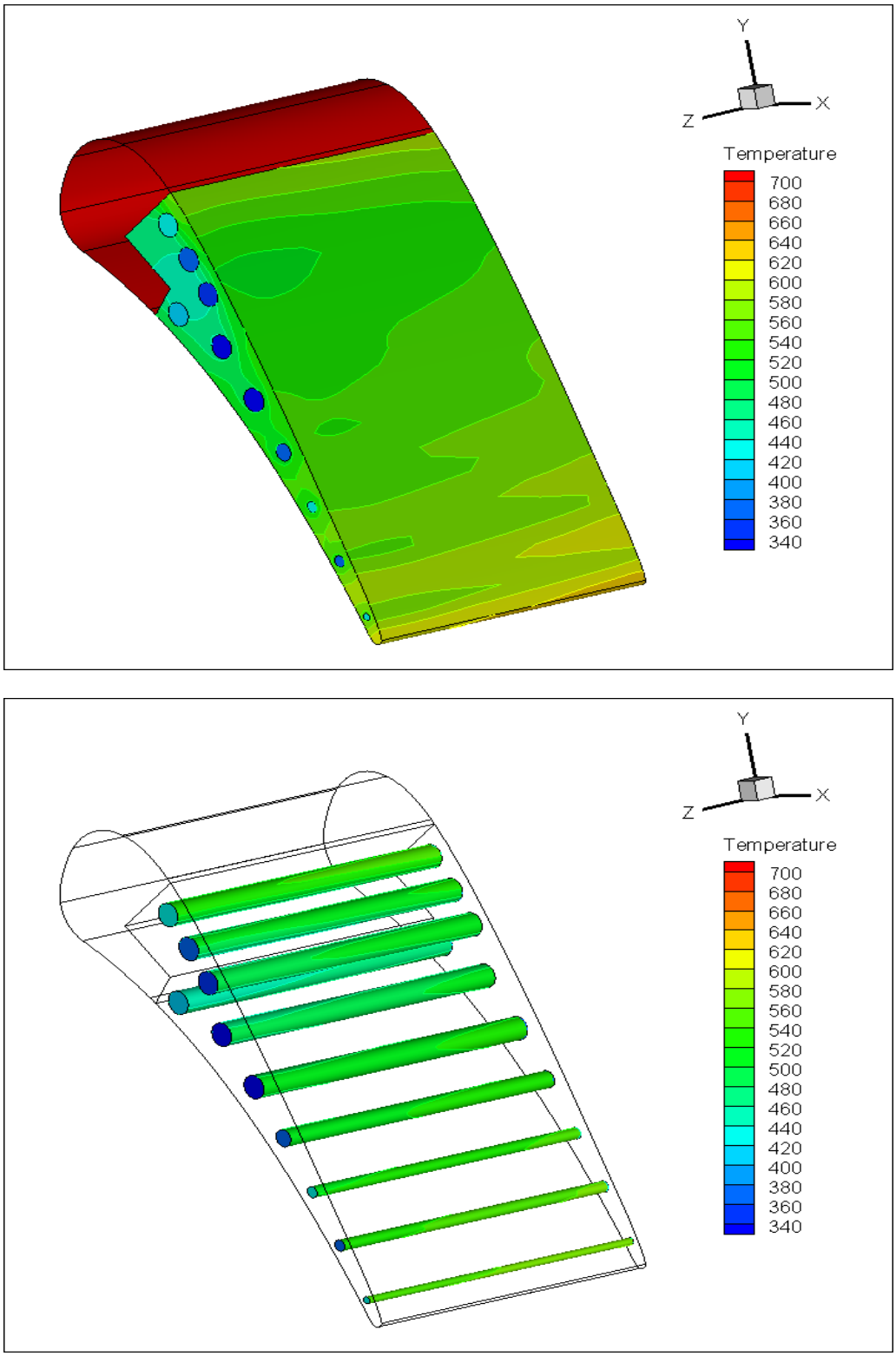

Figure 7-24a Temperature contour from 3D full conjugate simulation of C3X vane with no film cooling, **Run #44000**

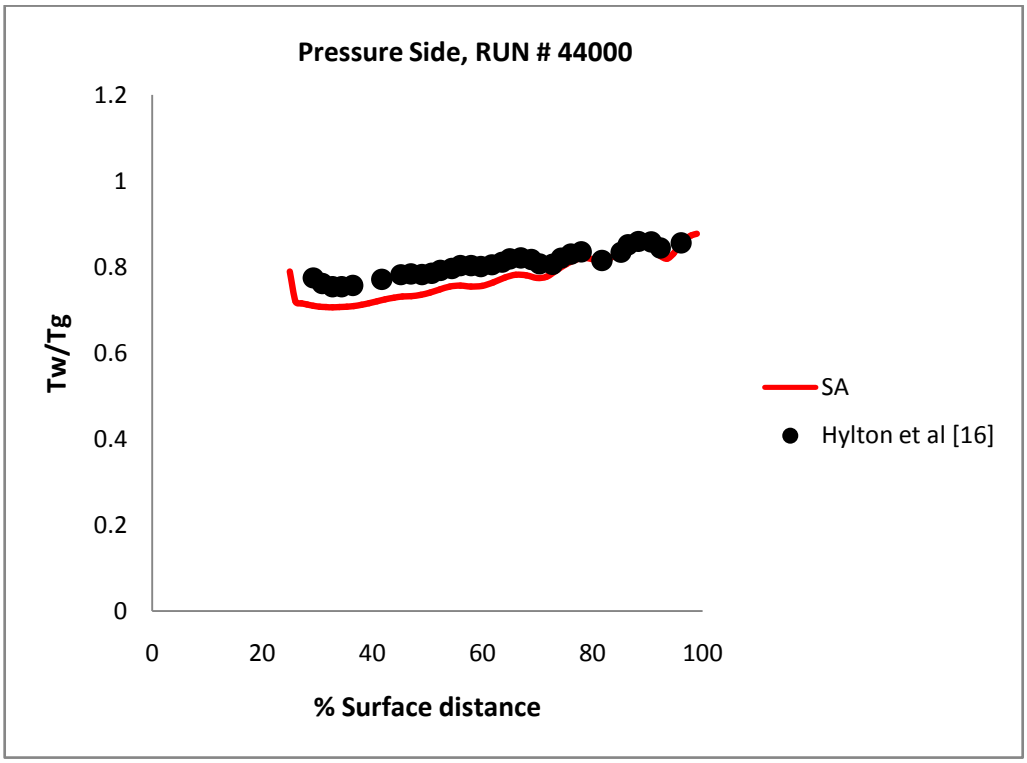

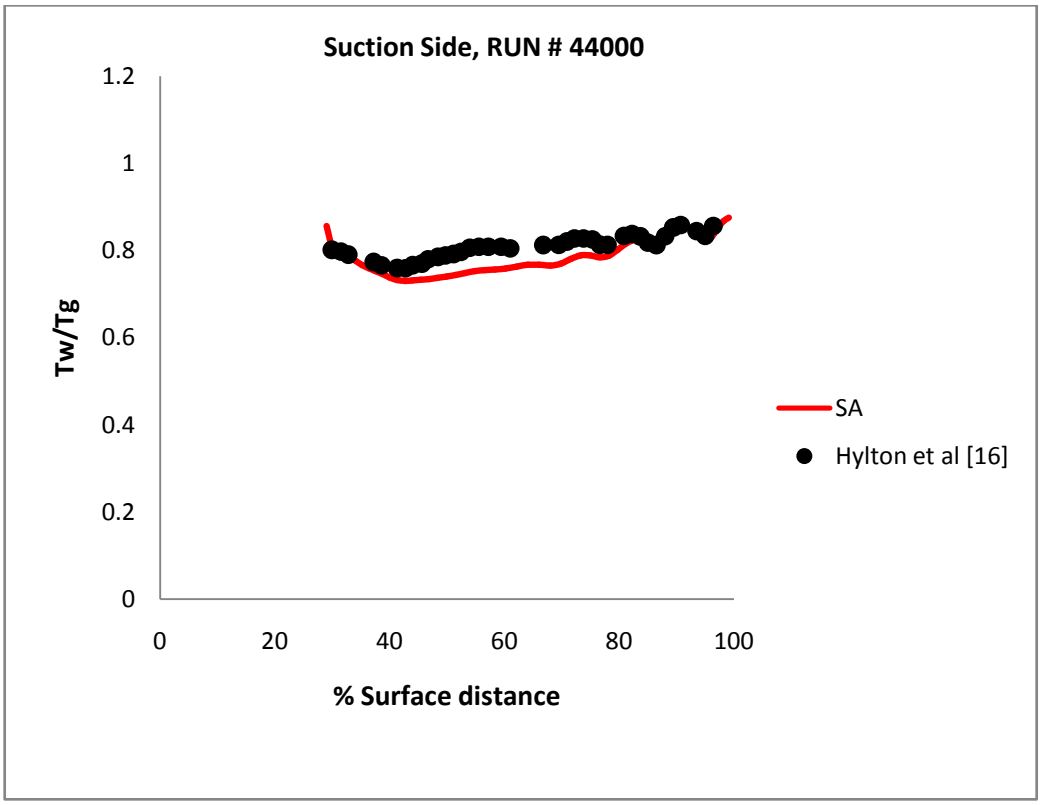

Figure 7-24b Surface temperature distribution at mid-span of the C3X vane using full conjugate 3D simulation with no film cooling, **Run #44000**

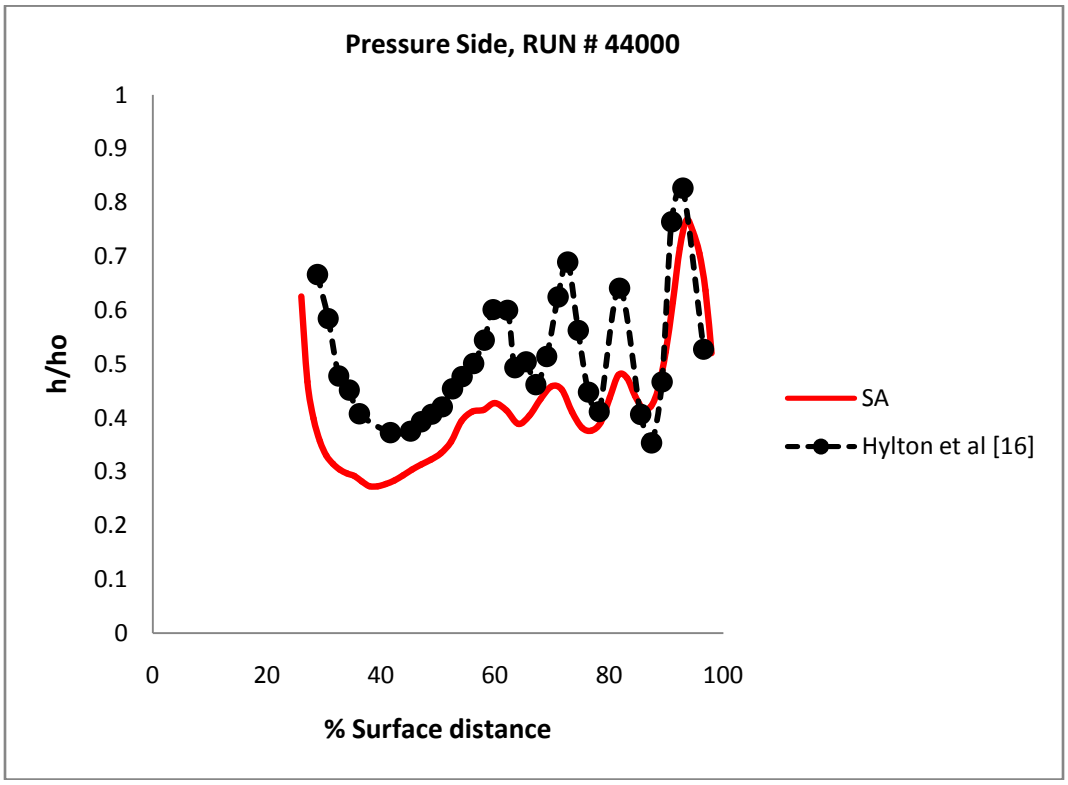

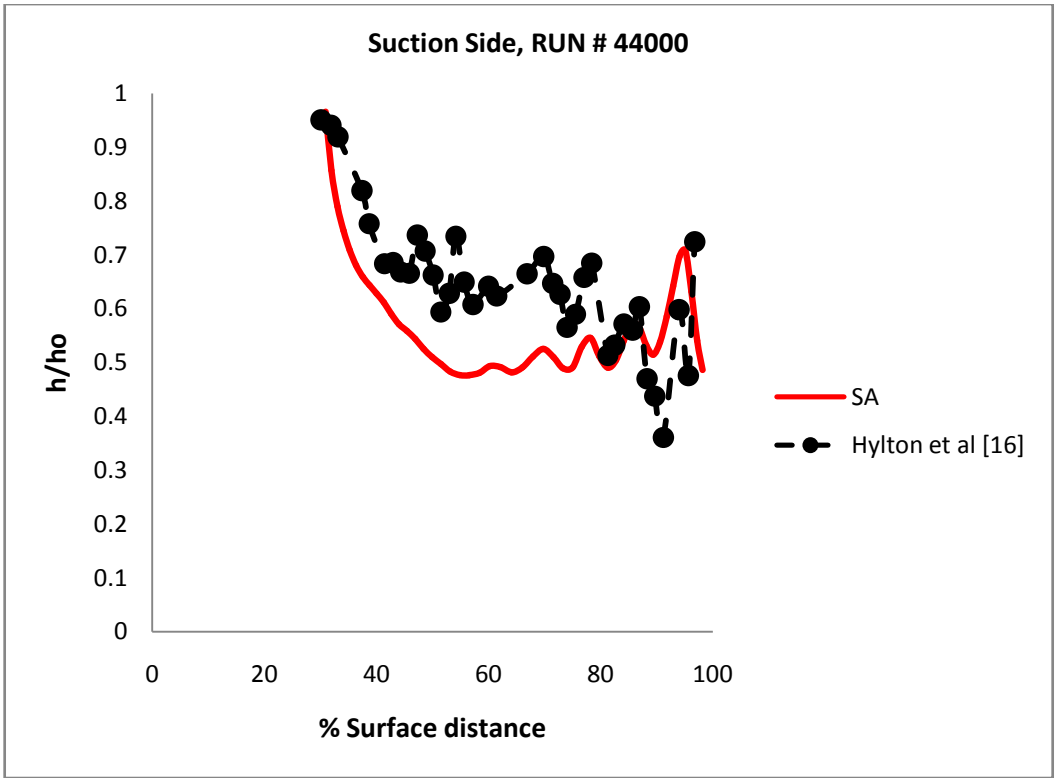

Figure 7-25 Heat transfer coefficient distribution at mid-span of the C3X vane using full conjugate 3D simulation with no film cooling, **Run #44000**

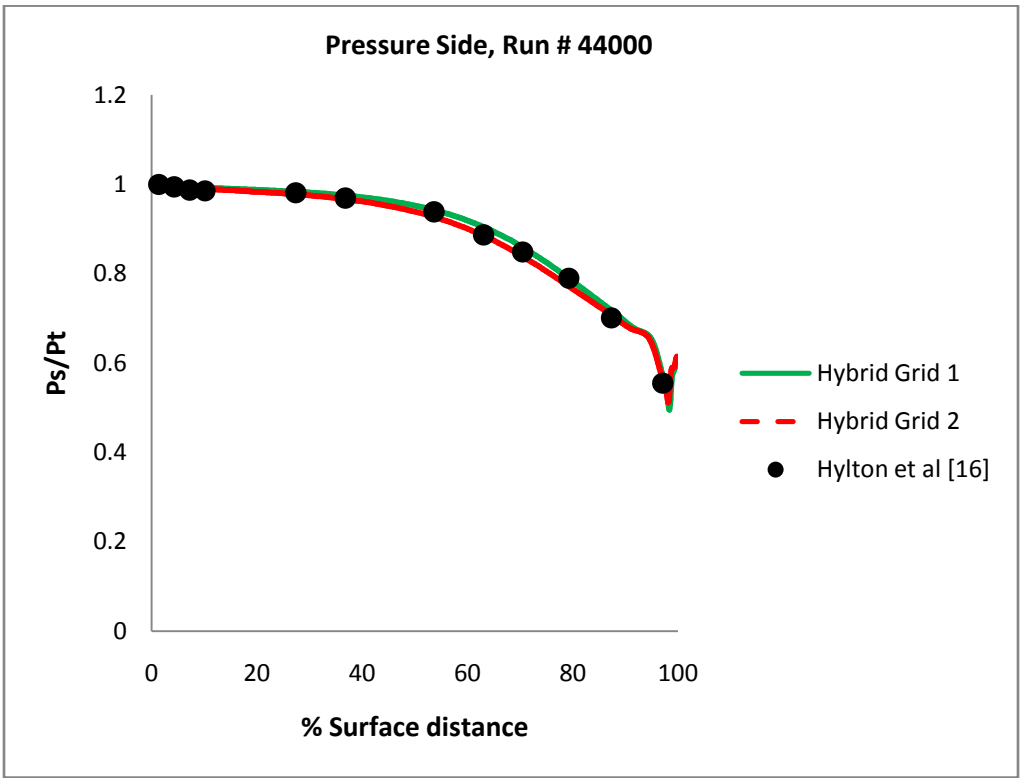

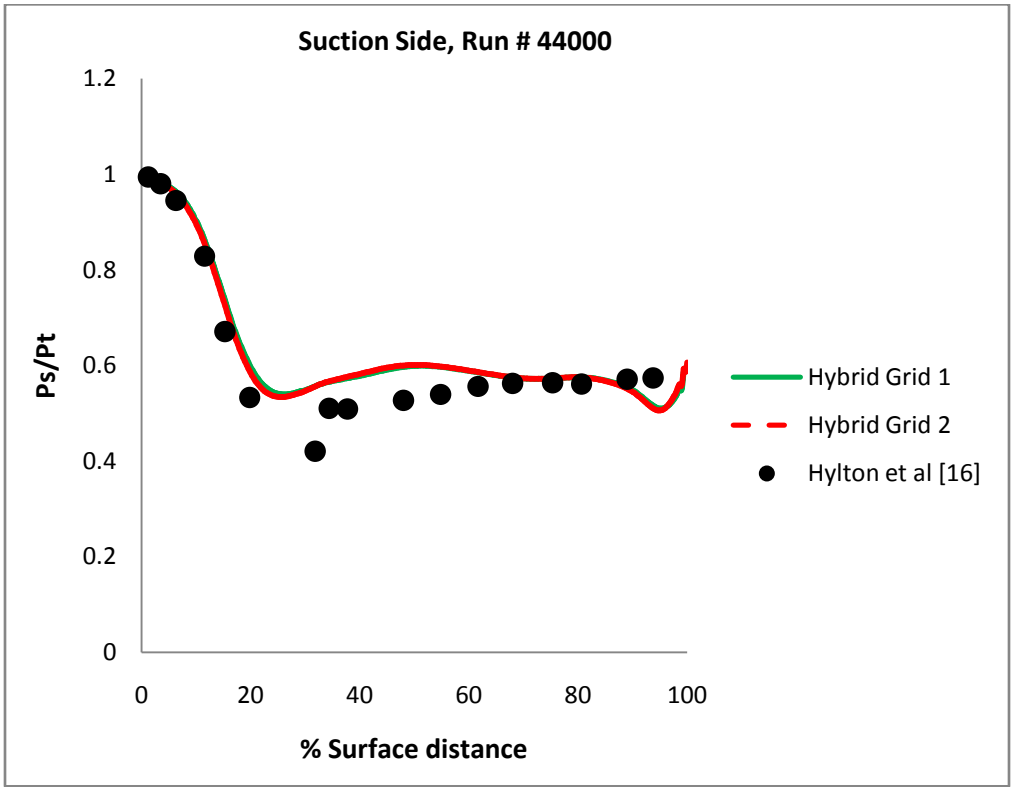

Figure 7-26a Surface pressure distribution comparison using *Hybrid Grid 1 & Hybrid Grid 2* obtained for C3X vane using full conjugate **2D** simulation with no film cooling, **Run #44000**

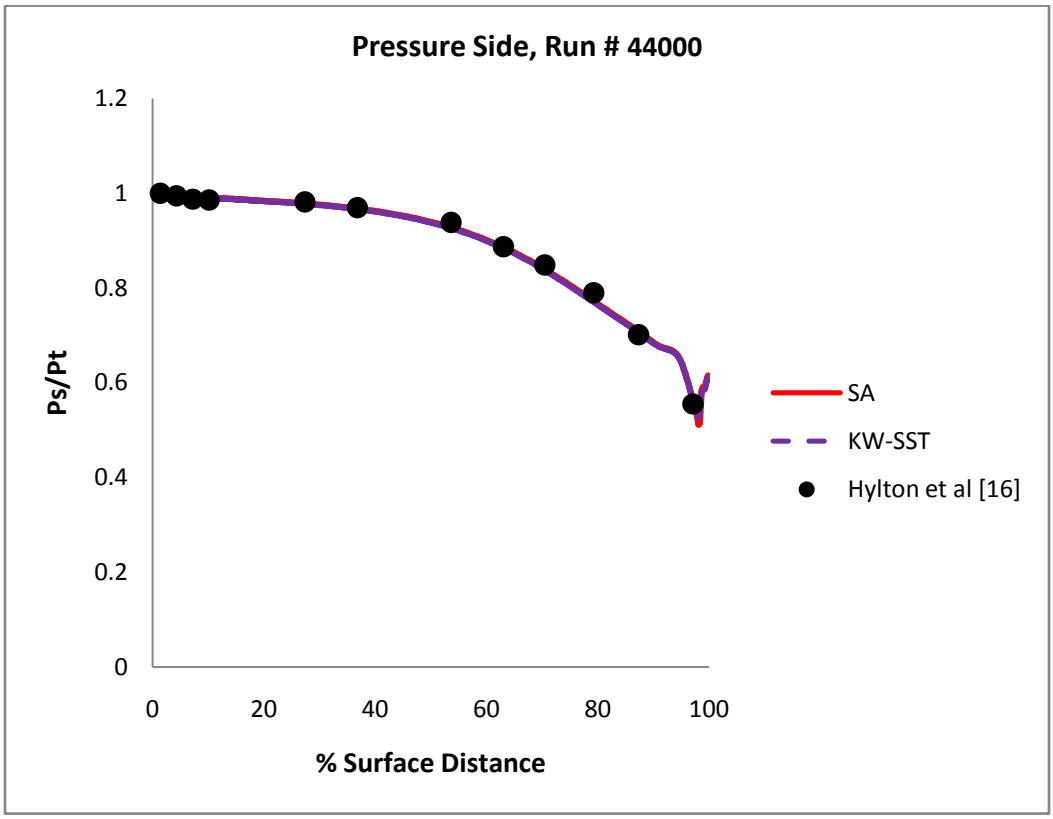

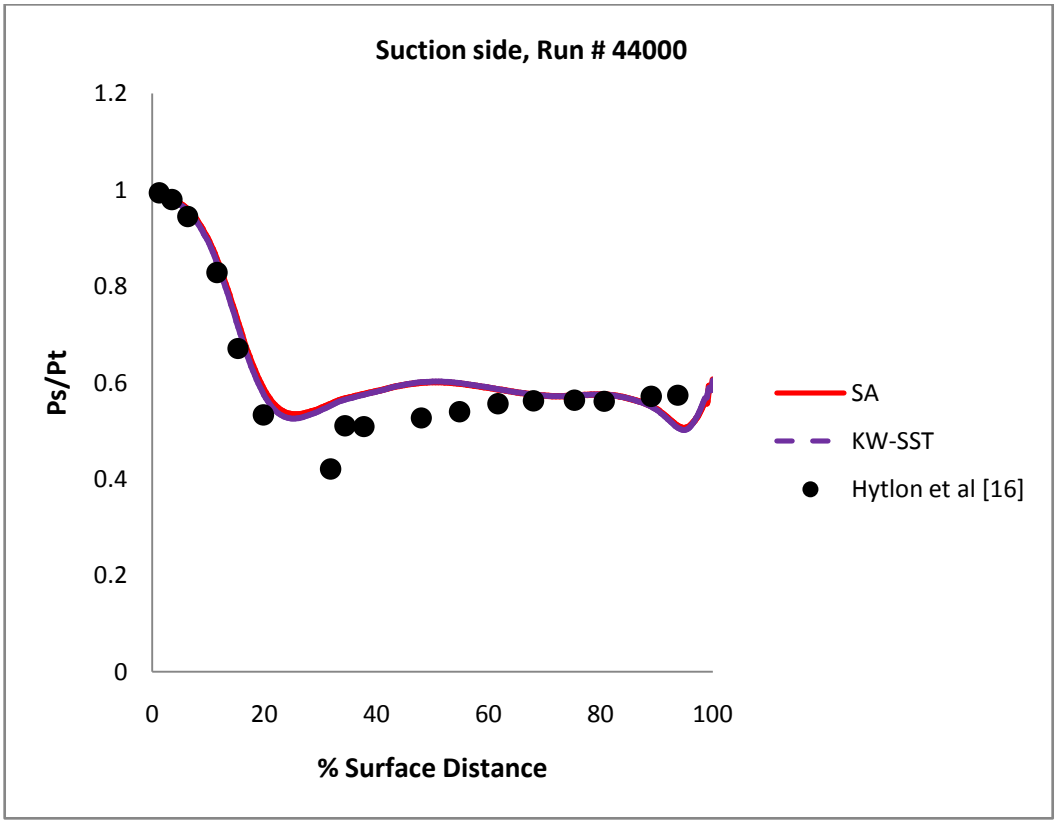

Figure 7-26b Surface pressure distribution of the C3X vane using full conjugate **2D** simulation with no film cooling, **Run #44000** on *Hybrid Grid 2*

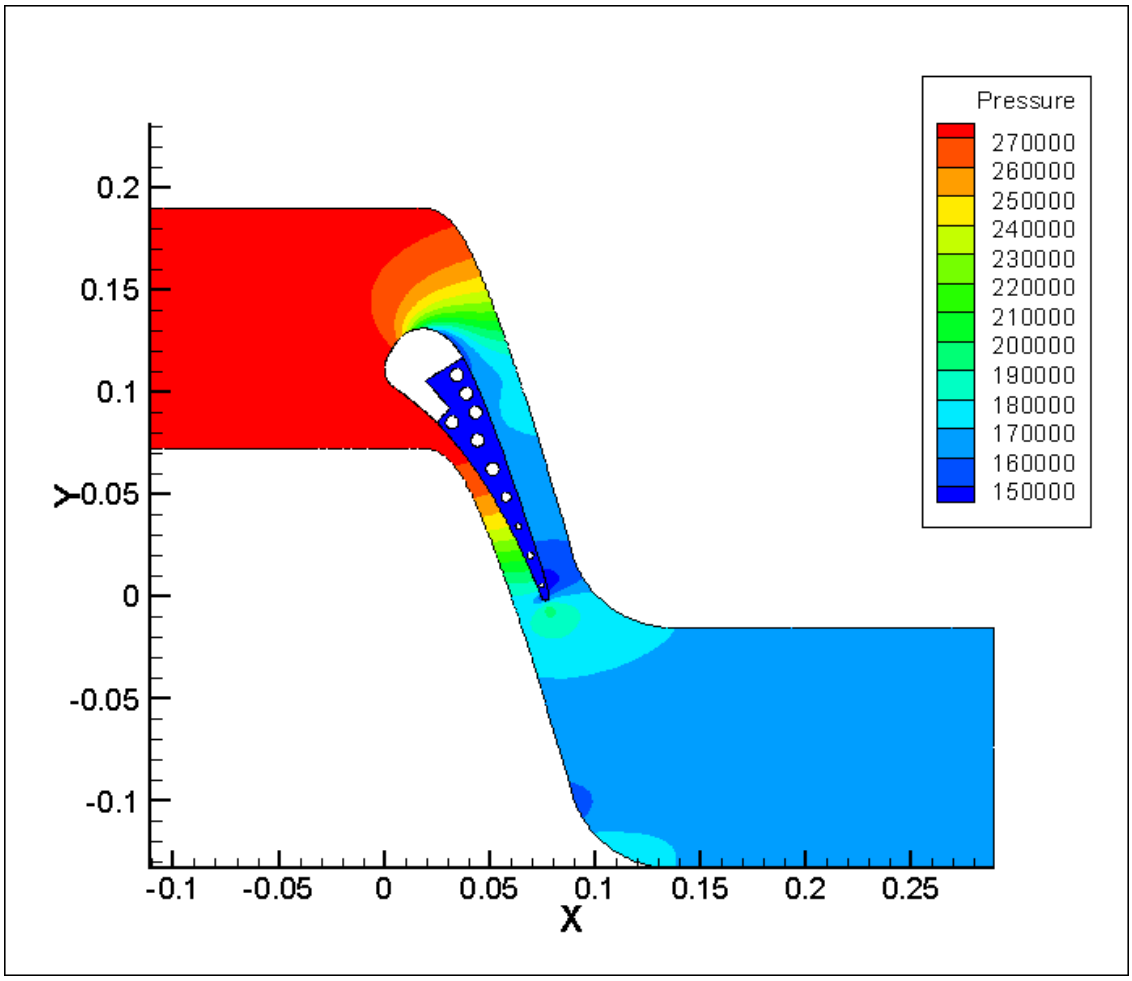

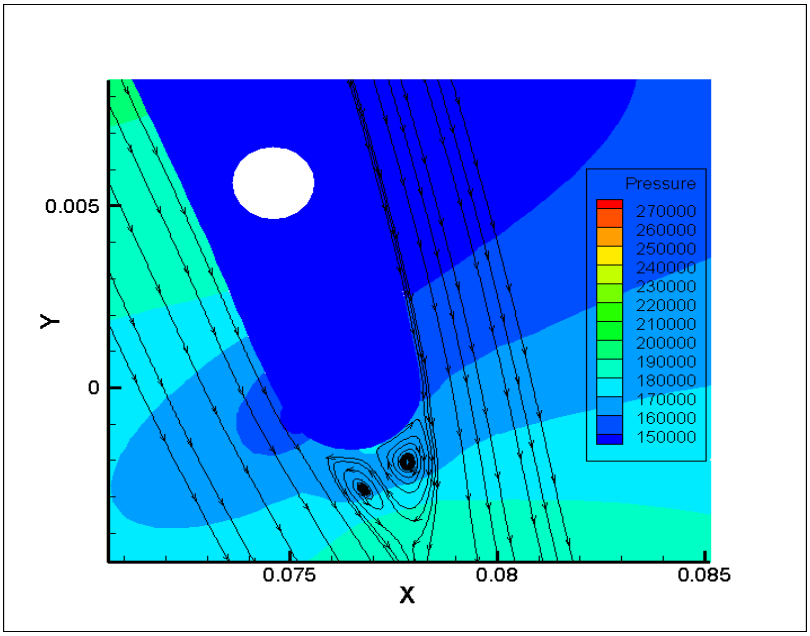

Figure 7-27 Pressure contour and trailing edge streamlines in the C3X vane using full conjugate 2D simulation with no film cooling, **Run #44000**

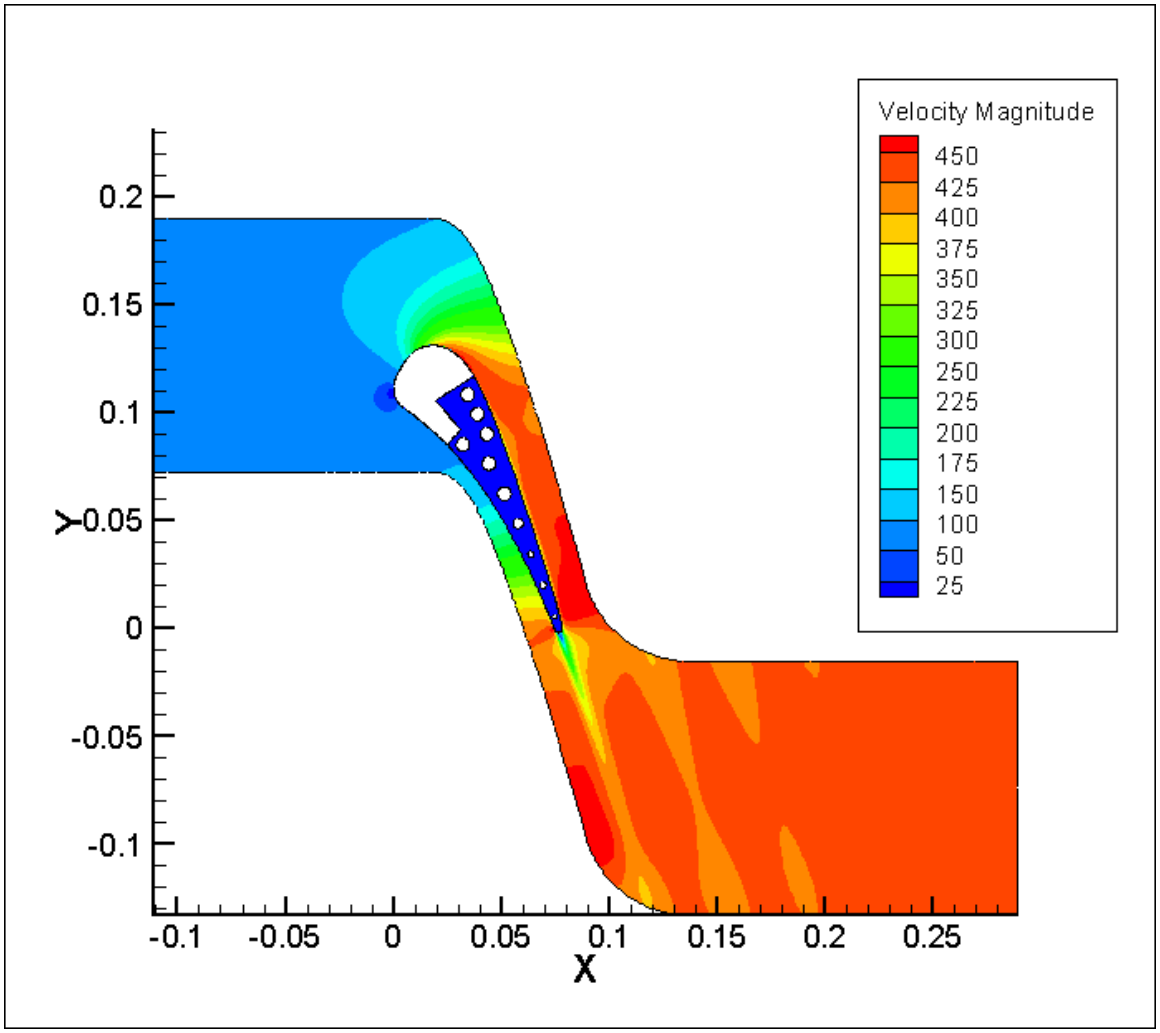

Figure 7- 28 Velocity contour in the C3X vane using full conjugate 2D simulation with no film cooling, **Run #44000**

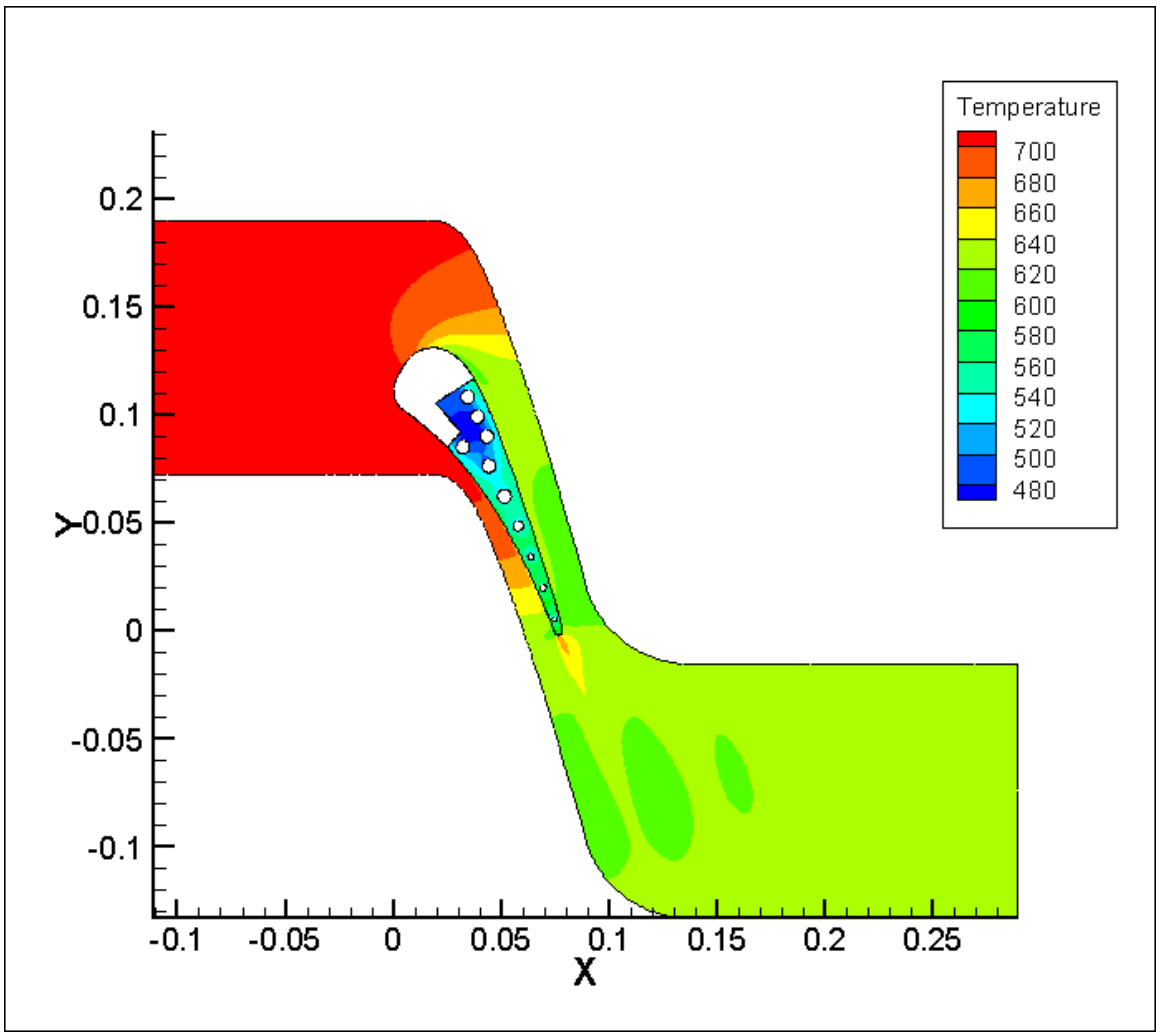

Figure 7- 29 Temperature contour in the C3X vane using full conjugate 2D simulation with no film cooling, **Run #44000**

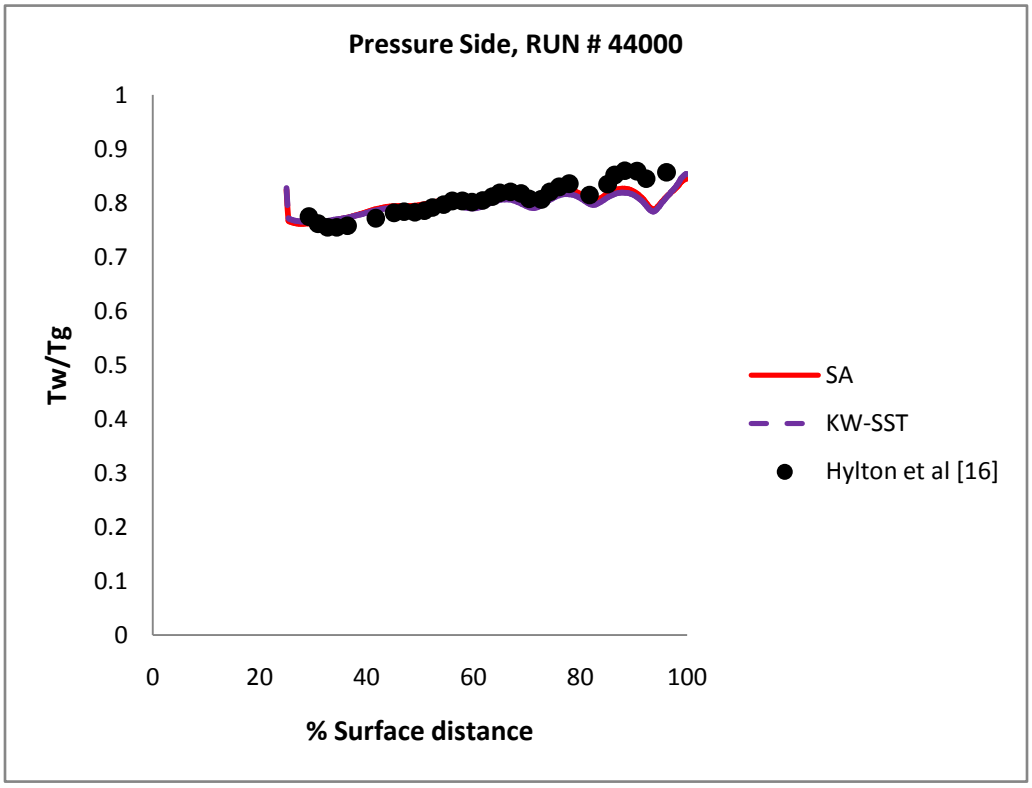

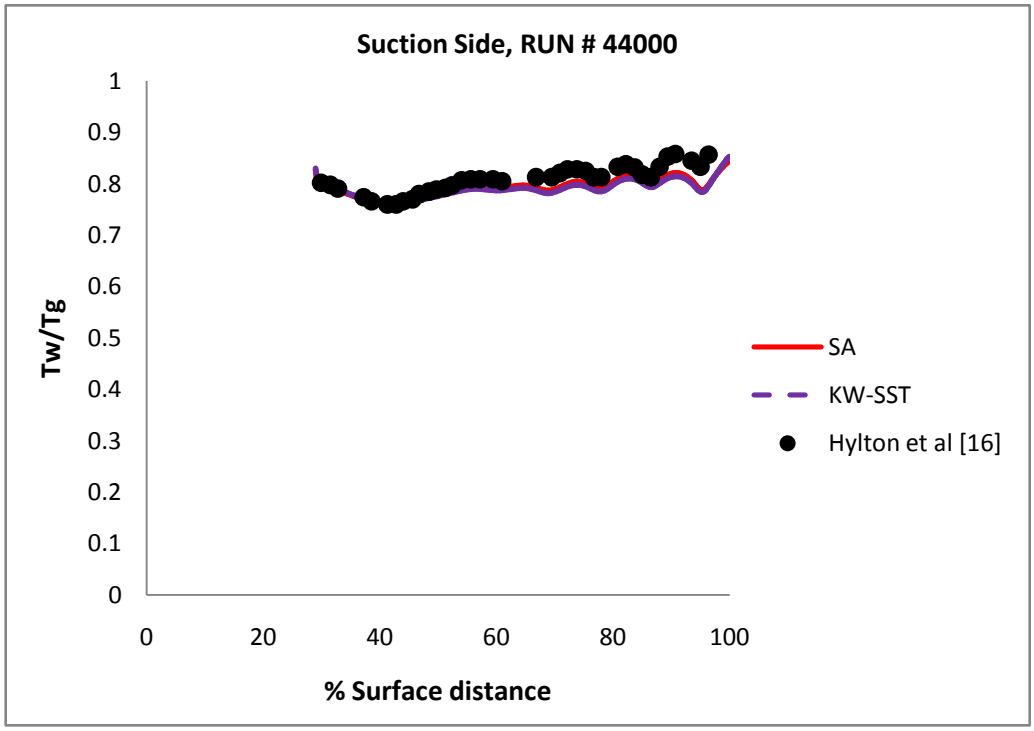

Figure 7-30 Surface temperature distribution of the C3X vane using full conjugate 2D simulation with no film cooling, **Run #44000** on *Hybrid Grid 2*

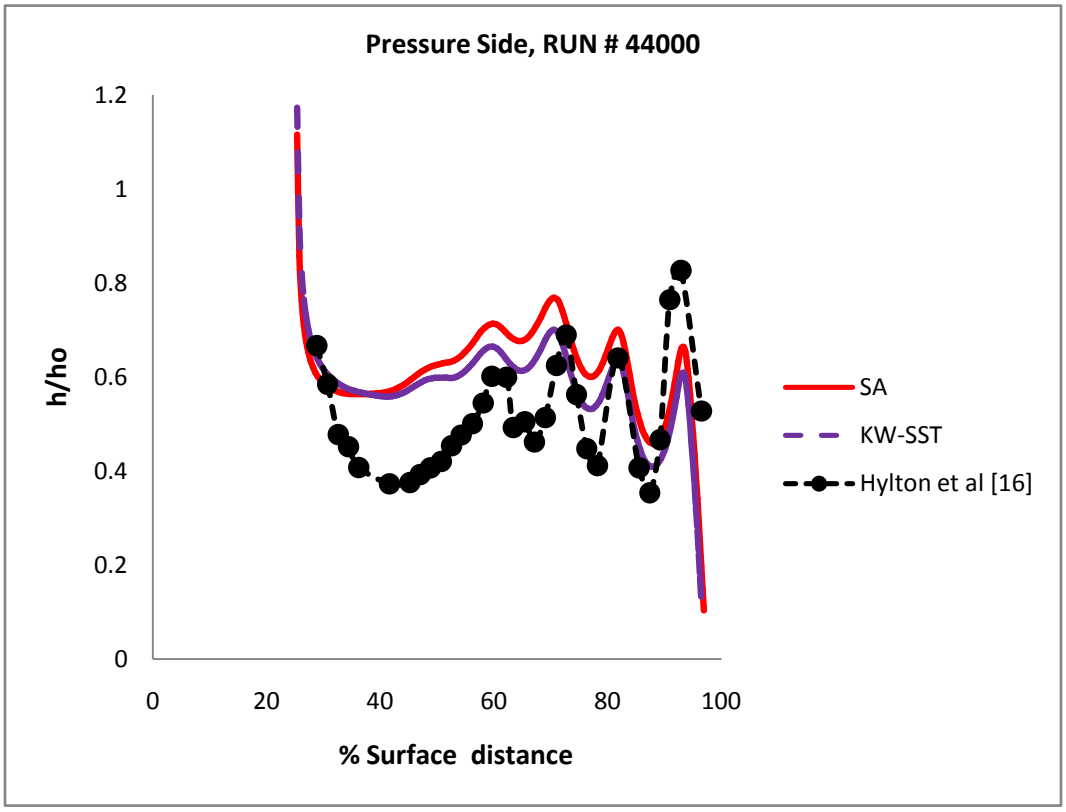

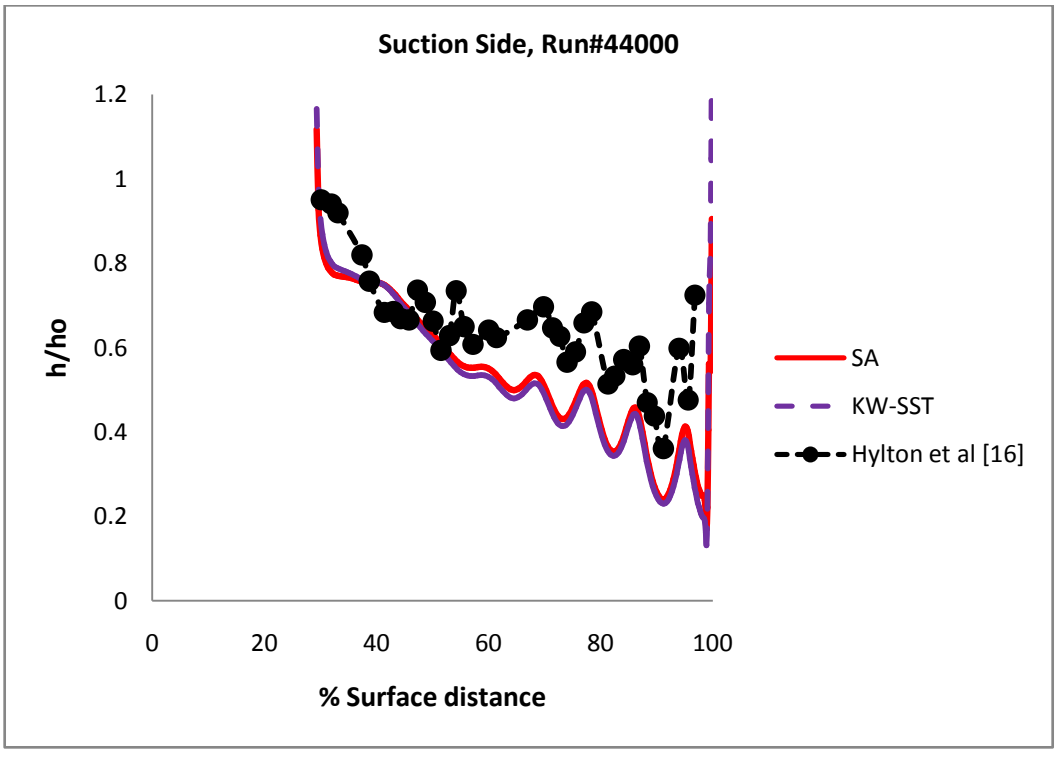

Figure 7-31 Surface heat transfer coefficient distribution of the C3X vane using full conjugate 2D simulation with no film cooling, **Run #44000**

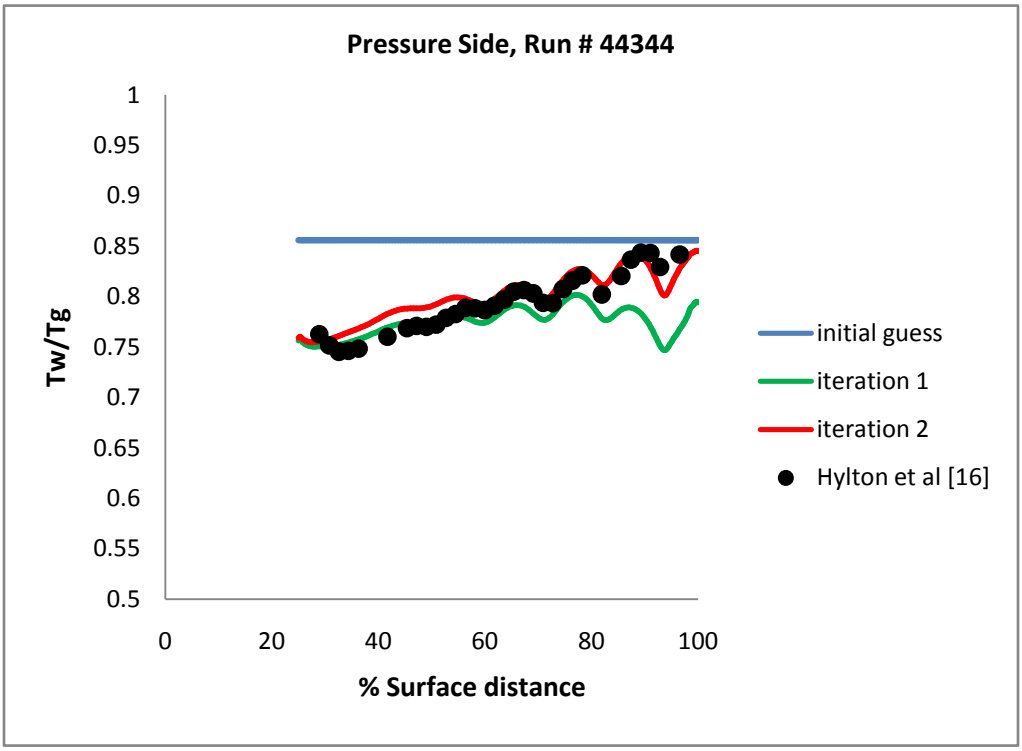

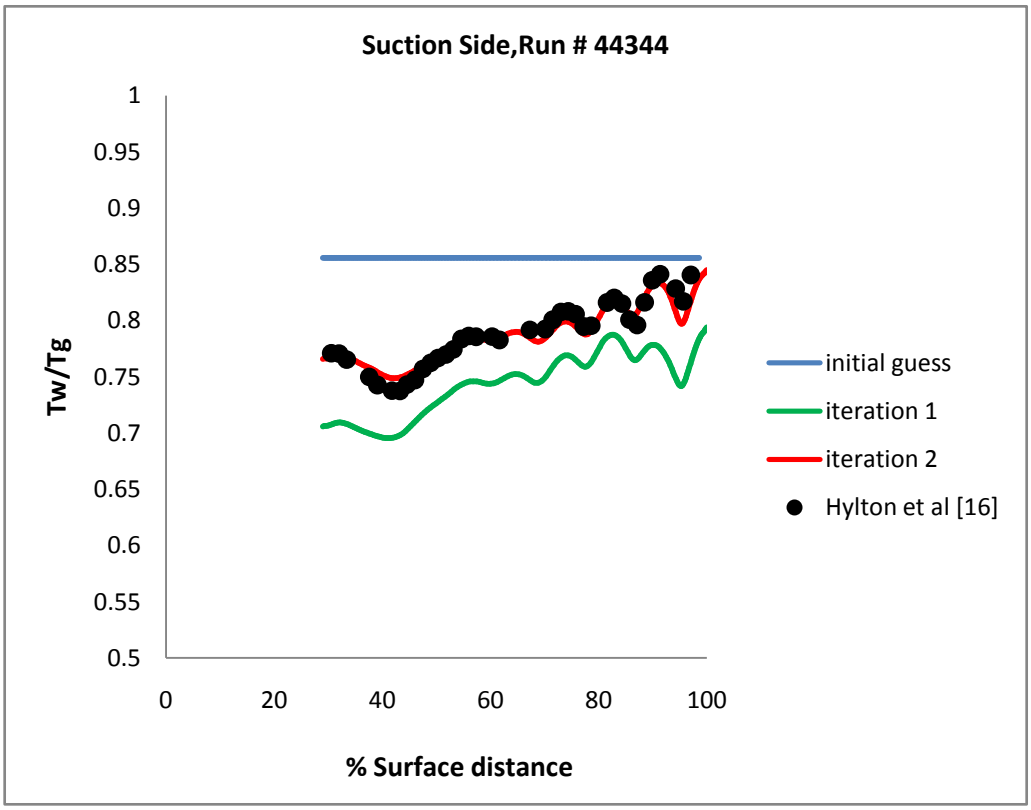

Figure 7-32 Surface temperature distribution on a film cooled C3X vane obtained using ICHT simulation, **Run #44344**

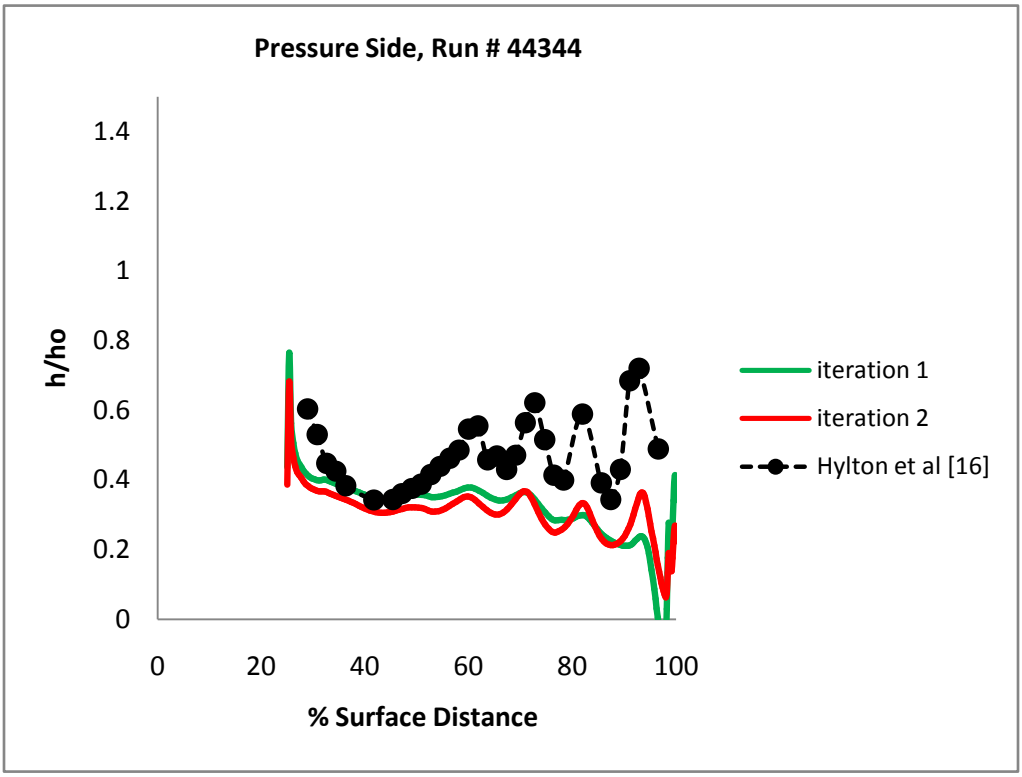

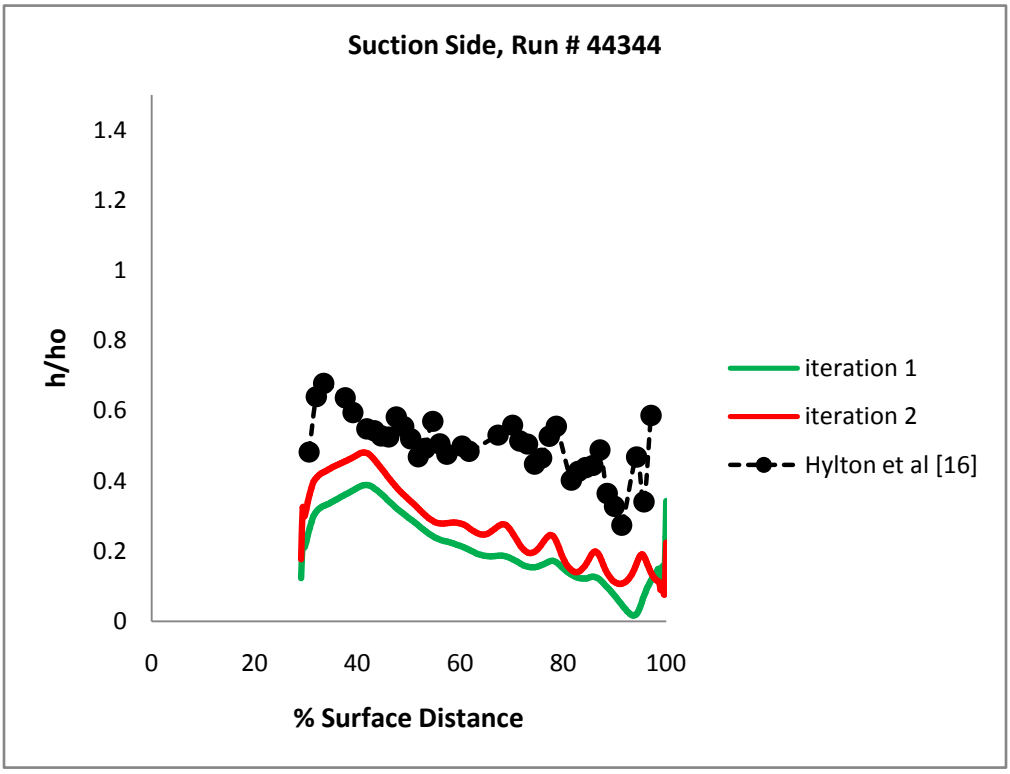

Figure 7- 33 Surface heat transfer coefficient distribution on a film cooled C3X vane obtained using ICHT simulation, **Run #44344**

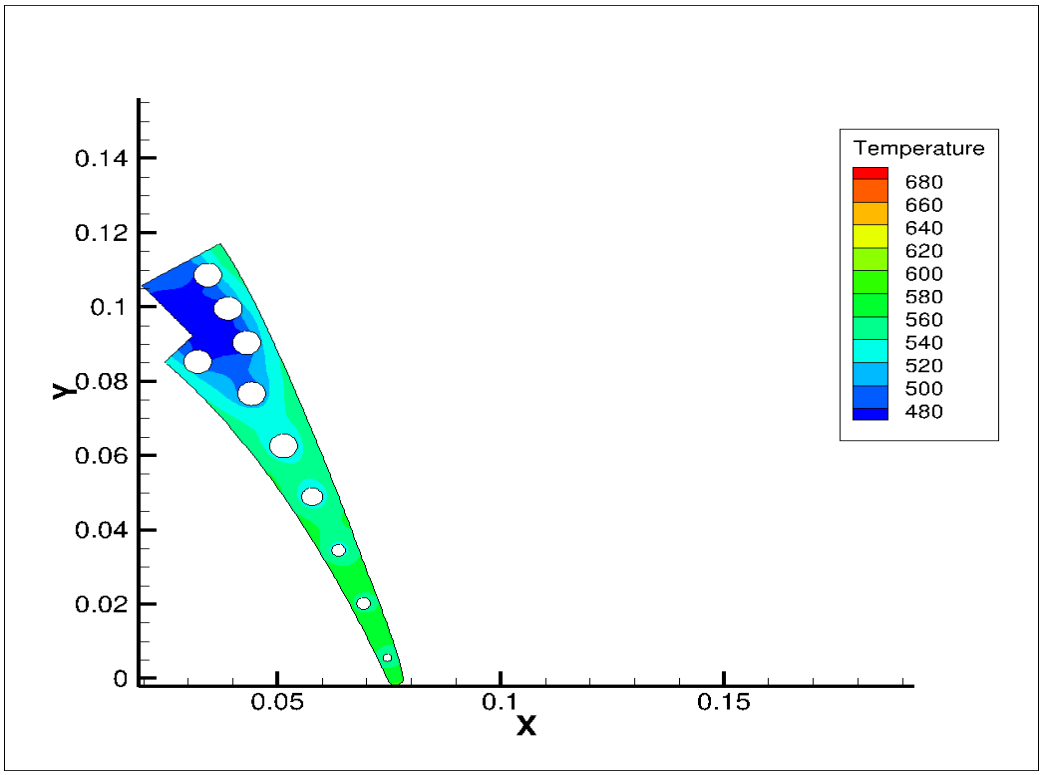

Figure 7- 34 Blade temperature distribution for non film cooled C3X blade, **Run #44344**

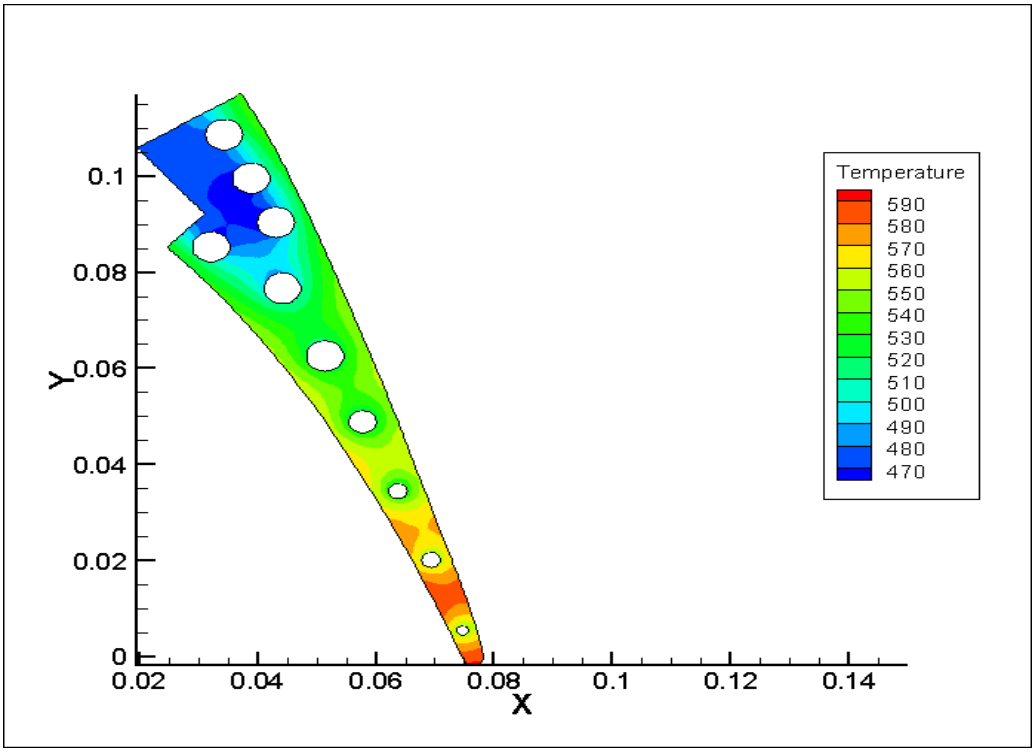

Figure 7-35 Blade temperature distribution for a film cooled C3X blade using ICHT, **Run #44344**

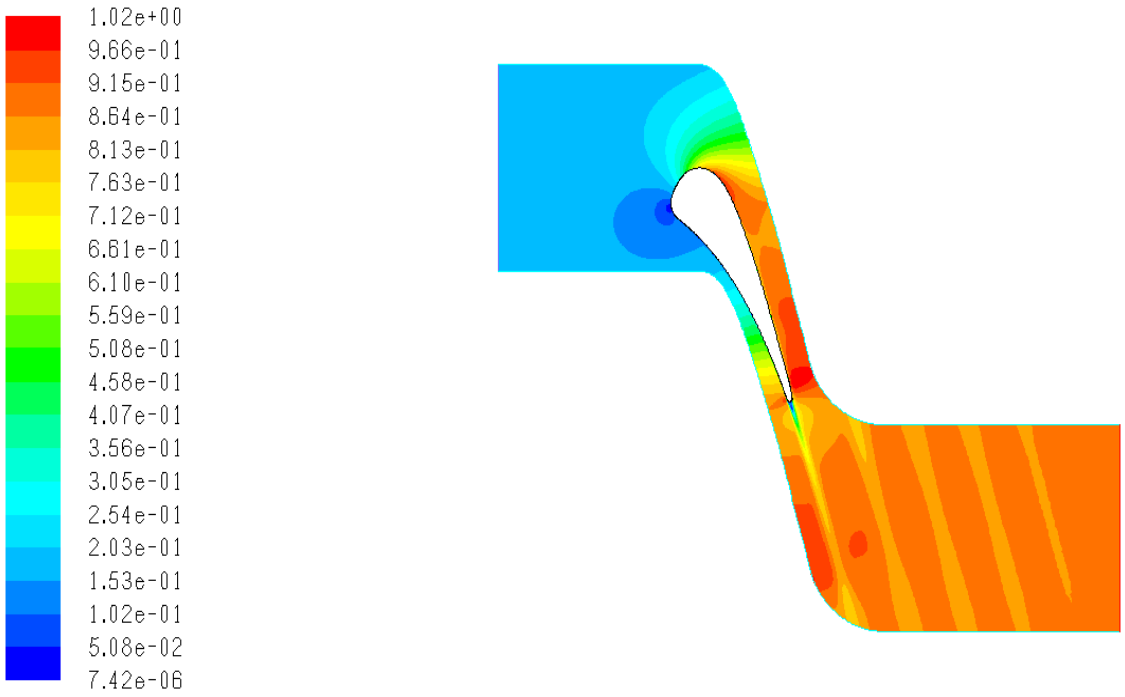

Figure 7-36 Mach number distribution for flow around a film cooled C3X vane obtained using ICHT simulation, **Run #44344**

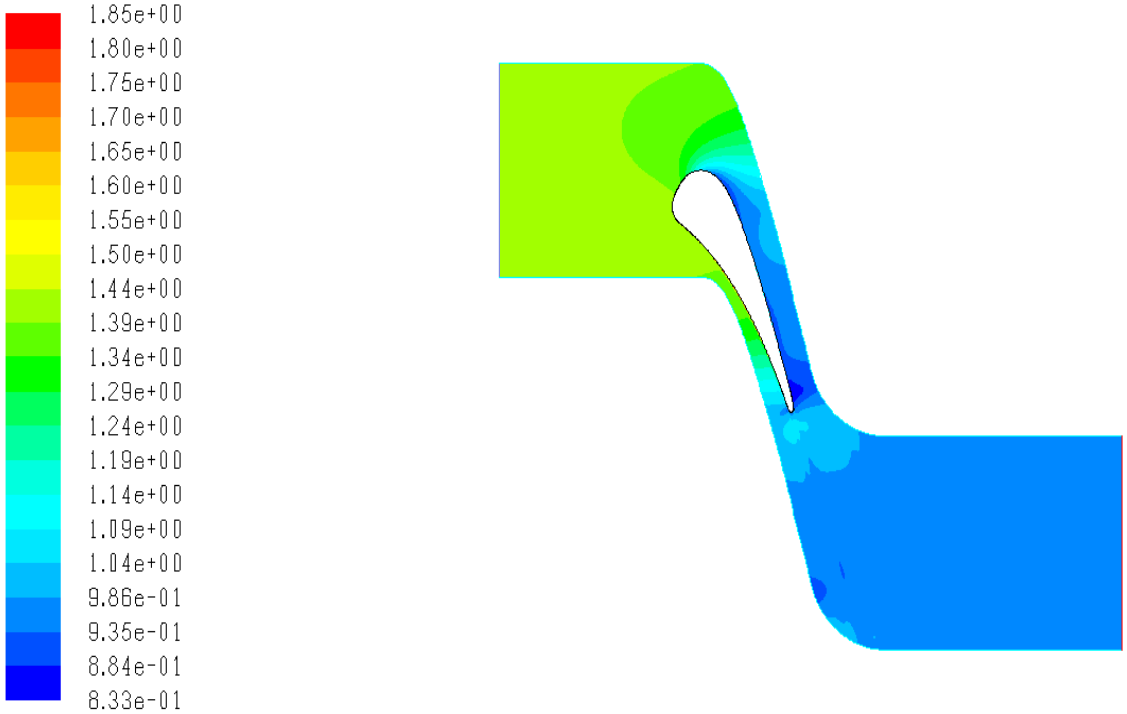

Figure 7-37 Density distribution for flow around a film cooled C3X vane obtained using ICHT simulation, **Run #44344**

Chapter 8

SUMMARY AND CONCLUSIONS

In this study ICHT technique is developed and applied to uncooled and film cooled flat plates and gas turbine blades using film cooling heat transfer coefficient corrections obtained from experimental data. Therefore, the need to numerically simulate complex film cooling flows is avoided in full conjugate calculations. This also avoids the shortcomings of present steady turbulence models in the near filed of film cooling jets thus avoiding inaccurate flow predictions. It also saves considerable time in preparation of the grid and running of the code, particularly when full coverage film cooling is being modeled. The effect of conjugate heat transfer is modeled successfully which makes the simulations more realistic and accurate.

Computational cost and resources required for such an analysis is minimal as external flow and blade conduction are solved separately. Thus at each step of convection or conduction a smaller computational matrix is solved as compared to full conjugate analysis. Further film cooling is not modeled but experimental data is used to correct for the conjugate heat transfer coefficient obtained from uncooled blades. Moreover, film cooling simulation can be performed with relatively simpler models like the one equation **SA** as the coolant jet is not directly simulated but only its effect is modeled. The results are also more reliable because it takes into account the effect of blade metal conduction which is usually ignored in conventional turbine blade design process.

This study therefore demonstrates the need for performing accurate film cooling simulation, under conjugate condition, using less computational cost and time. Test simulation performed using ICHT for film cooled flat plate reveal a difference of around 3% in wall temperatures from conventional technique under low temperature difference ($\Delta T \approx 20K$) and

around 10% from conventional technique under high temperature difference ($\Delta T \approx 550K$). Film cooled simulation, performed using ICHT, for a C3X vane with leading edge cooling revealed an improvement of around 7% on the pressure side and 10% on suction side, over conventional technique, for wall temperature distribution. Wall temperature distribution obtained using ICHT technique was found to be within 3% of the experimental value on pressure side and 2% of the experimental value on the suction side. These results thus confirm that ICHT can be a more effective tool for film cooling calculations than existing film cooling techniques.

Appendix A

SCHEME CODE

The ICHT process was fully automated using a List Programming (LISP) Code written in SCHEME language. Since ANSYS FLUENT has been scripted in SCHEME language, it was obvious to use this language for implementing ICHT technique.

SCHEME also has a unique advantage of invoking system commands from within the environment of ANSYS FLUENT which helps it communicating with MATLAB which performs the film cooling calculations. It is important to note that LISP languages are procedural based i.e. all the procedures used during the execution of the program have to be explicitly defined.

Text User Interface (TUI) commands were integrated with SCHEME code lines so that important procedures for following could be defined.

i. Reading checking and scaling the mesh
ii. Setting the appropriate turbulent model
iii. Settings boundary and other operating conditions
iv. Setting the discretization scheme and under relaxation factors
v. Settings convergence monitors
vi. Post processing

PLEASE NOTE – The SCHEME Code and MATLAB Script is a Proprietary Code developed for Pratt & Whitney which is not mentioned as a part of this thesis work and is not disclosed. It is at Pratt & Whitney's discretion to provide any information pertaining to it.

Following are the functions for important procedures developed in SCHEME code.

i. ***gui.scm*** - Creates a graphic user interface in FLUENT which could be used exclusively for setting important film cooling parameters.

ii. ***main.scm*** – All the various procedures are invoked from scheme code. It has flags to run all the operation in background mode and also performs file handling to get important results at each iteration level. It invokes MATLAB script for film cooling calculations.

iii. ***set-var.scm*** – Updates all boundary conditions and material property variables.

iv. ***set-model.scm*** – Sets the appropriate turbulence model

v. ***set-material.scm*** – Sets fluid and solid material properties

vi. ***set-bc.scm*** – Sets boundary conditions during convection or conduction run

vii. ***set-solution.scm*** – Sets discretization scheme and under relaxation factors

viii. ***check-res.scm*** – Checks for convergence criteria based upon scaled residuals

Appendix B

MATLAB SCRIPT

A MATLAB script is used which performs all the film cooling calculations. This MATLAB executable script is invoked from inside the FLUENT environment using SCHEME code. It is advantageous to use MATLAB since it can handle large and complex mathematical operations and the script can be changed from time to time without disturbing the main code.

The MATLAB script performs the following operations

i. Imports relevant data from DATA file generated by SCHEME code

ii. Loads experimental data for augmentation ratio and effectiveness stored in excel files

iii. Loads data quantities like temperature and baseline heat transfer coefficients etc from ANSYS FLUENT to perform film cooling calculations

iv. Performs 1-D curve fitting and interpolations along the length of the curved blade

v. Obtains heat transfer coefficient which incorporates the effect of film cooling

vi. Writes profile files for film cooling heat transfer coefficients

REFERENCES

[1] Han, J.C., Dutta, S., and Ekkad, S.V., 2000, "Gas Turbine Heat Transfer and Cooling Technology, Taylor & Francis, Inc.", New York, ISBN# 1-56032-841-X, 646 pages.

[3] R.J.Goldstein, "Advances in Heat Transfer, 1971,"Academic Press, New York, pp. 321–379.

[4] Ekkad, Srinath V.,Ou Shichuan., Rivir, Richard B, October 2004, "A transient infrared thermography method for simultaneous film cooling effectiveness and heat transfer coefficient measurements from a single test ASME J. Turbomach", v 126, n 4, p 597-603.

[5] Baldauf, S., Schulz, A., and Wittig, S., 2002 "Heat Flux Reduction from Film Cooling and Correlation of HeatTransfer Coefficients from Thermographic Measurements at Engine like Conditions".

[6] Baldauf, S., Scheurlen, M., Schulz, A., and Wittig, S., 2002, ''Correlation of Film-Cooling Effectiveness From Thermographic Measurements at Enginelike Conditions,'' GT-2002-30180, ASME J. Turbomach., 124, pp. 686–698

[7] Baldauf, S., Schulz, A., and Wittig, S., 1999, ''High Resolution Measurements of Local Heat Transfer Coefficients From Discrete Hole Film Cooling''. ASME J. Turbomach., 123, pp. 749–757.

[8] Baldauf, S., Schulz, A., and Wittig, S., 1999, ''High-Resolution Measurements of Local Effectiveness From Discrete Hole Film Cooling,'' ASME J. Turbomach., 123, pp. 758–765.

[9] C.H.N. Yuen, R.F., Martinez-Botas, January 2003 "Film cooling characteristics of a single round hole at various angles in a crossflow: Part I. Effectiveness", Int. J. Heat Mass Transfer

[10] C.H.N. Yuen, R.F., Martinez-Botas, January 2003 "Film cooling characteristics of a single round hole at various angles in a crossflow: Part II. Heat transfer coefficients", Int. J. Heat Mass Transfer.

[11] C.H.N. Yuen, R.F., Martinez-Botas, 2005, "Film cooling characteristics of rows of round holes at various angles in a crossflow: Part I. Effectiveness", Int. J. Heat Mass Transfer.

[12] C.H.N. Yuen, R.F. Martinez-Botas., 2005, "Film cooling characteristics of rows of round holes at various streamwise angles in a crossflow: Part II. Heat transfer coefficients", Int. J. Heat Mass Transfer.

[13] Gritsch, M., Schulz, A. Wittig, July 1998, "Adiabatic wall effectiveness measurements of film-cooling holes with expanded exits" ASME J. Turbomach, v 120, n 3, p 549-556,

[14] Gritsch, M., Schulz, A.,Wittig, S, 1998, "Heat transfer coefficient measurements of film-cooling holes with expanded exits"ASME, n GT, 1998

[15] Sargison, J.E., Guo, S.M., July 2002, Oldfield, M.L.G.,Lock, G.D.,Rawlinson, "A converging slot-hole film-cooling geometry-Part 1: Low-speed flat-plate heat transfer and loss" ASME J. Turbomach v 124, n 3, p 453-460

[16] Hylton, L.D., Nirmalan, V., Sultanian, B.K. and Kaufman,R.M., 1988, "The effects of leading edge and downstream film cooling on turbine vane heat transfer," NASA CR-182133.

[17] Yavuzkurt, Savas., Habte, Melaku., 2008, "Effect of computational grid on performance of two-equation models of turbulence for film cooling applications" ASME Turbo Expo, v 4, n PART A, p 133-143, 2008, Proceedings of the ASME Turbo Expo: Power for Land, Sea, and Air.

[18] Azzi, A., Lakehal, D. 2001, "Perspectives in modeling film-cooling of turbine blades by transcending conventional two-equation turbulence models" ASME,HTD, v 369, n 5, p 335-347, 2001, Proceedings of the Heat Transfer Division - Volume 5: Computational, Aerospace and Environmental Heat Transfer

[19] Hoda, A.,and Acharya, S.,1999,ASME-IGTI,Indianapolis.

[20] Acharya ,S.,Mayank, T., and Hoda, "Flow and Heat transfer predictions in Film cooling", Annals New York academy of science.

[21] Silieti, Mahmood., Divo, Eduardo., Kassab, Alain J. 2004 ,"Numerical investigation of adiabatic and conjugate film cooling effectiveness on a single cylindrical film-cooling hole. ASME,) HTD, v 375, n 1, p 333-343, 2004, Proceedings of the ASME Heat Transfer division.

[22] Bohn, Dieter E., Becker, Volker J., Kusterer, Karsten A.,1997, "3-D conjugate flow and heat transfer calculations of a film-cooled turbine guide vane at different operation conditions. Source" ASME, [d]10p.

[23] Lu, Xiaochen ., Jiang, Peixue., Sugishita, Hideaki; Uechi, Hideyuki; Suenaga, Kiyoshi. March 2006, "Conjugate heat transfer analysis of film cooling flows" . Journal of Thermal Science, v 15, n 1, p 85-91.

[24] Launder, B. E., and Spalding, D. B., 1974, "The Numerical Computation of Turbulent Flows," Computer Methods in Applied Mechanics and Engineering, Vol. 3, pp.269-289.

[25] Menter, F. R., 1994, "Two-Equation Eddy-Viscosity Turbulence Models for Engineering Applications," AIAA Journal, Vol. 32, pp. 598-1605.

[26] ANSYS Fluent 6.3 Documentation, 2006, Fluent Incorporated, Lebanon, NH.

[27] Spalart, P. R. and Allmaras, S. R., 1992, "A One-Equation Turbulence Model for Aerodynamic Flows" AIAA Paper 92-0439.

[28] Yakhot, V., and Orszag, S. A., 1986, "Renormalization Group Analysis of Turbulence: I. Basic Theory," Journal of Scientific Computing, 1(1):1-51.

[29] Shih, T. H, Liou, W. W., Shabbir, A., and Zhu, J., 1995, "A New k-ε Eddy-Viscosity Model for High Reynolds Number Turbulent Flows - Model Development and Validation," Computers Fluids, Vol. 24, pp. 227-238.

[30] Kays, W. M., and Crawford, M. E., 1993, "Convective Heat and Mass Transfer," 3rd edition, McGraw-Hill, New York, 1993.

[31] Chien, K. Y., 1982, "Predictions of Channel and Boundary-Layer Flows with a Low-Reynolds-Number Turbulence Model," AIAA Journal, Vol. 20, pp.33-38.

[32] Wieghardt, K., and Tillman, W., 1968, "On the Turbulent Friction Layer for Rising Pressure," Computation of Turbulent Boundary Layers, AFOSR-IFP-Stanford Conference, Volume II, edited by D. E. Coles and E. A. Hirst, Stanford University, CA, 1969, pp. 98-123.

[33] Eckert, E.R.G. 1983, "Analysis of film cooling and full-coverage film cooling of gas turbine blades", ASME 1983.

[34] Kane,Mangesh., Yavuzkurt, Savas. 2009, "Calculation of gas turbine blade temperatures using an iterative conjugate heat transfer approach" Int. Symp. on Heat Transfer in Gas Turbine Systems. 2009, Antalya, Turkey.

[35] Hylton, L. D., Millec, M. S., Turner, E. R., Nealy, D. A. & York, R. E., 1983, "Analytical and Experimental Evaluation of the Heat Transfer Distribution Over Surface of Turbine Vanes" NASA-Report CR 168015.

[36] Naeem, M., Jazayeri, S. and Rezamahdi,.N, "Failure Analysis of Gas Turbine Blades", Proceedings of The 2008 IAJC-IJME International Conference ISBN 978-1-60643-379-9.

[37] Luikov, A.V. "Conjugate convective heat transfer problems". Feb 1974 .International Journal of Heat and Mass Transfer, v 17, n 2, p 257-265.

[38] Montomoli, F. (Dipartimento di Energetica, Università di Firenze, Firenze, Italy). Adami, P. Martelli, F.. March 2009, "A finite-volume method for the conjugate heat transfer in film cooling devices", Proceedings of the Institution of Mechanical Engineers, Part A: Journal of Power and Energy, v 223, n 2, p 191-200.

[39] Laskowski, Gregory M., Ledezma, Gustavo A., Tolpadi, Anil K and Ostrowski, Michael C., 2008,"CFD simulations and conjugate heat transfer anaylsis of a high pressure turbine vane utilizing different cooling configurations", The 12th International Symposium on Transport Phenomena and Dynamics of Rotating Machinery Honolulu, Hawaii, February 17-22, 2008. ISROMAC12-2008-20065.

[40] Ledezma, Gustavo A., Laskowski, Gregory M., Tolpadi, Anil K., "Turbulence model assessment for conjugate heat transfer in a high pressure turbine vane model", Proceedings of the ASME Turbo Expo, v 4, n PART A, p 489-499, 2008, 2008 Proceedings of the ASME Turbo Expo: Power for Land, Sea, and Air.